Earth-Science Reviews 192 (2019) 285–316

Contents lists available at ScienceDirect

Earth-Science Reviews

journal homepage: www.elsevier.com/locate/earscirev

Detrital zircon provenance of Permo-Carboniferous glacial diamictites across Gondwana

John P. Craddock[a,*], Richard W. Ojakangas[b], David H. Malone[c], Alexandros Konstantinou[d], Arthur Mory[e], Wilfried Bauer[f], Robert J. Thomas[g], Suzanne Craddock Affinati[h], Kathryn Pauls[i], Udo Zimmerman[j], Greg Botha[k], Anthony Rochas-Campos[l], Paulo R. dos Santos[l], Eric Tohver[m,1], Claudio Riccomini[n], Joe Martin[o,2], Jonathan Redfern[o], Matthew Horstwood[p], George Gehrels[q]

[a] Department of Geology, Macalester College, St. Paul, MN 55105, USA
[b] Department of Geology, University of Minnesota-Duluth, Duluth, MN, USA
[c] Department of Geography, Geology and the Environment, Illinois State University, Normal, IL 61790-4400, USA
[d] ExxonMobil Exploration, Spring, TX 77389, USA
[e] Resources Branch, Industry Regulation and Safety, Government of W. Australia, Mineral House, 100 Plain Street, East, Perth, WA 6004
[f] AGEO Department, German University of Technology in Oman, PO Box 1816, 130 Athaibah, Oman
[g] Council for Geoscience, 3 Oos Street, Bellville 7535, South Africa
[h] School of Earth Sciences and Environmental Sustainability, Northern Arizona University, Flagstaff, AZ, USA
[i] Department of Geosciences, University of Wisconsin-Milwaukee, Milwaukee, WI 53211, USA
[j] Department of Petroleum Engineering, University of Stavanger, Ullandhaug, 4036 Stavanger, Norway
[k] Council for Geosciences, Geological Resources Division, 139 Jabu Ndlovu Street, Pietermaritzburg 3200, South Africa
[l] Instituto de Geociências, Universidade de São Paulo, São Paulo, Brazil
[m] Instituto de Astronomia e Geofísica, Universidade de São Paulo, 1226 Rua do Matão, Cidade Universitária, SP 05508-090, Brazil
[n] Institute of Energy and Environment, University of São Paulo, Av. Prof. Luciano Gualberto 1289, 05508-900 São Paulo, Brazil
[o] Basin Studies Group, University of Manchester, School of Earth and Environment, Manchester M13 9PL, UK
[p] NERC Isotope Geosciences Laboratory, British Geological Survey, Keyworth NG12 5GG, UK
[q] Department of Geosciences, University of Arizona, Tucson, AZ, USA

A B S T R A C T

Gondwana changed its high latitude location during the late Paleozoic (338–265 Ma), relative to the South Pole, and the style of glaciation evolved from localized alpine glaciers and ice fields to ~30 small ice sheets across the supercontinent. We report the analysis of heavy mineral populations ($n = 2217$) and the ages of detrital zircons ($n = 2920$ U-Pb LA-ICPMS results) from Gondwana diamictite deposits from eight landmasses: Africa (5 samples), Antarctica (5), Australia (8), the Ellsworth Mountains terrane (1, Antarctica), the Falkland Islands (2, diamictite plus U-Pb SHRIMP ages on granite clasts), India (1), Madagascar (1), Oman (3), the equatorial Lhasa terrane (2), the equatorial North Qiantang terrane (2) and South America (10). Heavy mineral separations (SEM-WDS analysis) identified one anomaly, pyrope garnets present only in Dwyka Group and Dwyka-equivalent samples suggesting an ultramafic Antarctic source. Statistical analysis of detrital zircon age distributions support the inference of local transport of sediment from many small ice centers with five examples of far-field ice transport (> 1000 km; four with ice flow > 2000 km), and three from ice fields located along coastal Antarctica. We propose that ice was distributed from five main ice-caps of different ages in southern Gondwana with ice flow away from central Gondwana. We also confirm that the Permo-Carboniferous detrital zircon populations of Euramerica (eolian and fluvial) and Gondwana (ash, detrital-glacial) are not mixed across the equator or seaway and ponder the possibility of a late Paleozoic snowball Earth.

1. Introduction

The Late Paleozoic Ice Age (LPIA), which occurred from the Visean (Mississippian) to the Capitanian/earliest Wuchiapingian (Middle-earliest Late Permian), was among the longest episodes of glaciation in Earth history, and the longest of the Phanerozoic (Figs. 1 and 2). Extensive reviews of the LPIA are provided by Fielding et al. (2008), Isbell et al. (2012) and Montañez and Poulsen (2013). The LPIA had profound effects on the Earth's physical, chemical and biological environments at all southern latitudes, and possibly in the northern hemisphere where glacial deposits of that age may exist (Crowell and Frakes, 1970; Crowell, 1978, 1999; Crowley and Baum, 1991, 1992;

* Corresponding author.
E-mail address: craddock@macalester.edu (J.P. Craddock).
[1] Now at: Instituto de Geociências, Universidade de São Paulo, São Paulo, Brazil.
[2] Now at: Shell Malaysia Ltd., Jalan Tun Sambanthan 211, Kuala Lumpur, 50,470, Malaysia.

https://doi.org/10.1016/j.earscirev.2019.01.014
Received 13 March 2018; Received in revised form 18 January 2019; Accepted 21 January 2019
Available online 14 February 2019

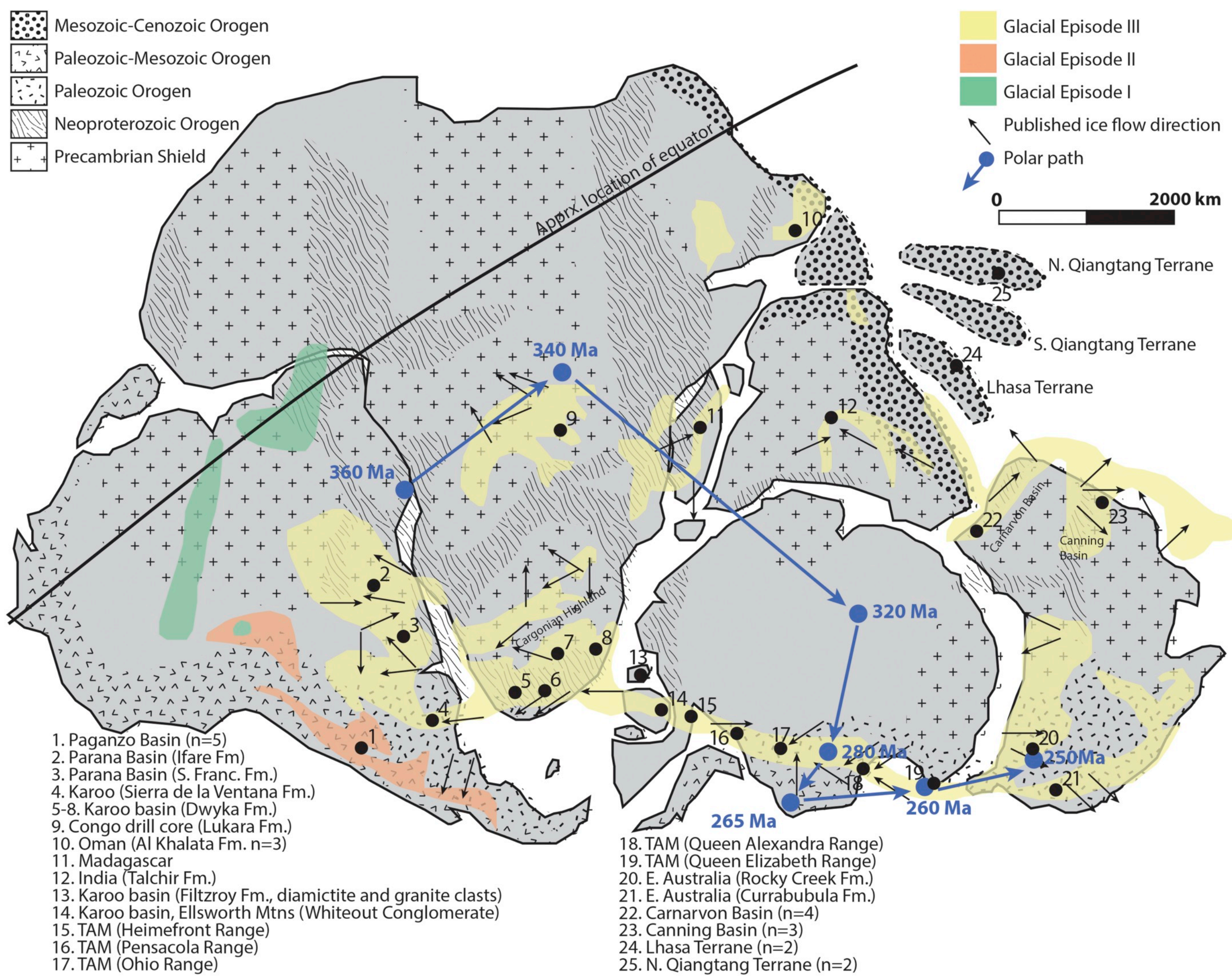

Fig. 1. Gondwana with schematic basement geology, the three episodes of LPIA glaciation indicated (Glacial Episode I: 360–342 Ma; Glacial Episode II: 334–313 Ma; Glacial Episode III: 315–265 Ma) and our sample sites (see Table 1).

Heckel, 1994, 2008; Isbell et al., 2003; Joachimski et al., 2006; Falcon-Lang, 2004; Grossman et al., 2008; Blakey, 2008; Lopez-Gamundi and Buatois, 2010; Isbell et al., 2012; Montañez et al., 2016; Isbell et al. (2016); Liu et al., 2017). Different parts of Gondwana were glaciated at different times as the supercontinent moved relative to the South Pole, with glaciation being most widespread during the Late Carboniferous–Early Permian, following local, alpine glacial episodes of lesser magnitude (Lopez-Gamundi and Buatois, 2010; Isbell et al., 2012). As ice volume changed, glacioeustatic sea-level change was widespread on both Gondwana and Laurasia, with the cyclothems of North America and Europe arguably the most prominent distal products (e.g. Heckel, 2008), although Pennsylvanian loess deposits are preserved in low-latitude settings in western North America (Soreghan et al., 2008).

The dynamics of glacial sedimentation does not favor preservation of interbedded ash deposits (i.e., primary zircons), so regional stratigraphic correlations have relied on relative age relationships. However, recent identification of interbedded ash beds and other volcanic rocks have better defined the absolute ages of local Gondwana glaciation (Fig. 3): 1) U-Pb zircon ages for the Dwyka Group of South Africa (Visser, 1990; Veevers et al., 1994; Key et al., 1998; Bangert et al., 1999 [U-Pb ages recalculated in Isbell et al., 2008]; Stollhofen et al., 2008), 2) For northwest Argentina (Gulbranson et al., 2010), 3) for eastern Australia (ignimbrites; Roberts et al., 1996; Fielding et al., 2008), and 4) for the Paraná Basin (Cagliari et al., 2014). The agents of diamictite deposition include ice sheets with various ice lobes, local alpine glaciers, ice caps, and floating ice shelves. These units are preserved because the depocenters were located along subsiding continental margins or in various types of subsiding basins, allowing Isbell et al. (2012) to delineate 30 basins in Gondwana with glacial deposits. These glacial deposits vary from terrestrial diamictites on striated basement (boulder pavements) to lacustrine and deep-marine sediments with dropstones (e.g., Lopez-Gamendi and Buatois, 2010) but often with syndepositional deformation (Isbell et al., 2008). Glacial striations and ice-flow directions are well-documented for Gondwana diamictites (Frakes et al., 1975; Matsch and Ojakangas, 1992; Hand, 1993; Veevers and Tewari, 1995; Visser et al., 1997, Visser, 1997; Fielding et al., 2008; Isbell et al., 2008a, 2008b; Mory et al., 2008; Rocha-Campos et al., 2008; and Isbell, 2010) but there is a paucity of detrital zircon and heavy mineral data to allow local and regional provenance analysis.

We document the provenance of Permo-Carboniferous diamictites based on heavy mineral (n = 2217) and detrital zircon U-Pb age populations across Gondwana (Fig. 1; 24 sample Sites including 5 cores, 2 with multiple samples, n = 2888 detrital zircon ages) to determine if glacial transport was local (Isbell et al., 2012), regional (i.e., entirely from Antarctica; Frakes et al., 1975; Veevers and Powell, 1987; Frakes et al., 1992; Ziegler et al., 1997; Hyde et al., 1999; Blakey, 2008;

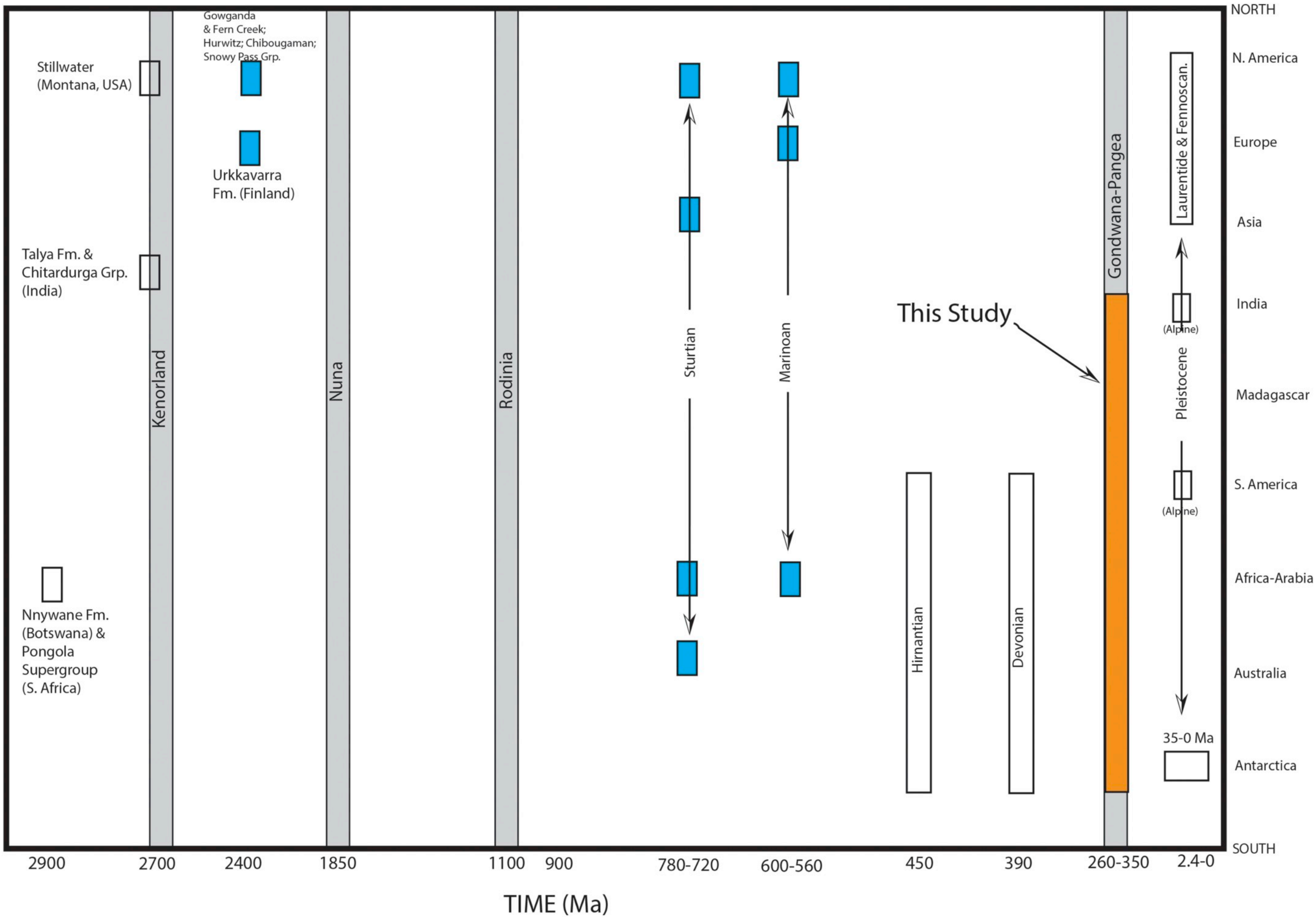

Fig. 2. Summary diagram of glacial epochs and sedimentation by continent and time (Eyles and Young, 1991; Crowell, 1999; Evans, 2000; Hoffman and Schrag, 2002; Halvorson et al., 2005). Supercontinents are in grey, snowball Earth events in blue. (For interpretation of the references to colour in this figure legend, the reader is referred to the web version of this article.)

Buggisch et al., 2011; Isbell et al., 2012), or both. We also include a published detrital zircon data set from late Paleozoic diamictites in the Himalayas and Tibet, which were in an equatorial setting during deposition (Gehrels et al., 2006a, 2006b, 2011), as well as three other existing diamictite detrital zircon data sets (Martin, 2008; Ramos et al., 2014; Linol et al., 2015) in northwest Australia, Argentina and South Africa, respectively. Ironically, Antarctica is again under a continental ice cap and analysis of Pleistocene glacial deposit zircons can be used to interpret what lies beneath Antarctic ice (Harley and Kelly, 2007; Veevers and Saad, 2008; Goodge et al., 2010; Licht and Palmer, 2013) and aid our provenance analysis. Preliminary results were presented at various Gondwana-related meetings (Craddock et al., 2008; Craddock, 2011; Craddock and Thomas, 2011).

2. Previous work

Whereas alpine glaciation was understood by the late 1700s in the Swiss Alps, the concept of continental glaciation developed slowly. Erratic boulders found over northern Europe were interpreted as the result of deposition by ancient (vanished) continental glaciers or from drifting icebergs, and hence the term "glacial drift" was coined. + +Von Charpentier (1834, but not published until 1841) and + +Agassiz (1837, but not published until 1840) presented the idea of widespread continental glaciers (see Crowell, 1999, p. 4–6.). We now recognize a wide array of primary sedimentary features in Pleistocene diamictites including striated boulder pavements, bullet-shaped boulders, glacial gouge and thrusting created by iceberg grounding (iceberg turbation), primary clast orientation (e.g., vertical clasts), convoluted beds, and soft-sediment deformation features such as flame structures, water-escape structures, rip-ups, clastic dikes and pebble nests (clast clusters) that likely originated by sediment dumps from overturned icebergs.

The first evidence for LPIA glaciation was described from the Permian of India (Blanford et al., 1856) and shortly thereafter in Australia, South Africa and South America. Wegener (1915, 1966) utilized these glacial deposits as a major line of evidence for his Continental Drift hypothesis, and later (1929) used Du Toit's, 1921 Gondwanaland reconstruction as further support. Du Toit's book, *Our Wandering Continents* (Du Toit, 1937) developed even further the significance of late Paleozoic glaciations. The forgoing studies of Permo-Carboniferous glaciations served as one line of evidence for the evolution of Continental Drift into Plate Tectonic theory.

Recent research indicates that the LPIA consisted of several short glacial events of < 10 million year duration, separated by similar short periods of warmer climate as Gondwana rotated and translated across the high southern latitudes (Fielding et al., 2008; Isbell et al., 2012). The LPIA started in South America at ~360 Ma, shifted to Africa at 340 Ma, to Antarctica from 320 to 260 Ma, and finally became widespread across Australia (e.g., Frank et al., 2008; Figs. 1 and 3). Gondwanan glaciation is subdivided into three episodes, with deposits of Episode I in northern South America (360–342 Ma), alpine deposits of Episode II in western South America (334–313 Ma), and deposits of widespread Episode III present on all the Gondwanan continents (315–265 Ma; López-Gamundí, 1997; Fig. 1). There are several

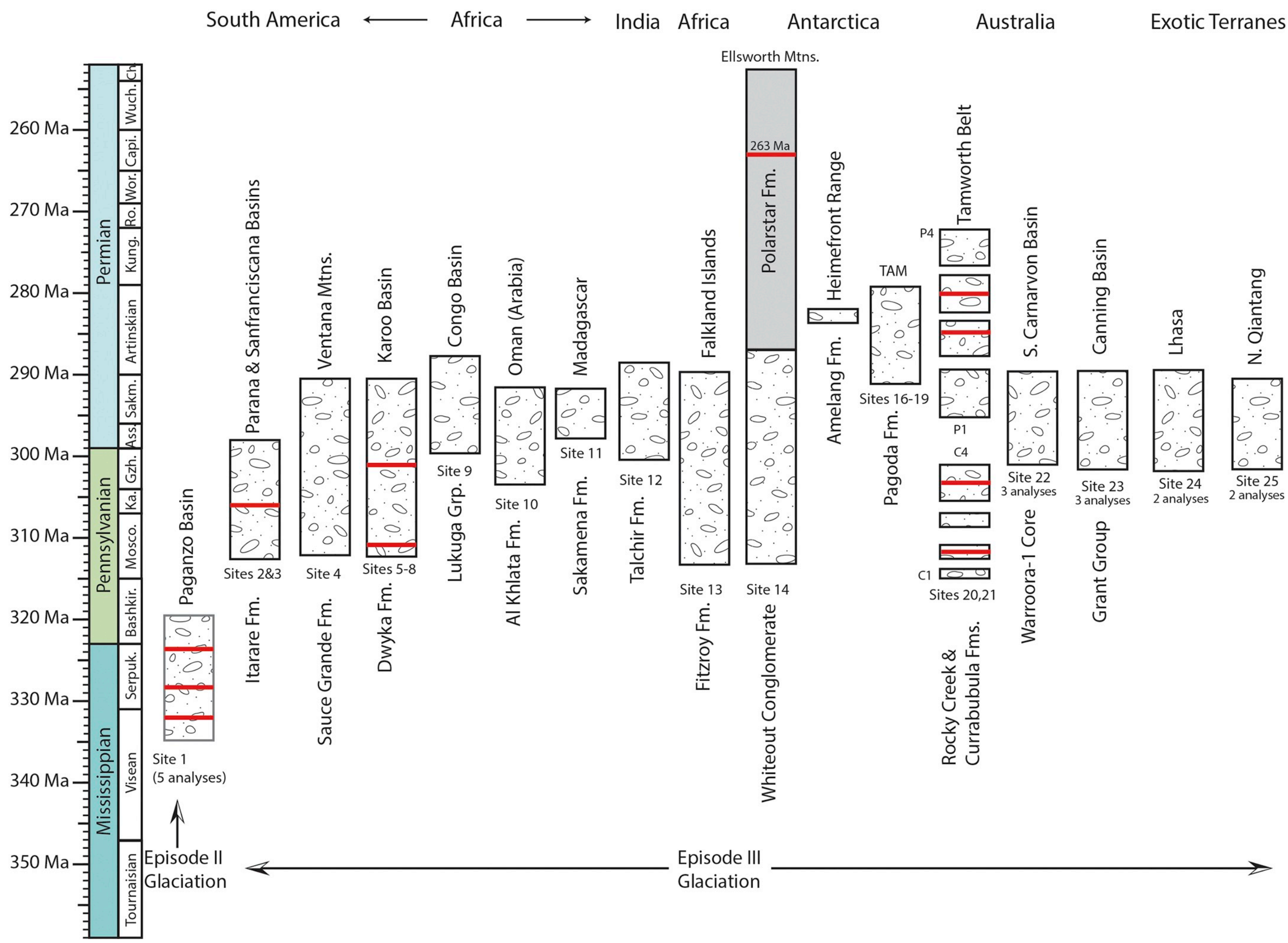

Fig. 3. Combined stratigraphy of glacial diamictites across Gondwana, modified from Isbell et al. (2012), with our tillite samples identified (see Fig. 1, Tables 1 and 2). Red lines indicate dated igneous layers. Additional sources: Gulbranson et al. (2010; Paganzo Basin), Rocha-Campos et al. (2008) and Cagliari et al. (2014; Parana Basin), Isbell et al. and Stollhofen et al. (2008; Dwyka Formation-Karoo Basin), Linol et al. (2015; Congo Basin), Webers et al. (1992), Elliot et al. (2014) and Craddock et al. (2017a, 2017b, 2017c); Ellsworth Mountains), Isbell et al., 2008a, 2008b, Transantarctic Mtns.); Lindström, 1995; Heimefront Range); Roberts et al. (2004) and Fielding et al. (2008; E. Australia), and Gehrels et al. (2011; Lhasa and N. Qiantang terranes). (For interpretation of the references to colour in this figure legend, the reader is referred to the web version of this article.)

excellent volumes of compilations and reviews of ancient glacial deposits, including those of the LPIA (Hambrey and Harland, 1981; Deynoux et al., 1994; Crowell, 1999; Fielding et al., 2008; Lopez-Gamundi and Buatois, 2010), all nicely summarized in Isbell et al. (2012). We have adopted the three-episode events of the LPIA, with samples from Episode II (Paganzo basin, Argentina, $n = 5$) and Episode III (everything else; Fig. 3).

3. Methods

Diamictite samples analyzed here were collected over many years and some are repository samples from central Antarctica (Table 1). Zircon crystals were extracted from samples by traditional methods of crushing and grinding, followed by separation with a Wilfley table, heavy liquids, and a Frantz magnetic separator as described on the University of Arizona LaserChron website. Samples are processed such that all zircons are retained in the final heavy mineral fraction; all the grains are < 500 µm in diameter. The non-zircon heavy mineral split was placed on a puck and analyzed using the SEM for additional provenance information (Table 2). A large split of the zircon grains (of all available sizes as to avoid bias) was incorporated into a 1″ epoxy mount together with fragments of our Sri Lanka standard zircon. The zircon mounts are sanded down to a depth of ~20 µm, polished, imaged, and cleaned prior to isotopic analysis. U-Pb geochronology of zircons is conducted by laser ablation multicollector inductively coupled plasma mass spectrometry (LA-MC-ICPMS) at the Arizona LaserChron Center (Gehrels et al., 2006c, 2008; *www.laserchron.org*). Data reduction was done using Isoplot (Ludwig, 2008) and K-S statistical software available on the LaserChron website.

Zircons from granite clasts in the Fitzroy Diamictite, Falkland Islands were analyzed using the SHRIMP at the John de Laeter Centre for Geochronology at Curtin University, Australia. Heavy minerals were analyzed using the SEM-WDS at Macalester College and Northern Arizona University; Sites 2 and 3 only include detrital zircon ages and samples reported in Gehrels et al. (2011). Sites 24 and 25 were processed in the field (see Table 2).

4. Results

Our data are presented, generally, from west (South America; oldest) to east (Australia, youngest) with respect to sample locales within Gondwana, and include detrital zircon results in glacial deposits reported by Gehrels et al. (2011) from the Himalaya and Tibet, the Sauce Grande Formation, Argentina (Ramos et al., 2014), Linol et al.

Table 1
Gondwana (Carboniferous-Permian) Tillite Detrital Zircons.

Sample	*Locality*	*Latitude*	*Longitude*	*Country*	*State/province*	*Region*	*Geological province*	*Zircons (n=)*	*Youngest Zircon Age*	*Stratigraphic unit*	*Position within unit*/Comment*
1	Malanzán	30.811222	66.573361	Argentina	Sierra de Malanzán	southwest	Paganzo Basin	24	412 Ma	Malanzán Formation	within Section L2 of Net and Limarino (2006)
	Loma Larga	30.795861	66.543639		Sierra de Malanzán	Unquillal	Paganzo Basin	50	362	Loma Larga Formation	within Section L5 of Net and Limarino (2006).
	Famatina Ranges	28.862889	67.600278			Precordillera Ranges	Navidad Arizaro Basin	95	389	Agua Colorada Formation	
	Huaco	30.144611	68.542556			Precordillera Ranges		50	404	Guandacol Formation	
	west of Huaco	30.059750	68.540528			Precordillera Ranges		19	385	Tupe Formation	
2				Brazil			Paraná Basin	38	365	Itararé Group	
3				Brazil			San Franciscana Basin	88	323	Itararé Group	
4	Ventana Mountains			Argentina			Ventana Mountains	194	386	Sauce Grande Formation	This study; Ramos et al. (2014)
5	Western Cape Dwyka			South Africa			Karoo Basin	93	498	Dwyka Group	
6	central Cape Dwyka			South Africa			Karoo Basin	92	507	Dwyka Group	
7	eastern Cape Dwyka			South Africa			Karoo Basin	85	499	Dwyka Group	
8	KwaZulu-Natal			South Africa	KwaZulu-Natal		Karoo Basin	90	499	Dwyka Group (basal)	
9	Dekese			central Africa			Congo Basin	157	528	Lukuga Group	Linol et al. (2015)
10	Oman-1			Oman		Huqf Hills		83	604	Al Khlata Formation P1	undisclosed drill holes
	Oman-2							98	272	Al Khlata Formation P5	
	Oman-3							100	346	Al Khlata Formation P9	
11	east of Ranohira	45.496850	22.508500	Madagascar		upper Ihazofotsy Valley	Morondava Basin	59	442	Sakamena Group	
12	Dhanbad,			India		Damodar Valley		46	431	Talchir Formation	
13		51.046450	60.046450	Falkland Islands				96	479	Fitzroy Diamictite Formation	
								11	447.3	granite clasts	SHRIMP ages
14				Antarctica	Ellsworth Mountains	Meyers Hills	Ellsworth-Whitmore terrane	90	519	Whiteout Conglomerate	Craddock et al. (2017a, 2017b, 2017c)
						Sentinel Range				Whiteout Conglomerate	
15				Antarctica	Dronning Maud Land	Heimefront Range		100	521	Amelang Plateau Formation	Pole Research Repository
16				Antarctica	Transantarctic Mountains	Pensacola Mountains	Ellsworth-Whitmore terrane	91	498	Gale Mudstone	Pole Research Repository
17						Ohio Range		95	493	Buckeye Tillite	Pole Research Repository
18						Queen Alexandra Range		91	474	Pagoda Fm	Pole Research Repository
19						Queen Alexandra Range		91	506	Pagoda Fm	Pole Research Repository
20	Rocky Creek	−31.263879	150.731203	Australia	NSW		Tamworth Belt	45	288	Rocky Creek Conglomerate	Unknown; Rocky Creek Syncline. MDA: 302 Ma
21	Currabubula	−30.032821	150.313231	Australia	NSW		Tamworth Belt	30	313	Currabubula Formation	Unknown; Werris Creek Syncline. MDA: 317 Ma

(*continued on next page*)

Table 1 (*continued*)

Sample	*Locality*	*Latitude*	*Longitude*	*Country*	*State/province*	*Region*	*Geological province*	*Zircons (n=)*	*Youngest Zircon Age*	*Stratigraphic unit*	*Position within unit*/Comment*
22	Warroora 1	−23.509678	113.881853	Australia	WA	Carnarvon Shire	S. Carnarvon Basin	23, 13, 85	562	Lyons Group	core 4: 412.4–416.05 m (Gascoyne Platform)
									1125		core 10: 830.3–831.8 m
									503		core 17: 1374.65–1375.9 m
23	Drossera 1	−19.678043	125.040742	Australia	WA	East Pilbara	Canning Basin	61	327	'lower' Grant Group	192.9 m (Crossland Platform; Martin et al., 2008)
	Capparis 1	−19.450542	125.102405			West Kimberley		62	363		106.9 m (Barbwire Terrace)
	Cycas 1	−19.008217	126.016122			West Kimberley		61	295		999.6 m (Fitzroy Trough)
								n = 2506			
N. Hemisphere (Carboniferous) Tillites											
24	Himalaya Mountains			Tibet	Lhasa Terrane			216	507		Gehrels et al. (2011)
25	Himalaya Mountains			Tibet	N. Qiangtang Terrane			198	523		Gehrels et al. (2011)
								n = 414			
								n = 2920			

* or depth within exploration well
MDA: Maximum depositional age.

(2015) from the Congo Basin subsurface and the Australian Canning Basin (Martin, 2008; Fig. 1). Sample sites can be referenced to local stratigraphy (Fig. 3) and sample details are presented in Table 1. Field photos can be found in Figs. 4–6 and Appendix 3a-h (for most sample groupings), heavy mineral populations are tabulated in Table 2, and detrital zircon relative probability plots in Figs. 7–12 (full data sets are found in Appendix 1, and the K-S statistical analyses in Appendix 2). Each sample site sub-heading also includes the figure number with the appropriate detrital zircon relative probability plot. Several of our samples had relatively small numbers of zircons analyzed. This was because of the small sample size and paucity of zircons in the heavy mineral suites. We decided to use all data sets in our analysis so that we our geographic coverage is as comprehensive as possible. We caution that the low number of zircons analyzed in some samples may impact our interpretations (see Vermeesch, 2004).

4.1. Paganzo Basin, northern Argentina, South America (Site 1, 5 samples; Fig. 7)

Five samples from the Paganzo Basin (middle-Carboniferous glaciation) were collected across the extent of the basin (Table 1; Appendix 3a). These units were deposited during to the glacial stage from that occurred from Visean to the early Bashkirian (i.e. equivalent to the European stages of Visean and Namurian) of the Protoprecordilleran region of the Paganzo Basin in Argentina (Azcuy, 1975; Net and Limarino, 1999; Heckel and Clayton, 2006; Net and Limarino, 2006; Limarino et al., 2014b). In the eastern Paganzo Basin, the samples are from a paleovalley complex, while the western Paganzo Basin samples are from the Protoprecordilleran mountain belt that bounded the basin to the west and existed along the Panthalassic margin of Gondwana. The Paganzo Group strata are correlated using zircon ages, facies, palynomorphs, as well as paleoflora occurrences (Gulbranson et al., 2010; Pérez Loinaze and Césari, 2012; Limarino et al., 2014b). The glacial deposits of the Guandacol and Agua Colorado Formations in the western Paganzo Basin are younger 335 Ma (Serpukhovian), and are correlated to the non-glacial deposits of the Malanzán Formation in the eastern portion of the basin (Pankhurst et al., 1998; Drobe et al., 2011; Gulbranson et al., 2010; Pérez Loinaze and Césari, 2012; Limarino et al., 2014b; Moxness et al., 2018). The middle units, the Loma Larga Formation in the east and Tupe Formation in the west, rest conformably on their older units, and therefore have been determined to have a Bashkirian-middle Moscovian age (323–310 Ma; Limarino et al., 2014b).

The Malanzán Formation samples were collected from the southwestern portion of a paleovalley that cuts through the Sierra de Malanzán, a small northern extension of the Sierra de Chepes, close to the town of Malanzán (30°48′40.4″, W 066°34′24.1″). The Malanzán Formation rests unconformably on metamorphosed sedimentary and igneous rocks of the Olta and Chepes formations of Ordovician ages (Pankhurst et al., 1998). The basal facies in this area of the paleovalley consists of siltstones with rare pebbles and medium-grained sandstones, which are poorly sorted, and dominated by quartz with a weak calcite cement (Qtz 61% F 35% L 4%). Conglomerates, which are interpreted as fan deltaic and debris flow deposits, dominate the upper Malanzán Formation (Moxness et al., 2018). Heavy minerals include garnet, barite, zircon, rutile, apatite, monazite, ilmenite and hematite (Table 2). Grain shape varies from well-rounded to angular in every grain size fraction and the matrix is < 15% (Net and Limarino, 2006). Twenty four concordant U-Pb zircon ages were acquired with an age peak of ~500 Ma. The youngest zircon is 362 Ma; the oldest is 973 Ma (Appendix 1). The Loma Larga Formation samples were taken from just 1 km west of the village of Loma Larga (S 30°47′45.1" W 066°32′37.1″). The Loma Larga Formation contains conglomerates and sandstones interbedded with siltstone and organic-rich layers (Qt 59% F 33% L 8%; Net and Limarino, 2006). The heavy mineral suite includes abundant of hematite and ilmenite, with lesser zircon, monazite, and barite

Table 2
Heavy Minerals, Gondwana Diamictites (SEM-WDS).

Continent/Site	Glacial Episode	Location	Sample	Garnet	Garnet	Garnet	Garnet	Sphene	Apatite	Rutile
				Spessartine	Pyrope	Almandine	Andradite			
1-S. America	II	Huaco-A(Arg.)	301	35	0	0	1	0	0	2
1-S. America	II	Unquillal (Arg.)	175	2	0	0	0	0	0	0
1-S. America	II	Famatina (Arg.)	259	6	0	5	1	0	0	5
1-S. America	II	Malazan (Arg.)	203	49	0	3	1	0	0	3
1-S. America	II	Huaco-B (Arg.)	318	33	0	0	0	0	1	2
4-S. America	III	Ventana Mtns.	GHR-3*	0	1	0	0	5	15	25
5-Africa	III	W. Cape Mtns.	Dwyka2*	0	23	1	5	0	6	0
6-Africa	III	Central Cape	Dwyka3	7	12	5	1	0	13	7
7-Africa	III	E. Cape Mtns.	Dwyka4	14	21	3	5	9	11	3
8-Africa	III	KwaZulu Natal	KZN (Dwyka)	3	40	0	0	0	0	0
10-Arabia	III	S. Oman	Al Khlata Fm-1	1	0	9	0	0	2	2
10-Arabia	III	S. Oman	Al Khlata Fm-2	13	0	36	0	0	3	1
10-Arabia	III	S. Oman	Al Khlata Fm-3	21	0	28	0	1	4	0
11-Africa	III	Ranohira (Mad.)	Sakamena	8	0	2	4	0	5	14
12-India	III	Dhanbad	Talchir	22	0	4	6	0	4	7
13-S. America	III	Falkland Is.	Falk-06-01*	0	52	3	0	10	0	22
14-Antarctica	III	Sent. Range	OM-79–7*	0	46	4	0	21	5	0
14-Antarctica	III	Meyers Hills	OM-79-219*	0	52	0	0	15	9	0
15-Antarctica	III	Heimefront R.	KS31	0	0	0	0	0	0	65
16-Antarctica	III	Pensacola Mtns.	PRR 16746	65	0	0	0	0	0	4
17-Antarctica	III	Ohio Range	PRR 1749	2	0	0	0	0	0	16
18-Antarctica	III	Queen Alex. R.	PRR 2732	85	0	0	0	0	1	0
19-Antarctica	III	Queen Eliz. R.	PRR 2921	89	0	0	0	0	0	1
20-E. Australia	III	Rocky Creek	Rocky Creek	6	0	14	7	0	12	9
21-E. Australia	III	Currabubula	Currabubula	3	0	7	12	0	9	4
22-W. Australia	III	Carnarvon Basin	AUS-4	70	0	4	0	0	0	3
22-W. Australia	III	Carnarvon Basin	AUS-5	44	0	0	0	0	0	3
22-W. Australia	III	Carnarvon Basin	AUS-10	8	0	0	0	0	0	0
22-W. Australia	III	Carnarvon Basin	AUS-17	6	0	2	0	0	0	33

Continent/Site	Ilmenite	Zircon	Monazite	Hematite	Barite	Galena	Pyrite	Chalcopyrite	Chromite	Total
1-S. America	1	0	4	0	6	0	0	0	0	49
1-S. America	15	5	2	69	1	0	0	0	0	94
1-S. America	2	29	20	7	7	0	1	0	0	83
1-S. America	5	8	4	2	22	0	0	0	0	97
1-S. America	0	0	3	0	4	0	0	0	0	43
4-S. America	0	0	0	0	0	0	0	0	0	46
5-Africa	0	11	0	0	0	0	0	0	0	46
6-Africa	0	5	0	0	0	0	0	3	0	53
7-Africa	0	8	0	0	0	0	5	8	0	87
8-Africa	0	0	0	0	0	0	1	8	0	52
10-Arabia	0	44	0	1	0	0	15	8	0	82
10-Arabia	0	33	0	2	0	0	28	8	0	124
10-Arabia	0	34	0	2	0	1	35	8	0	134
11-Africa	0	5	1	1	0	0	9	14	0	63
12-India	0	8	0	3	0	0	0	8	0	62
13-S. America	0	0	0	0	0	0	0	0	0	87
14-Antarctica	0	0	0	0	0	0	0	0	0	76
14-Antarctica	0	0	0	0	0	0	0	0	0	76

(*continued on next page*)

Table 2 (*continued*)

Continent/Site	Ilmenite	Zircon	Monazite	Hematite	Barite	Galena	Pyrite	Chalcopyrite	Chromite	Total
15-Antarctica	0	25	1	0	0	0	7	0	0	98
16-Antarctica	4	20	1	2	1	0	0	0	0	97
17-Antarctica	4	23	0	4	1	0	30	2	5	87
18-Antarctica	0	0	1	7	0	0	0	0	0	94
19-Antarctica	1	0	1	0	0	0	0	0	0	92
20-E. Australia	0	7	0	3	0	1	6	1	0	66
21-E. Australia	0	11	0	4	0	0	12	0	0	62
22-W. Australia	4	4	0	0	0	0	10	0	0	95
22-W. Australia	3	0	0	0	0	0	1	0	0	51
22-W. Australia	0	0	0	0	1	2	11	0	0	22
22-W. Australia	3	24	5	0	1	0	17	1	7	99
										n = 2217

Heavy mineral separates for the Canning Basin samples (Site 23; CYC, CAP and DRO) can be found in Martin (2008).
[*] Heavy mineral analysis done on thin sections; Samples from the Lesser Himalaya, Tethys, Lhasa, S & N. Qiangtang were field separated and no heavy mineral splits remain.

(Table 2). The facies are interpreted as meandering fluvial and flood plain deposits, and are interpreted as the terminal mid-Carboniferous glacial stage (Bashkirian to the earliest Cisuralian 323 Ma to c. 290 Ma; Shen et al., 2013). We acquired 50 concordant U-Pb zircon ages with a peak age of ~500 Ma; the youngest zircon is 412 Ma, the oldest 2133 Ma.

Samples from the Agua Colorada Formation were collected in the Famatina Range (listed as Famatina in Fig. 7 and portrayed stratigraphically in Appendix 3), and are from the northernmost outcrop in this study and are located in the northern Paganzo Basin (S 28°51′46.4" W 67°36′01.0″). The rocks are conglomeratic sandstones with some larger clasts (8–30 cm) of igneous rocks in a mainly feldspathic sandy matrix. The grains are poorly sorted and angular, indicating a short transport history. The heavy mineral composition shows a dominance of zircon and monazite, with lesser garnet, barite, rutile and hematite (Table 2). These are interpreted terrestrial sediments related to a glacially-influenced environment, and a glacio-lacustrine environment post-glacial succession (Limarino and Gutierrez, 1990; Limarino et al., 2002). The correlation and paleontological evidence point to a Serpukhovian age (Limarino et al., 2002). In the sample area, the rocks were unconformably deposited on Lower Paleozoic igneous rocks (extension of the Ñuñorco Granite; 484 Ma, Pankhurst et al., 1998) and Cambrian metasedimentary successions (Negro Peinado Formation; Limarino and Gutierrez, 1990; Collo et al., 2009) of the Famatina Range and border a granite of unknown age. One age peak of ~500 Ma, is apparent from 95 concordant U-Pb zircon ages. The youngest zircon age is 389 Ma, the oldest 2116 Ma.

The samples for the Guandacol Formation were collected west of Huaco, a town in the Precordillera Ranges (Net, 2002; S 30°08′40.6" W 068°32′33.3). Here, the formation is overturned and rests unconformably on the Ordovician San Juan Formation. Here we sampled the sandy matrix of a diamictite. The rocks are greyish to bluish and poorly sorted with a wide range of grain shapes from well-rounded to angular. Net (2002) reports an average sandstone composition of Q 62.9 F 27.4 L 9.7, with matrix proportions exceeding 15% of the rock volume. The heavy mineral suite is dominated by garnet, barite and rutile (Table 2). Thes rocks are interpreted to be of glacial and deltaic origin (Net et al., 2002). The age of the rocks is well constrained by isotopic dating, and range in age from 320 Ma for the glacial deposits and 315 Ma for the fluvial successions and are Bashkirian in age (Gulbranson et al., 2010; Limarino et al., 2014b). The Guandacol-Huaco sample has a peak age of ~500 Ma ($n = 50$) with smaller peaks at 1000, 1500 and 2000 Ma. The youngest zircon age is 385 Ma, the oldest 2059 Ma. The Tupe Formation (S 30°03′35.1" W 068°32′25.9″) consists of medium-grained sandstone units that are interbedded with siltstone and organic-rich units. Net et al. (2002) reports an average composition of Q 62.5 F 23.2 L 14.3, with a larger amount of lithoclasts in comparison to the Guandacol Formation. The Tupe Formation represents a stacked fluvial and coal-bearing facies succession, and is interpreted as part of the terminal glacial phase that is comparable to the Loma Larga Formation (Gulbranson et al., 2010; Césari et al., 2011; Limarino et al., 2014a). Only 19 zircons were obtained from this sample, and an age peak of ~500 Ma is observed. The youngest zircon is 404 Ma, the oldest 2761 Ma.

4.2. *Paraná Basin, Brazil, South America (Sites 2 and 3; Fig. 7)*

As in other glaciated basins, the primary data on the provenance of the glacial strata in the Paraná Basin derive from the sense of flow of glaciers interpreted from the orientation of subglacial micro-, macro- and mega-erosional features, such as striae and furrows, roches moutonnés and whale backs, as well as depositional featurures like drumlins, eskers, and moraines (Santos et al., 1996; Rocha-Campos et al., 2008). This is corroborated by sandstone paleocurrent directions associated with diamictites and sedimentary petrology, fabrics of local basement clasts dispersed in diamictite and correlation with similar

Fig. 4. Gondwana glacial diamictites from Rocky Creek, Australia (A; outcrop with is 1 m) and the Heritage Range of the Ellsworth Mountains, Antarctica (B). Dick Ojakangas is standing on the boulder pavement in the Whiteout Conglomerate in the Meyers Hills. The white arrow indicates the ice flow direction, north toward the Sentinel Range. Inset C shows the striations on the boulder pavement.

basement rocks exposed along the eastern and western outcrop belts in the Paraná Basin which includes the < 1400 m of Itarare Formation (Maack, 1961; Bigarella et al., 1967; Rocha-Campos, 1967; Frakes and de Figueiredo Filho, 1967; Frakes and Crowell, 1969). Recent ash bed geochronology by Cagliari et al. (2014) provides an age of 307 Ma for the Itarare Formation.

The Itarare Formation is present in the Paraná Basin and in its northern equivalent, the San Franciscana Basin (Fig. 1; Appendix 1, 3a), as part of the depositional system that covered ~1 million km^2 of South America between 318 and 300 Ma. Only detrital zircons were retained from the heavy mineral splits (no entry in Table 2), and the southern Itarare (Paraná Basin) sample yielded 38 concordant zircon ages. Four small peaks between 440 and 800 Ma are observed; the youngest zircon ages is 323 Ma and the oldest is 2606 Ma. The San Franciscana Basin Itarare sample yielded 88 zircons with small age peaks at 600, 1800 and 2000 Ma. The youngest zircon is 365 Ma, the oldest 2743 Ma. All these detrital zircon ages are known from the basement in the vicinity of the Paraná Basin (e.g., Mantovani and Brito Neves (2005).

4.3. Sierra de la Ventana Mountains, Argentina, South America (Site 4; Fig. 7)

The Ventana Mountains (10 × 40 km), in central Argentina, west of Buenos Aires, were visited by Darwin (1846) and Du Toit (1937) and they both recognized the similarity of the stratigraphy and structure with the Cape Mountains in southern Africa (we regard this as as the equivalent of the Karoo Basin in Fig. 7). The Sauce Grande diamictite in the Ventana Mountains was thoroughly described by Coates (1969), relative to Gondwana stratigraphy, following earlier work by Keidel (1922, 1940), Du Toit (1929, 1937), Fossa-Mancini (1943) and Harrington (1947). The Sauce Grande Formation is a diamictite that unconformably overlies the Devonian Lolen Formation and grades upward into the Permian marine Piedra Azul Formation allowing a Carboniferous-Permian age designation. The diamictite is ~800 m thick and contains abundant glacially faceted and striated clasts, and correlates with the Dwyka diamictite in South Africa (Buggisch, 1987; Appendix 3b). The Gondwanide orogen deformed the Ventana region, resulting in NE-vergent folds with an axial planar cleavage and a

Fig. 5. Al Khlata Formation in Oman with a granite dropstone in diamictite (A) that includes a heavy mineral population dominated by garnet (grey and rounded in inset) and pyrite (bright in inset; image width is 1000 μm) and glacial striations on the Edicaran Khufal Limstone from the type locale at Wadi Al Khlata, southern Hugf (B). GPS unit for scale in A and B.

greenschist metamorphic overprint (Von Gosen et al., 1990, 1991), and a typical thin-skinned strain pattern (Craddock et al., 1998).

One Sauce Grande thin section was analyzed for heavy minerals (n = 46) and it is populated by rutile, apatite, sphene and garnet (Table 2). We analyzed 92 detrital zircons from the Sauce Grande and added samples SLV-VE-14 and 15 from Ramos et al. (2014), making a total of 194 concordant zircons included in our analysis. The youngest grains having a U-Pb age of 386 Ma and the oldest is 3330 Ma (Table 1, Appendix 1). The age peak is ~500–600 Ma with a lesser peak at ~1100 Ma.

4.4. Southern Africa (Sites 5–8; Fig. 8)

Glaciogenic rocks of the Dwyka Group form the base of the Karoo Supergroup in the main Karoo Basin of South Africa and associated smaller sub-basins of southern Africa (e.g. Catuneanu et al., 2005). In the central to northern part of KwaZulu-Natal (KZN) Province, the Early Permian Dwyka Group is sub-divided into the northern Mbizane Formation (heterolithic valley- fill facies in a dissected highland region) and the southern Elandsvlei Formation (platform homogeneous diamictite facies; Visser, 1987, 1990; Von Brunn, 1996). In the north the regressive glacial deposits of the Mbizane Formation overlie the homogeneous Elandsvlei Formation diamictite that extends across the Main Karoo Basin to the south and west. Near the Umlaas Road sampling site the Dwyka Group is about 120 m thick and the Elandsvlei Formation has a basal heterolithic unit (Kayeni Member), comprising interbedded laminated shale, sandstone, conglomerate and sandy diamictite (Botha and Botha, 2002). The coarse diamictite in the Durban-Pietermaritzburg area is interpreted as the result of ice grounding on highs in the irregular basement topography during the rapid retreat of the ice sheet (Von Brunn, 1996; Haldorsen et al., 2001). This succession represents rapid ice-withdrawal at the close of the late Paleozoic

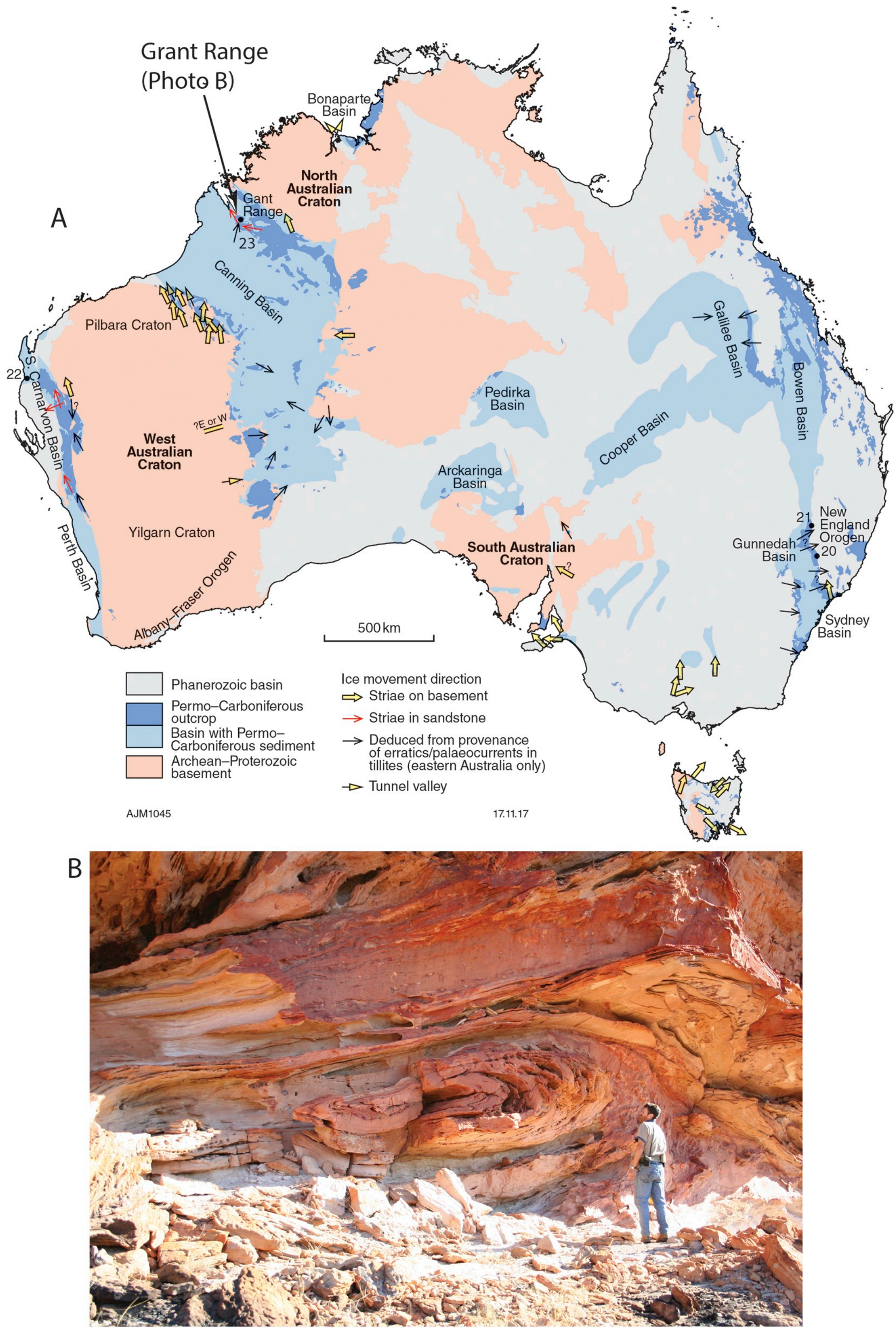

Fig. 6. Ice flow directions for the LPIA in Australia (A; Osborne and Browne, 1921; Brakel and Totterdell, 1990; Bourman and Alley, 1999; Mory et al., 2008; Haines et al., 2011 and Preiss and Preiss, 2015) with Sites 20–23 located (see Table 1). (B) Ice flow deformation in the Grant Group, Grant Range, Canning Basin. (For interpretation of the references to colour in this figure legend, the reader is referred to the web version of this article.)

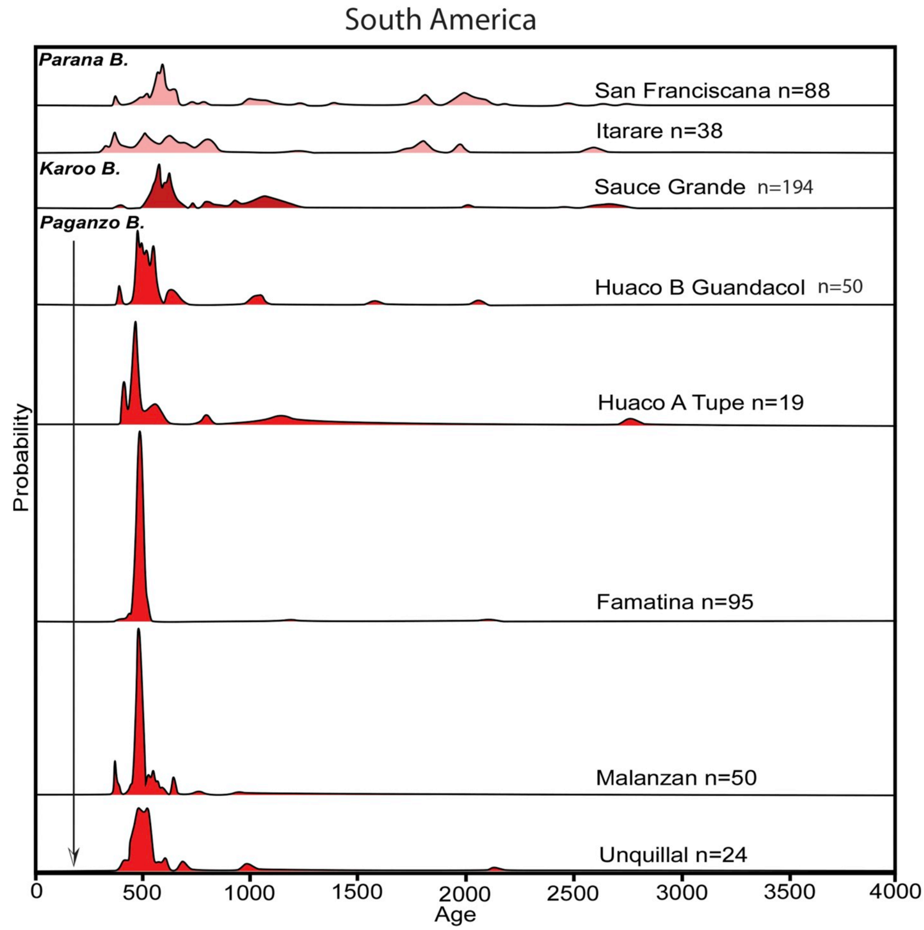

Fig. 7. Relative probability plots for South American samples (Sites 1–4; see Table 1 and Appendix 1).

glaciation (Thomas et al., 1990) with the main body of sediment accumulating as massive glaciomarine muds with dropstones in an ice-free open marine basin (Haldorsen et al., 2001) where icebergs were generated from marine glacial fronts located to the northeast.

The Dwyka Group is diachronous (younger in the north where continental glaciation lasted longer than in the south), due to deglaciation during warming in the early Permian (Catuneanu et al., 1998). Ice movement directions can be determined from glacially polished and striated surfaces of the underlying rocks (Haldorsen et al., 2001). The northern pre-Dwyka upland of the Karoo Basin directed ice movement from the northwest across the Kaapvaal Craton to the Tugela region of KZN where irregular paleorelief developed on the older basement rocks (von Brunn, 1996). The present distribution of the Dwyka Group is controlled by Cretaceous faults related to Gondwana breakup. Reconstructions of Gondwana show that the Falkland Islands lie on a rotated microplate that originally lay off the Eastern Cape- KZN provinces of South Africa (Marshall, 1994), showing that the Permo-Carboniferous diamictites of the two areas were once contiguous.

In the Western Cape Province, South Africa, thin tuff layers within the Dwyka Group have been dated at 302 Ma (U-Pb zircon with SHRIMP), close to the Permian-Carboniferous boundary (Bangert et al., 1999; recalculated in Isbell et al., 2008a, 2008b; Stollhofen et al., 2008). In our study, U-Pb ages from detrital zircons, extracted from four samples of the Dwyka diamictite (all Elandsvlei Formation) were collected from the western Cape (near Laingsberg), the southern Cape (east of Oudtshoorn), the eastern Cape and central KZN (near Pietermaritzburg). Sample Sites 5–7 are within the Cape fold belt, sample 8 is from the Karoo Basin foreland (Fig. 1). All the samples are from the matrix of massive diamictite (photo in Appendix 3b). Published models of ice sheet flow directions in South Africa, show ice movements generally from NE to SW across the area (Isbell et al., 2008a, 2008b). There is evidence of possible glacial sediments of Visean age in the Witteberg Group of South Africa that underlie the Dwyka Group (Streel and Theron, 1999; see review in Isbell et al., 2008a, 2008b). These diamictites and sparse lonestones in mudstone may be equivalent to the Bluff Cove Formation in the inverted Falkland Islands and the glacial Episode II Paganzo Basin units in Argentina; we did not sample this unit.

The eastern Cape Dwyka detrital zircon age spectrum (n = 85) ranges from 499 to 3491 Ma (Site 7 on Fig. 1; Dwyka East on Fig. 8). Peak ages are 508, 628, 1086, 2074, 2972, and 3108 Ma. The central Cape Dwyka (n = 92) detrital zircon age spectrum ranges from 507 to 1667 Ma (Site 6 on Fig. 1; Dwyka Central on Fig. 8). Peak ages are 540, 589, and 1050 Ma. The western Cape Dwyka detrital zircon age spectrum (n = 93) ranges from 499 to 2817 Ma (Site 5 on Fig. 1; Dwyka Wast on Fig. 8). Peak ages are 571 and 1093 Ma. The KZN Dwyka detrital zircon age spectrum (n = 90) ranges from 499 to 2817 Ma (Site 8 on Fig. 1; Dwyka East on Fig. 8). Peak ages are 511, and 2649 Ma.

4.5. *Central Africa (Congo Basin; Site 9; Fig. 8)*

Linol et al. (2015) report detrital zircon results (n = 157) from core samples D1400 and D1595 from the Carboniferous-Permian Lukuga Group diamictites of the Dekese section from the Congo Basin. Concordant ages from 157 zircons reveal three peaks at 1930 Ma, 1040 Ma and 680 Ma, with the oldest zircon age at 2925 ± 8 Ma (Fig. 8).

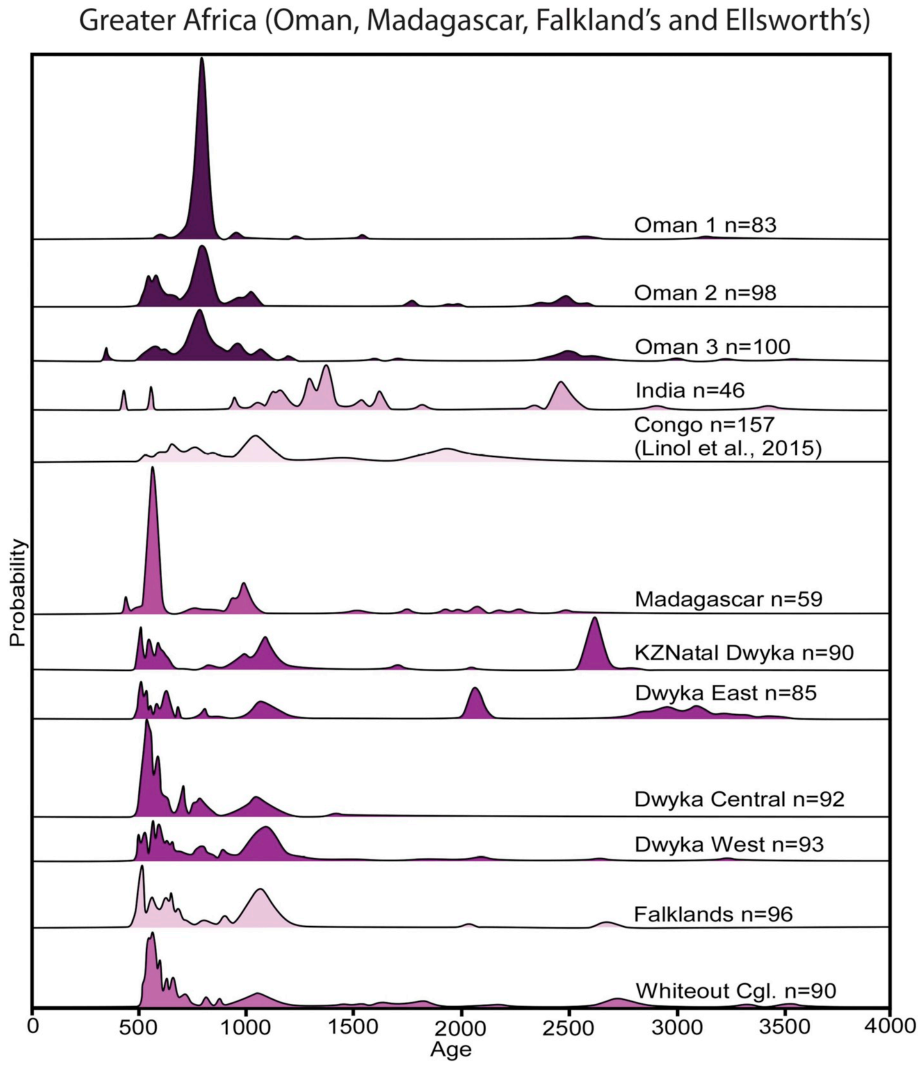

Fig. 8. Relative probability plots of detrital zircon samples from Greater Africa (Sites 5–14; see Table 1, Fig. 1 and Appendices 1 and 3).

4.6. Oman (Site 10; Fig. 8)

All Upper Carboniferous/Lower Permian diamictites in Oman are included in the Al Khlata Formation (Martin et al., 2008, 2012; Forbes et al., 2010). This formation is exposed along the western margin of the Huqf Hills in southern Oman (Fig. 5) and in a tectonic window in the Oman Mountains south of Muscat, however, drilling for hydrocarbon reservoirs has revealed a widespread occurrence of this formation in central and southern Oman (Appendix 3c and d)

Levell et al. (1988) subdivided the Al Khlata Formation in four subunits that have been named from top to bottom, Rahab Shale, P1, P5 and P9. In the Huqf Hills only the upper subunits P1 and P5 are exposed, but since the outcrops are lying in a game sanctuary, sampling is forbidden. Outside the Huqf Hills the outcrops in Wadi Daiqa have been recently flooded after the construction of a dam, therefore Petroleum Development Oman provided us some drillcores for analytical purposes. The three analyzed samples come from (undisclosed) wells southwest of the Huqf Hills and they represent the diamictites from the base of P1, P5 and P9 subunits. The ages of the units are based on sample palynology: P1 diamictites, Sakmarian (palynomorph zone 2141; ~293 Ma); P5 diamictites, late Kasimovian (palynomorph zone 2165; ~305 Ma); P9 diamictites, mid-Kasimovian (palynomorph zone 2159; ~304 Ma; Al-Hussein, 2015).

The Al Khlata diamictites are coarse-grained, poorly-sorted clastic rocks with a matrix-supported texture. Clasts range in size between 0.5 and 1 m. The clasts are highly variable in composition, mostly granites and other igneous rocks like gabbros, rhyolites, basalts, and quartzo-feldsphatic porphyrys. Finely bedded sandstones, homogeneous grey sandstones and black cherts are ubiquitous sedimentary clasts. Metamorphic clasts are absent. The matrix is a greenish to bluish grey sandstone to arkosic sandstone without micas. The heavy mineral separates are dominated by rounded almandine and spessartine garnet (Fig. 5), zircon and pyrite (Table 2).

Detrital zircons were recovered from each of the three core samples (Appendix 3c and d). Sample Oman-1 (P1) is from a separate core and produced 83 concordant U-Pb zircon ages with the youngest age 604 Ma and the oldest 3152 Ma. The peak age is 799 Ma. Samples Oman-2 (middle = P5) and Oman-3 (deep = P9) are from a different core: Oman-2 has 98 concordant ages that ranged from 511 to 2600 Ma. Age peaks are at 590 and 813 Ma. Oman-3 has 100 concordant ages that range from 347 to 3559 Ma. Age peaks are at 788 and 2518 Ma.

4.7. Madagascar (Site 11; Fig. 8)

The western third of Madagascar is covered by a succession of Phanerozoic sedimentary rocks. The lower part of the sedimentary

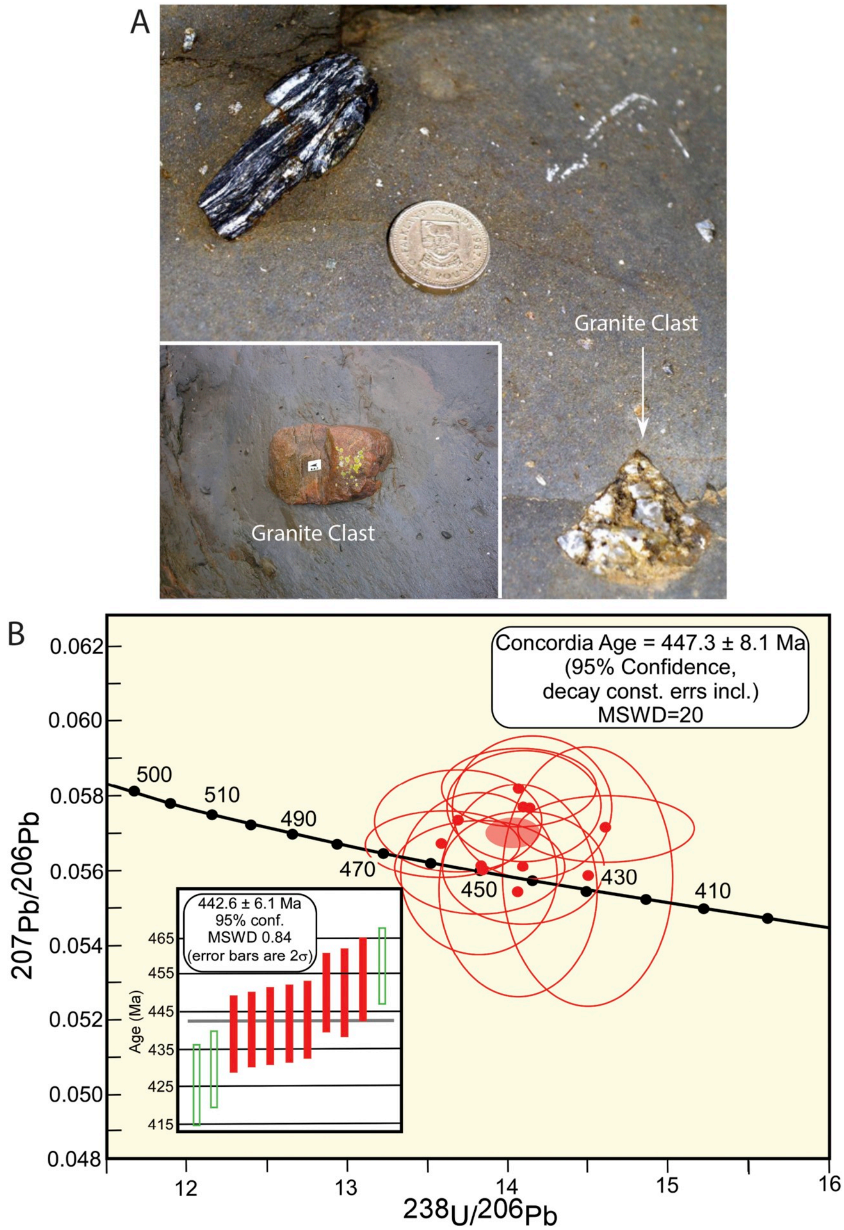

Fig. 9. Field photos of the Fitzroy Formation diamictite in the Falkland Islands (A) and a U-Pb concordia age plot of zircons from granite clasts (B).

cover, characterized by thick siliciclastic strata, ranging from the uppermost Carboniferous to the Early Jurassic, is an equivalent of the Karoo Supergroup in mainland Africa (Wescott and Diggens, 1998). This sequence has been deposited during a long-lasting phase of crustal extension between East Africa and what is now Madagascar, which predates the decay of Gondwana (Hankel, 1994; Schandelmeier et al., 2004).

The sampling site is located at the eastern margin of the Morondava Basin, about 15 km east of the town of Ranohira in the valley of the upper Ihazofotsy River (45°29.811′ E 22°30.510′ E). Here, the basal unconformity between the Precambrian and the overlying Sakamena is well exposed (Appendix 3c). The sedimentary succession begins with 1.5 to 2 m of a grey, poorly sorted, polymict conglomerate. Individual clasts are made up of amphibolite, milky quartzite, light grey orthoquartzite, and garnetiferous paragneisses, embedded in a fine- to medium-grained quartz matrix. This assemblage reflects the composition of the crystalline basement within the next 5 km east of the outcrop and is probably the reworked local debris of the underlying Precambrian. The conglomerate is overlain by a light yellow-grey, laminated mudstone of 2.5 m thickness, which contains a layer of iron oxide nodules with up to 10 cm diameter half a meter below its top. With a sharp erosional contact a second approximately 60 cm thick conglomerate is lying on top of the mudstones. The upper conglomerate contain additional to the components recorded in the basal conglomerate, also pink granites and dark granulites, which do not appear near the exposure and may represent an input from a larger provenance area. Clasts are subangular to well-rounded and the largest components are up to 8 cm in diameter (Appendix 3c). The sample was collected from this second conglomerate. The upper conglomerate is overlain by a light brown arkosic sandstone. Heavy mineral populations are dominated by rutile and chalcopyrite (Table 2). Detrital zircon (n = 59) age peaks are at 560 and 1000 Ma. The youngest zircon is 442 Ma and the oldest 2496 Ma (Fig. 8). The exposed basal sequence of the sedimentary cover represents a part of the approximately 2500 m thick lower Sakamena Formation, which was dated with pollen and spores (260 Ma; Wescott and Diggens, 1998).

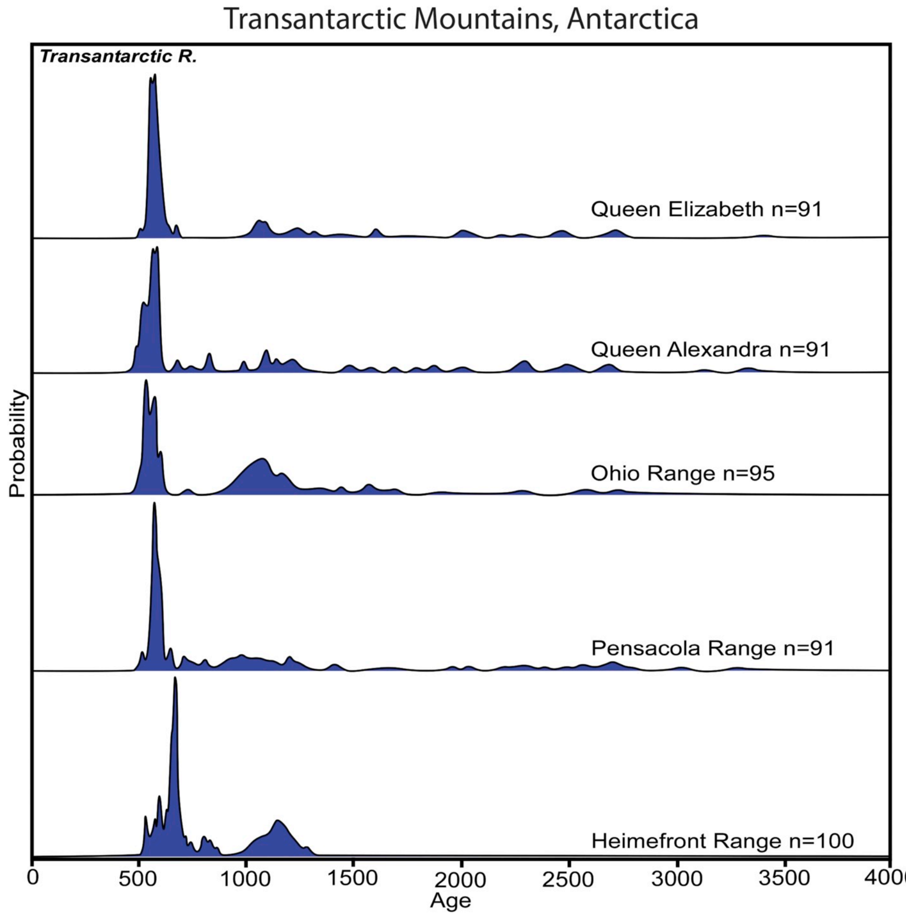

Fig. 10. Relative probability plots for detrital zircon samples in the Transantarctic Mountains, Antarctica (see Table 1, Fig. 1 and Appendices 1 and 3).

4.8. India (Site 12; Fig. 8)

The Gondwanan diamictites of India are known as the Talchir Boulder Beds (Talchir Formation) and are Late Carboniferous to Early Permian in age. The Talchir series of diamictite, shale and sandstone may be as thick as 250 m at other places in India, and generally overlies Archean rocks; paleocurrent indicators show a south to north movement of the glaciers (Ahmad, 1981). The diamictite sample and photos herein (diamictite and lonestones in shale) are from small, weathered exposures in the Damodar Valley region of east-central India (Appendix 3c). They are within the city limits of Dhanbad, about 10 km south of the campus of the Indian School of Mines. The Talchir is stratigraphically beneath the Permian Barakar coal-bearing formation that is being actively mined. Sandstone and shale overlie the diamictite–these are in separate but nearby outcrops, each about 1 m thick. A thin section of the diamictite matrix shows it to be a poorly sorted mixture of sand (quartz, feldspars and schistose rock fragments), silt, and clay, with minor larger clasts of granite, schist, and till pellets.

Heavy minerals include a variety of non-pyrope garnets (60%), rutile, apatite and pyrite. Detrital zircons ($n = 46$) are dominantly 900–1300 Ma with a small age peak at 2600 Ma. The youngest zircon age is 431 Ma, and the oldest 3436 Ma (Fig. 8).

4.9. Falkland Islands (Site 13; Figs. 8 and 9)

In the Falkland Islands, glacial diamictites of the Lafonian Diamictite (Frakes and Crowell, 1967) or Fitzroy Diamictite Formation of the Lafonia Group (Aldiss and Edwards, 1999) outcrop on both of the main islands. The diamictite is massively bedded, and almost completely lacking internal stratification to indicate its structural attitude. Frakes and Crowell (1967) report a range in thickness for this unit of 350 to 850 m, and they identify a continental to proximal marine depositional setting. Based on the abundance and size of continent-derived clasts as well as linear sand bodies suggested to be subglacial eskers, Frakes and Crowell (1967) and Trewin et al. (2002) surmise a west-to-east (modern coordinates) transport direction for the glacial sediments, effectively toward the SE margin of Africa when the Falklands (Malvinas Islands) are restored to their pre-Jurassic position within the Gondwana supercontinent (Adie, 1952; Mitchell et al., 1986; see also a tectonic review by Ramos et al., 2017). The detrital zircon ($n = 96$) age spectrum includes age peaks at 521 and 1085 Ma. The youngest grain in 480 and the oldest is 2707 Ma (Table 1, Fig. 9). Pyrope garnets (60%) dominate the heavy mineral population (Table 2).

As noted, the Fitzroy Diamictite contains abundant sub-rounded to sub-angulose, dropstone clasts up to 7 m (Fig. 9a). These clasts are of a diverse origin. A population of 100 clasts from Port Purvis, West Falkland Islands (coordinates 51°27′37.24”S, 59°30′03.57”W) has shown the following distribution: quartzite 43%, sandstone 24%, granite 22%, foliated granite and gneiss 3%, schist 3%, quartz (from veins) 2%, felsic volcanic (rhyolite?) 1%, mylonite 1%, carbonate rock 1%. Within this population, 2 clasts of granite are faceted and striated. Eight clasts of granite lithology were obtained from the north shore of Byron Sound, West Falkland Islands (coordinates 51°27′10.83”S, 60°02′47.22”W) for zircon SHRIMP geochronology to help establish the provenance of the Fitzroy Diamictite. Zircons from three individual clasts were analyzed, yielding a Concordia age of 447.3 +/− 8.1 Ma with errors at the 1 sigma level (Fig. 9; Table 3). Minor amounts of discordance are observed from these two samples, as well as the

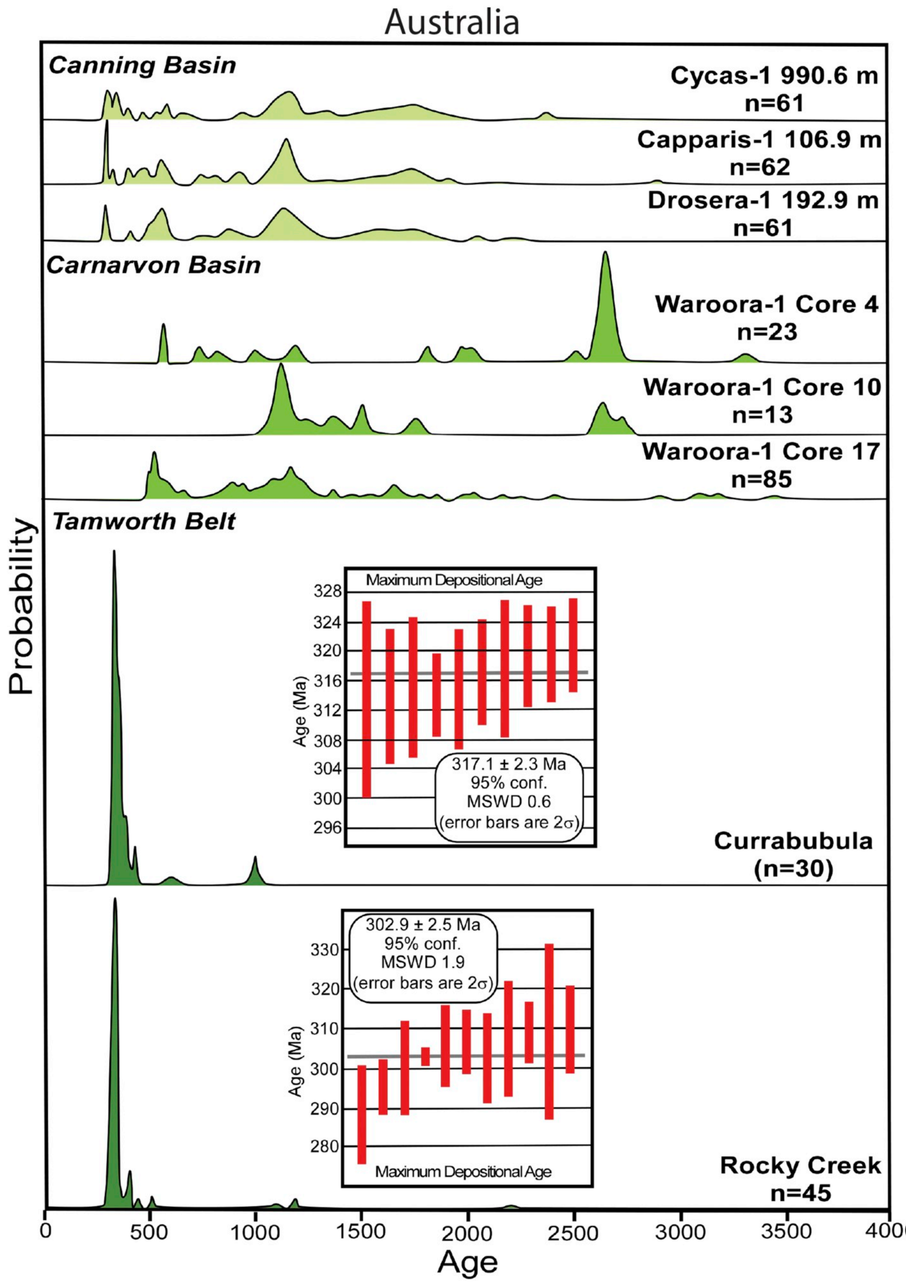

Fig. 11. Relative probability plots for detrital zircon samples from Australia (Sites 20–22; see Table 1, Fig. 1 and Appendices 1 and 3). Canning Basin data from Martin (2008).

presence of individual inherited grains of Neoproterozoic (ca. 630 Ma). Zircons from the third sample presented a larger proportion of discordant analyses, with a mean-weighted U/Pb age of 435 ± 14 Ma calculated from two concordant analyses of individual zircon grains.

4.10. Ellsworth Mountains, Antarctica (Site 14; Fig. 8)

The Ellsworth Mountains are part of the Ellsworth-Whitmore terrane in central Antarctica and contain a Cambrian-Permian stratigraphic section, deformed in the Gondwanide orogeny, that overlies Grenville-aged basement rocks (Millar and Pankhurst, 1987; Craddock et al., 2017a, 2017b, 2017c). The stratigraphic section is ~13,000 m thick with more than half of the thickness being Cambrian sediments (Webers et al., 1992; Sporli and Craddock, 1992). The Gondwana section is well preserved: the Crashsite Quartzite (Cambrian?-Devonian; 1000 m thick), the Whiteout Conglomerate (Carboniferous-Permian; 1000 m thick) and the Polarstar Formation (Permian; 1000 m thick). The Whiteout Conglomerate is thought to be equivalent to the late Paleozoic diamictites in the Transantarctic Mountains (see below), an observation aided when the Ellsworth-Whitmore terrane is rotated 90° clockwise to its tectonic position adjacent to the Pensacola Mountains during the Paleozoic (Watts and Bramall, 1981; Grunow et al., 1987). Exposures of the Whiteout Conglomerate in the Ellsworth Mountains include the massive, folded diamictite in the northern Sentinel Range and the thinly-bedded, interbedded diamictite-diamictite in the southern Meyers Hills of the Heritage Range (Matsch and Ojakangas, 1992). Exposures in the Meyers Hills include diamictite zones with boulder pavements (the grounding line) and abundant glacially striated

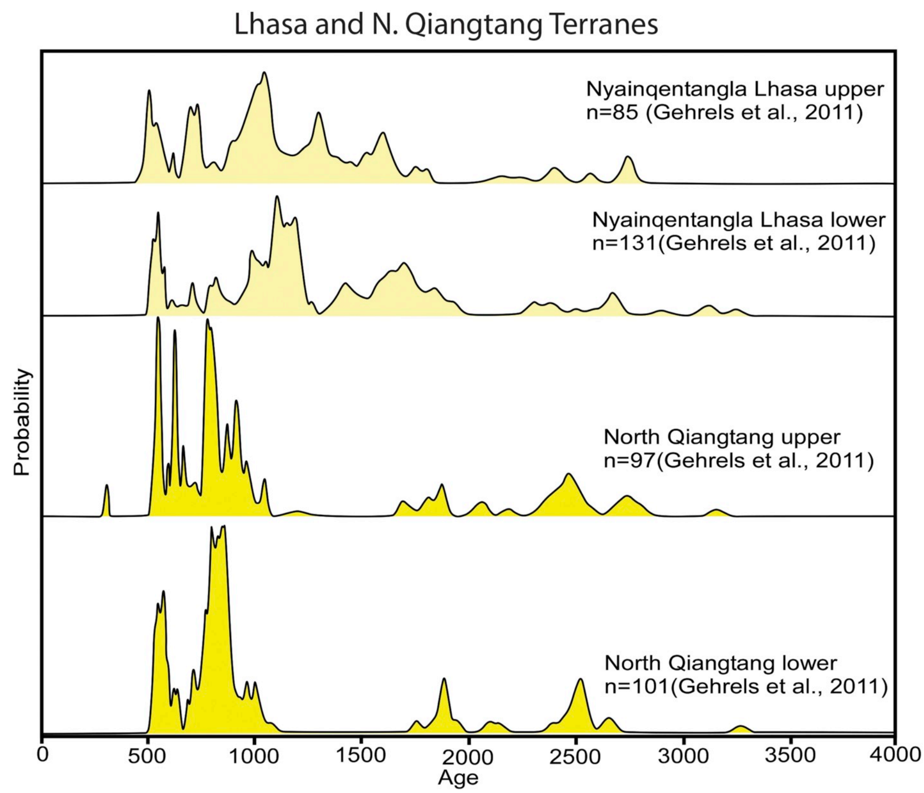

Fig. 12. Relative probability plots for detrital zircons from the Lhasa and North Qiangtang terranes (see Table 1, Fig. 1, Appendices 1 and 3 g; Samples 613,021, 05AL46, 05GT42 and 05GT56 from Gehrels et al., 2011).

clasts (Fig. 4; see also Appendix 3b) all indicating the ice flowed from the Meyers Hills (south) toward the open ocean (Sentinel Range to the north). Meyers Hills diamictites contain numerous 2–3 cm diameter pyrope garnets (SiO_2: 43.4%; Al_2O_3: 21%; FeO: 12.9%; MgO: 16.9%; CaO: 4.7%; MnO: 0.8%) in the basal layer.

Matsch and Ojakangas (1992) report that the Whiteout is populated by quartzite (66%) and granite clasts (17%) and petrographic analysis reveals a variety of feldspars and garnet. We analyzed thin sections from the northern Sentinel Range and Meyers Hills for their heavy mineral populations (SEM-WDS) and report the presence of much pyrope garnet (64%; Table 2). The detrital zircons ($n = 90$) from the Whiteout of the northern Sentinel Range range from 520 to 3569 Ma, with peak ages of 564 and 1065 Ma. The Whiteout Conglomerate contains the highest proportion of pyrope garnet.

4.11. Heimefront Range, Dronning Maud Land, Antarctica (Site 15; Fig. 10)

The Permo-Carboniferous diamictites of the Heimefront Range are part of the Amelang Plateau Formation (Wolmarans and Kent, 1982). On the basis of palynologic analyses, the age of the basal Amelang Plateau Formation has been narrowed down to the Early Permian, i.e. Asselian to Artinskian (Larsson et al., 1990; Lindström, 1995). The most complete section in the Heimefront Range is exposed on the northern flank of Mount Schivestolen where the diamictites form the 0.8 to 3 m thick basal part of the 160 m Permian cover, resting on a striated basement of metamorphic rocks (see Appendix 3e).

The diamictite has a dark grey, sandy matrix that contains individual silty lenses which define a poor bedding. Embedded in this matrix are granite and gneiss pebbles with diameters between 10 and 30 cm. The facies interpretation of the diamictites as glaciogenic deposits is based on provable contact with the glacially abraded and striated basement as well as striated and faceted clasts in the diamictites. A paleo-ice flow direction of 335° ± 10° was determined from the striated basement. The diamictite is overlain by 12 m of pale grey, well-stratified sandstones. Parallel small furrows, probably produced by floating icebergs sliding on the ground, were found within these strata. Poscher (1994) assumes glacial to periglacial conditions during the deposition in a fluviolacustrine environment, which is substantiated by dropstones and ice-dump tills. A decrease of dropstones and an increase of phytoclasts to the top of this unit suggest a change from a glacial to a periglacial paleoclimate. The heavy mineral suite is unremarkable, lacking a pyrope garnet population (Table 2). The detrital zircons ($n = 100$) include the youngest and oldest ages of 521 and 1282 Ma, which correlate with age peaks of 671 and 1142 Ma (Fig. 10).

4.12. Transantarctic Mountains, Antarctica (Sites 16–19; Fig. 10)

Tectonic reconstructions place the Ellsworth-Whitmore terrane (EWT; Dalziel and Elliot, 1982; Storey et al., 1988; Craddock et al., 2017a, 2017b, 2017c) in a position north of the Pensacola Mountains adjacent to the Falkland Islands as part of Gondwana. The Whiteout Conglomerate in the Ellsworth Mountains (above) is correlated with a variety of late Paleozoic glacial deposits that are present throughout the Transantarctic Mountains, and to the Dwyka-Sauce Grande formations in South Africa and South America. (Figs. 1, 3; Table 1). From north (Pensacola Mountains) to south to north (Darwin Glacier, South Victorialand) these units are: the Gale Mudstone (Pensacola Mountains, 600 m; Schmidt and Williams, 1969; Tessensohn et al., 1999), the Buckeye Diamictite (Ohio and Wisconsin Ranges, 300 m; Long, 1962), the Metschel Formation (Queen Maude Range, 50 m; Barrett, 1965), the Pagoda Formation (Queen Alexandra Range, 100 m; McDougall and Grindley, 1965) and the Darwin Diamictite (Darwin Glacier, South Victorialand; Haskell et al., 1965) all of which is summarized in Schmidt and Williams (1969), Isbell et al. (2003) and Isbell et al., 2008a, 2008b; Fig. 3; see also Appendix 3e). Koch and Isbell (2013)

Table 3
SHRIMP U-Pb Ages for Fitzroy Fm. Granite Clast Zircons, Falkland Islands.

Sample name, Spot no.	ppm U	ppm Th	ppm 206*	% comm 206Pb	232Th/238 U	Ln UO/U	Ln Pb/U	Obs 206Pb/238 U	± %	Corr 206Pb/238 U	± %	Age S-K comm Pb
f3–7	526	189	30.9	−0.04	0.37	1.934	−1.640	0.194	1.2	0.068	2.5	427
f3–10	532	284	32.4	0.05	0.55	1.958	−1.534	0.216	0.4	0.071	2.3	441
f3–11	225	112	14.1	−0.12	0.52	1.939	−1.560	0.210	1.2	0.073	2.5	454
f3–12	314	176	19.1	−0.07	0.58	1.906	−1.657	0.191	0.5	0.071	2.3	443
f3–13	141	74	8.83	0.45	0.54	1.922	−1.604	0.202	0.8	0.073	2.3	450
f3–14	642	366	37.3	0.00	0.59	1.967	−1.542	0.214	0.4	0.068	2.3	422
f3–15	518	194	32.7	−0.07	0.39	1.964	−1.504	0.222	0.5	0.073	2.3	458
f3–16	126	20	11.2	0.23	0.16	1.961	−1.160	0.314	1.4	0.104	2.6	634
f3–17	93	48	6.43	0.92	0.53	1.927	−1.499	0.225	1.0	0.080	2.4	492
f3–18	69	55	3.49	−1.48	0.83	1.723	−2.194	0.110	2.6	0.059	3.5	376
f8–1	237	217	14.6	0.75	0.94	1.902	−1.657	0.192	0.6	0.072	2.3	443
f8–2	252	170	15.7	0.19	0.70	1.963	−1.562	0.210	1.2	0.072	2.5	450
f8–3	571	292	32.7	0.09	0.53	1.981	−1.567	0.209	0.4	0.067	2.3	415
f8–4	572	616	25.7	1.56	1.11	2.021	−1.756	0.175	1.0	0.052	2.4	324
f8–5	168	128	10.3	0.17	0.79	1.962	−1.538	0.215	0.8	0.071	2.4	442
f8–6	604	512	34.4	0.43	0.88	1.967	−1.617	0.199	1.4	0.066	2.6	412
f9-3a	172	129	10.4	−0.17	0.78	1.949	−1.562	0.209	0.7	0.071	2.3	440
f9–6	670	651	35.1	0.21	1.00	1.784	−2.049	0.129	0.5	0.061	2.3	381
f9–7	957	917	34.9	1.91	0.99	2.034	−1.950	0.145	0.7	0.042	2.3	263
f9–8	234	162	14	0.65	0.71	1.957	−1.578	0.208	0.9	0.069	2.4	430

Sample name, Spot no.	(3) 206Pb/238 U Age		(1) 207Pb /206Pb Age		(1) 208Pb/232Th Age		% Dis-cor-dant	(1) 208Pbr/232Th	± %	7corr 206Pbr/238 U	err	(3) 206Pbr/238 U
f3–7	427.3	11.0	496	± 22	414	± 12	16	0.02	2.8	0.0683	0.0017	0.0685
f3–10	441.3	10.6	518	± 38	442	± 12	17	0.02	2.7	0.0707	0.0016	0.0709
f3–11	454.2	12.0	504	± 34	457	± 14	11	0.02	3.0	0.0729	0.0019	0.0730
f3–12	442.4	10.7	538	± 25	446	± 11	22	0.02	2.6	0.0709	0.0016	0.0710
f3–13	450.4	11.2	449	± 56	447	± 15	0	0.02	3.3	0.0723	0.0017	0.0724
f3–14	423.8	10.2	502	± 20	406	± 11	19	0.02	2.6	0.0675	0.0016	0.0679
f3–15	457.7	10.7	480	± 23	454	± 12	5	0.02	2.6	0.0735	0.0017	0.0736
f3–16	635.5	16.3	629	± 53	558	± 44	−1	0.03	7.9	0.1033	0.0028	0.1036
f3–17	493.4	12.7	424	± 88	477	± 20	−14	0.02	4.1	0.0795	0.0020	0.0795
f3–18	369.6	14.4	798	± 75	423	± 20	112	0.02	4.8	0.0592	0.0021	0.0590
f8–1	451.8	11.7	430	± 76	385	± 12	−3	0.02	3.1	0.0711	0.0017	0.0726
f8–2	459.7	12.3	455	± 32	364	± 13	1	0.02	3.4	0.0723	0.0019	0.0739
f8–3	419.1	9.9	499	± 25	363	± 9	20	0.02	2.6	0.0663	0.0015	0.0672

(continued on next page)

Table 3 (*continued*)

Sample name, Spot no.	(3) 206Pb/238 U Age		(1) 207Pb /206Pb Age		(1) 208Pb/232Th Age		% Dis-cor-dant	(1) 208Pbr/232Th	± %	7corr 206Pbr/238 U	err	(3) 206Pbr/238 U
f8–4	343.2	9.4	592	± 70	224	± 7	83	0.01	3.3	0.0511	0.0013	0.0547
f8–5	445.0	11.8	455	± 39	418	± 17	3	0.02	4.2	0.0709	0.0017	0.0715
f8–6	420.3	12.1	543	± 45	358	± 11	32	0.02	3.1	0.0658	0.0017	0.0674
f9-3a	441.1	11.3	517	± 48	433	± 12	18	0.02	2.9	0.0705	0.0017	0.0708
f9–6	383.7	10.0	429	± 37	367	± 10	12	0.02	2.6	0.0608	0.0014	0.0613
f9–7	256.9	7.4	903	± 96	298	± 9	243	0.01	3.0	0.0407	0.0010	0.0407
f9–8	438.9	11.3	446	± 90	350	± 14	4	0.02	4.1	0.0689	0.0017	0.0705

Sample name, Spot no.	err	238 U/206Pbr	± %	207Pbr/ 206Pbr	± %	207Pbr/235 U	± %	206Pbr/238 U	± %	err corr	Comments
f3–7	0.0018	14.62	2.5	0.0571	1.0	0.539	2.7	0.0684	2.5	0.932	
f3–10	0.0018	14.11	2.3	0.0577	1.7	0.564	2.8	0.0709	2.3	0.799	
f3–11	0.0020	13.69	2.5	0.0573	1.6	0.577	3.0	0.0730	2.5	0.850	
f3–12	0.0018	14.07	2.3	0.0582	1.2	0.571	2.6	0.0711	2.3	0.893	
f3–13	0.0019	13.83	2.4	0.0559	2.5	0.558	3.5	0.0723	2.4	0.681	
f3–14	0.0017	14.77	2.3	0.0573	0.9	0.535	2.4	0.0677	2.3	0.929	rejected
f3–15	0.0018	13.60	2.3	0.0567	1.0	0.575	2.5	0.0735	2.3	0.913	
f3–16	0.0028	9.68	2.6	0.0607	2.4	0.865	3.6	0.1033	2.6	0.733	rejected
f3–17	0.0021	12.61	2.4	0.0553	4.0	0.605	4.7	0.0793	2.4	0.524	rejected
f3–18	0.0024	16.65	3.5	0.0657	3.6	0.544	5.0	0.0601	3.5	0.696	rejected
f8–1	0.0019	14.07	2.3	0.0554	3.4	0.543	4.1	0.0711	2.3	0.563	
f8–2	0.0021	13.83	2.5	0.0561	1.4	0.559	2.9	0.0723	2.5	0.871	
f8–3	0.0016	15.05	2.3	0.0572	1.1	0.524	2.5	0.0665	2.3	0.892	rejected
f8–4	0.0015	19.42	2.4	0.0597	3.2	0.424	4.1	0.0515	2.4	0.601	rejected
f8–5	0.0020	14.09	2.4	0.0561	1.8	0.549	3.0	0.0710	2.4	0.799	
f8–6	0.0020	15.14	2.6	0.0584	2.1	0.532	3.3	0.0661	2.6	0.785	rejected
f9-3a	0.0019	14.15	2.3	0.0577	2.2	0.562	3.2	0.0707	2.3	0.730	
f9–6	0.0017	16.41	2.3	0.0554	1.7	0.466	2.8	0.0609	2.3	0.809	
f9–7	0.0012	24.02	2.4	0.0691	4.7	0.397	5.2	0.0416	2.4	0.450	
f9–8	0.0019	14.51	2.4	0.0558	4.1	0.531	4.7	0.0689	2.4	0.511	

Errors are 1-sigma; Pb_c and Pb^* indicate the common and radiogenic portions, respectively.

provide a poignant description of the Permian Pagoda Formation diamictites and ice flow dynamics (thrusting) in the Diamictite glacier area of the Transantarctic Range.

Our samples come from the Pensacola Mountains ($n = 91$), Ohio Range ($n = 95$), Queen Alexandra Range (n = 91), and Queen Elizabeth Range (n = 91; Fig. 1). All the samples have detrital zircon age spectra with a primary peak at ~600 Ma (Pan-African), a secondary peak around 1100 Ma (Grenville), and a smattering of older ages. The youngest and oldest ages are 498 and 3276 Ma (Pensacola Range), 493 and 2741 Ma (Ohio Range), 474 and 3347 Ma (Queen Alexandra Range), and 507 and 3414 Ma (Queen Elizabeth Range; Fig. 10). The heavy mineral populations are unremarkale and do not include any pyrope garnets as found in the Ellsworth, Falkland and Cape (Dwyka Group) diamictites (Table 2).

4.13. East Australia (Sites 20 & 21; Fig. 11)

Eight glacial intervals, four during the late Mississippian–Pennsylvanian (C1–C4) and four in the Permian (P1–P4), spanning the period from 327 to 255 Ma, have been identified in eastern Australia within the southern New England Orogen (Roberts et al., 1995, 1996, 2006; Glen, 2005; Birgenheier et al., 2009; Fielding et al., 2008; Roberts and James, 2010; Laurie et al., 2016). Diamictite facies include faceted, striated and bullet-shaped clasts. These facies are interbedded with laminated mudstone, sandstone and conglomerate. Clast penetration structures (dropstones) within laminated mudstone support an origin from floating ice. Age control for these facies is almost exclusively from SHRIMP dating of zircons from the volcanic facies.

The Currabubula Formation in the central part of the Tamworth Belt encompasses glacial episodes C3–4 (Fielding et al., 2008). The formation consists of up to 1200 m of thick alluvial sandstone and conglomerate beds with a significant volcanic component. Prominent interbedded ignimbrites have yielded U-Pb zircon ages of 319.1 to 308.9 ± 2.8 Ma (Roberts et al., 2004, 2006). Three intervals of glacially-influenced facies can be recognized and their complex internal facies reflect the ice-proximal position of the formation. The Rocky Creek Conglomerate (Fig. 4b; see also Appendix 3 g), in the northern Tamworth Belt, is from the C3 interval (Fielding et al., 2008) and has a similar depositional history and thickness (up to 880 m; Roberts et al., 2003). Its age is constrained by U-Pb zircons from an interbedded ignimbrite dated at 319 ± 2.7 Ma (Roberts et al., 2003).

Heavy mineral separates for both samples are similar (Table 2). Overall the detrital zircon populations in the Rocky Creek Conglomerate ($n = 45$) and Currabubula Formation ($n = 30$) samples are also similar, each with one age peak presumably close to the depositional age, and a smattering of Proterozoic zircons (Fig. 11). The oldest zircons are 992 Ma (Currabubula) and 2209 Ma (Rocky Creek). However, the maximum depositional ages (MDA), based on the 10 youngest zircons, are 302.9 ± 2.5 Ma for Rocky Creek and 317.1 ± 2.3 Ma for Currabubula (Fig. 11). The latter is consistent with other isotopic ages in that area (Roberts et al., 2004; Fielding et al., 2008) but the former is at least 1 Ma younger than basal pyroclastics from the overlying Lark Hill Formation (310.6 ± 4.0 Ma; Roberts et al., 2003, Fig. 8). This discrepancy probably relates to the large errors inherent in both SHRIMP and LA-ICPMS techniques that make both unsuitable for determining depositional ages in relatively young strata.

4.14. Western Australia (Carnarvon and Canning basins; Figs. 1 and 11)

Upper Carboniferous – Lower Permian (Gzhelian – mid-Sakmarian) glacial deposits are widespread in all Phanerozoic basins in west Australia (apart from the Mesozoic–Cenozoic basins) and have been intersected in many onshore petroleum wells and mineral boreholes. The absence of associated volcanic facies or diverse faunas means that the age of the glacial succession is based on spore-pollen zones in subsurface sections (outcrops are usually too oxidized) and marine faunas largely from outcrop of stratigraphically enclosing units. Glacial facies in west Australia contain 'Stage 2' (now *Microbaculispora tentula*) and overlying *Pseudoreticulata confluens* spore-pollen zones (Kemp et al., 1977; Backhouse, 1991, 1993; Mory et al., 2008). In east Australia these zones are associated with rare volcanic tuffs from which zircons dated by ID-TIMS indicate that the *M. tentula* Zone likely spans the Carboniferous–Permian boundary and the *P. confluens* Zone covers much of the Asselian (Bodorkos et al., 2016).

Whereas previous provenance studies in Western Australia incorporating the Permian had no samples from glacial facies (e.g. Cawood and Nemchin, 2000; Veevers et al., 2005; Dillinger et al., 2018) distinctive clasts in outcrop, particularly those derived from Proterozoic basement within the Nangetty Formation (Perth Basin; Playford et al., 1976) indicate an input from nearby sources. By comparison, clasts in the Grant Group (Canning Basin) indicate sources from both the Proterozoic Kimberley Basin to the north (Playford et al., 2009) as well as the Pilbara Craton to the south (O'Brien and Christie-Blick, 1992).

In the Petrel sub-basin of the Bonaparte Basin Gorter et al. (2005, 2008) placed the commencement of glacial conditions in the early Pennsylvanian, whereas in the Canning Basin unambiguous glacial facies do not appear until the latest Pennsylvanian (Mory, 2010). Further south the glacial affinity of mid-Carboniferous (late Visean – Serpukhovian) strata in the Perth and Carnarvon basins has recently been questioned (Playford and Mory, 2017). Even if there are variations in the onset of glaciation across Western Australia, such a relationship may have more to do with local tectonics (and hence accommodation) than uplift providing local seeding points for the onset of glaciations as implied by Eyles (2008).

Southern Carnarvon Basin, west Australia (Site 22, 3 samples; Fig. 11).

In the Southern Carnarvon Basin Warroora-1 (Johnstone and Pudovskis, 1955; Crostella and Iasky, 1997), drilled within the northern part of the Gascoyne Platform, is one of the few wells with core showing distinct glacial characters including diamictite, exotic clasts and contorted bedding (cores 4 to 17 from 412 to 1376 m). Four of the 14 short cores within the glacial succession in this well were selected for zircon dating (Appendix 3f).

The zircon age profiles of the productive Warroora-1 samples (cores 4, 412.4–416.05 m; 10, 830.3–831.8 m; and 17, 1374.65–1375.9 m) show overlapping as well as different ages (Fig. 11), but the only ones in common to all three are around 1100–1200 Ma. In terms of Western Australian Precambrian terranes (summarized by Southgate et al., 2011, Fig. 1), this best matches the younger parts of the Albany–Fraser Province (~1000–1500 Ma) over 1000 km south of the well. More striking are similarities in the 2600–2750 Ma peaks between the samples from cores 4 and 10 that match ages from the Yilgarn Craton, and peaks within 500–580 Ma also shown by the Madagascan and Indian samples. The comparison of cores 10 and 17 is hindered by the disparity in zircon yields, but shows some similarity over 1020–1800 Ma. In addition, the age profile from core 17 shows a conspicuous similarity to that of the Perth Basin for ages < 1700 Ma implying reworking of early Paleozoic deposits rather than direct transportation from the original source areas. The lowest sample from Waroora-1 has detrital zircons with Archean ages of 2917, 3099, 3117, 3205, 3207 and 3460 Ma, likely sourced from the Yilgarn or Pilbara cratons, but Paleoarchean zircons are known from Jack Hills (Compston and Pidgeon, 1986) approximately 400 km southeast of Warroora-1.

Overall, the age profiles are typical of the 'pan-Gondwanaland' signature (Veevers et al., 2006) for which an origin from (now subglacial) mountains in Antarctica has been suggested (Veevers and Saeed, 2008). Such an origin is consistent with Cawood and Nemchin's (2000) conclusion of "an overall longitudinal supply of detritus from the south" even though they did not analyse lowermost Permian glacial samples. Given the near-polar position for most of Gondwana during the Late Paleozoic ice age, a common southern provenance is not surprising. Similarities between non-contiguous provinces (e.g., the two youngest peaks in the oldest Western Australian sample and the Madagascan sample) imply longevity of uplift in the central source area as well as for the pattern of ice movement during this glacial episode.

4.15. Canning Basin, northwest Australia (Site 23; n = 3; Fig. 11)

The Canning Basin in northwest Australia lay at mid- to high latitudes in East Gondwana during the Permo-Carboniferous, with proximal Precambrian highlands (Arunta Inlier, Musgrave Block) and rifting along its northwestern margin as a prelude to break-up with India and Himalayan terranes (Veevers and Tewari, 1995; Hand et al., 1999; Betts et al., 2002; Veevers, 2004; Glen, 2005). Deposition of the Grant Group in the NW-SE trending Canning Basin was associated with deglaciation following ice motion toward the NW (Martin et al., 2007; Playford et al., 2009). Samples from three petroleum wells drilled in the central part of the basin (Fig. 6; Drosera-1, −19.678043, 125.040742; Capparis-1, −19.4505, 125.1024; and Cycas-1, −19.0082, 126.0161) yielded detrital zircons dominantly from central Australia discussed in detail by Martin et al. (in press). The age profile of the 1000–2000 Ma components are close to that from the basal sandstone of the Neoproterozoic Murabba Basin (Haines and Allen, 2017) whereas the younger tail is similar to zircon ages from the Neoproterozoic Amadeus Basin (see Maidment et al., 2007). Core from the underlying Upper Carboniferous Reeves Formation was not sampled as its strong fluvio-deltaic character is likely to reflect local provenance and/or input from central (and possibly eastern) Australia, largely driven by the Alice Springs Orogeny (Haines et al., 2001) rather than ice-related transport.

Sample DRO is from the 'lower' Grant Group (latest Carboniferous) interval of Drosera-1 (192.9 m) on the Barbwire Terrace (Fig. 6; also Appendix 3 g). Sixty-one U-Pb age determinations were obtained from DRO zircons, ranging from 2828 to 306 Ma, with 62% of the grains > 90% concordant (Table 1, Appendix 1). Noteable age populations include: 1) Paleoproterozoic to early Mesoproterozoic ages of 1796–1449 Ma, and 2) Mesoproterozoic ages of 1289–1164 Ma (Fig. 11). Late Neoproterozoic to Cambrian ages of 602–508 Ma also form a population. Remaining zircons yielded a single Archean age of 2828 Ma, several Palaeoproterozoi ages between 2220 and 058 Ma, Neoproterozoic ages between 966 and 743 Ma, and four Devonian to Pennsylvanian ages between 427 and 306 Ma. The youngest zircon from this sample (dro66c) has an age of 306 ± 8 Ma (2σ, 96% concordant).

Sample CAP, from the 'lower' Grant Group of Capparis-1 (106.9 m) on the Barbwire Terrace (Fig. 4.1), yielded a total of 60 zircon U-Pb age determinations that range from 2908 to 298 Ma, with 72% of the grains > 90% concordant (Table 1, Appendix 1) Age populations include: 1) Palaeoproterozoic to early Mesoproterozoic ages of 1802-1492 Ma and 2) Mesoproterozoic ages of 1329–1086 Ma. Late Neoproterozoic to Devonian ages of 604–408 Ma also form a population Remaining ages include a single Archean age of 2908 Ma, several Paleoproterozoic ages from 2140 to 1919 Ma, Neoproterozoic ages from 943 to 750 Ma, and several Mississippian to Early Permian ages of 335–298 Ma. The youngest zircons from this sample have ages of 298 Ma and 304 Ma. Additional ablations yielded ages of 305 and 306 Ma, respectively.

Sample CYC is from a cross-bedded sandstone in the 'lower' Grant Group interval of Cycas-1 (999.6 m) in the Fitzroy Trough (Fig. 6). Sixty U-Pb age determinations were obtained from CYC zircons, ranging from 3359 to 297 Ma, with 68% of the grains > 90% concordant (Table 1, Appendix 1). Age peaks include: 1) Paleoproterozoic to early Mesoproterozoic ages of 1866–1472 Ma, and 2) Mesoproterozoic ages of 1374–1037 Ma. Remaining ages include Archean to early Paleoproterozoic ages of 3359–2304 Ma, Neoproterozoic ages of 955–585 Ma, and Cambrian to Early Permian ages of 537–297 Ma. The youngest zircon is 297 Ma.

4.16. Lhasa and North Qiangtang terranes (Sites 24 & 25; Fig. 12)

Diamictites are common in upper Paleozoic strata belonging to several of the main assemblages that make up the Himalayan-Tibetan orogen (Fig. 12; Appendix 3 h). Several samples were collected from diamictite-bearing strata in each assemblage, with results reported by Gehrels et al. (2011). This includes samples 05AL46 and 613,021 (n = 216) from the Lhasa terrane and 06GT56 and 05GT42 (n = 198) from the North Qiangtang terrane. The Lhasa terrane diamictites preserve age peaks of 47–580, 940–1230 and 1530–1870 Ma. Diamictites from the North Qiangtang terrane include zircon age spectra of 520–630 and 740–1030 Ma. Both sample suites include minor age peaks ~2500 Ma with a few Paleoarchean grains (n = 6, between 3115 and 3271 Ma). These results were included in one K-S analysis and all glacially-related results from Gehrels et al. (2011) were included in a second analysis (see Discussion and Figs. 15 and 16). We also used detrital zircon age data for diamictites and interbedded sands from the Tethyan Himalayan sub-terranes (see inset box, Appendix 3 h; DeCelles et al., 2000, 2004; Gehrels et al., 2006a, 2006b; McQuarrie et al., 2008; Myrow et al., 2010). There is a paucity of glacial striation data in these terranes but the detrital zircon provenance connects Oman with the Qiangtang terranes and the southern Tethys and Lhasa terranes with northwest Australia.

5. Discussion

We preformed a K-S statistical analysis on all the detrital zircon age populations in various 30 by 30 matrices (Appendix 2) as this is a more rigorous evaluation of correlations and provenance than visual inspection of the relative probability plots (Figs. 7–12) and can be compared with the heavy mineral (pyrope garnet) provenance (Table 2). Of the 428 possible detrital zircon site correlations, 45 yielded a reliability coefficient > 0.050 (yellow highlights in Appendix 2) and, after additional evaluation (see below), only 38 correlations appear meaningful (**boldface type**, yellow highlight in Appendix 2). As a first pass, 38 provenance correlations of 428 (or, 390 failures of 428 = 88%) does not support the hypothesis that Gondwana-aged diamictites all came from the same Antarctic source. There are many additional analyses that support the hypotheses of Isbell et al. (2012) where three glacial phases existed between 338 and 256 Ma in a multitude of glacial centers across Gondwana. We have adopted the use of Episodes I-III (oldest to youngest) for the LPIA in Gondwana (Fig. 1).

5.1. Episode II heavy mineral provenance

Heavy mineral suites from five samples from the Paganzo Basin were analyzed (n = 366). The samples preserve a wide range of heavy minerals (spessartine garnet, zircon, hematite, ilmenite and barite) in a wide range of concentrations (Table 2) within the section from samples around the basin indicating local sourcing.

5.2. Episode II detrital zircon correlations

We did not sample any Episode I diamictites in northern Brazil but we do present results from five samples from the Paganzo Basin, Argentina of Episode II glaciation (Site 1, Fig. 1). Details of the Paganzo stratigraphy and a few field photos can be found in Appendix 3a. The Paganzo heavy mineral provenance was locally sourced (Table 2) and the detrital zircon relative probability plots show a demonstrable age peak at 500 Ma (Fig. 7) with many older 2nd and 3rd order peaks, and

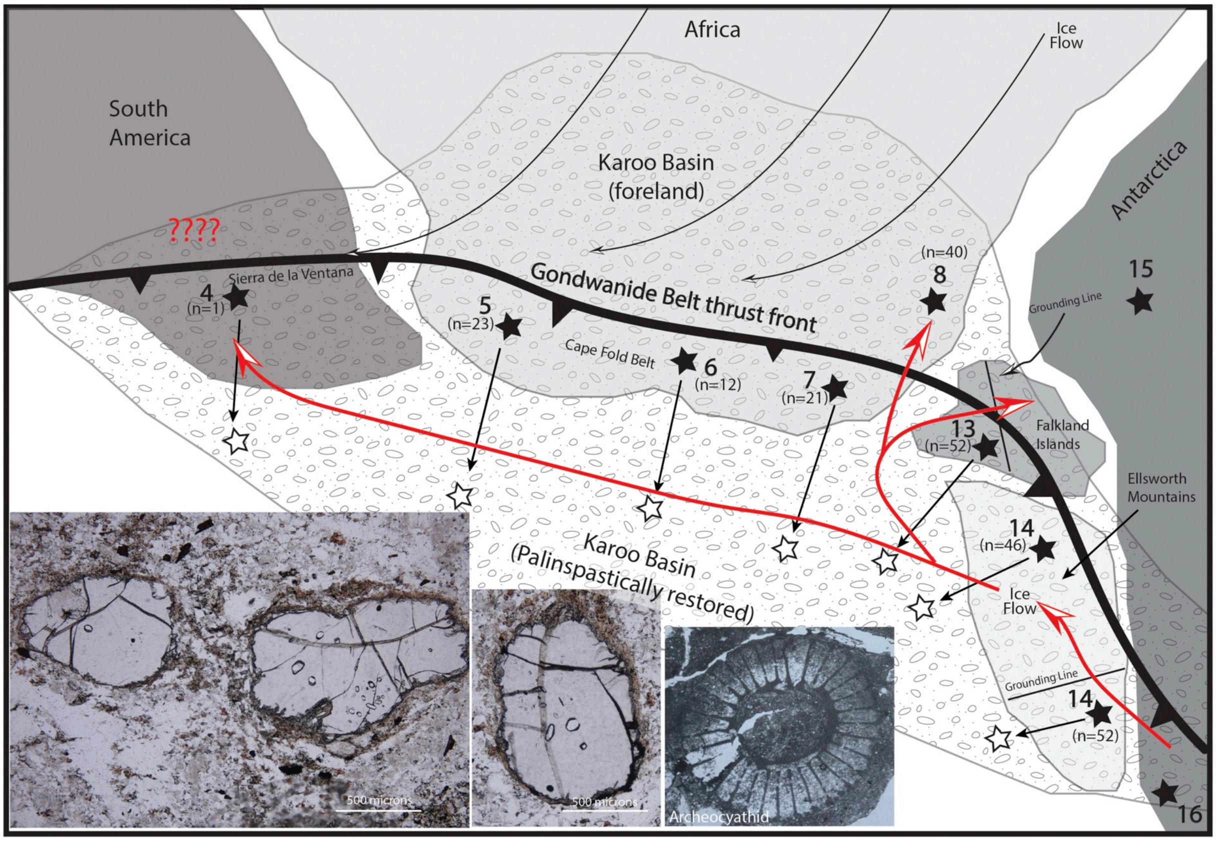

Fig. 13. Schematic drawing of the southern margin of Gondwana showing the Karoo Basin and Dwyka-equivalent diamictites after restoration of the Permian.

no zircons as young as the predicted depositional age (Table 1; Gulbranson et al., 2010). The statistical analysis demonstrates a provenance correlation in only 5 of 25 possibilities, with K-S correlation values between 0.707 and 0.122, some up-section, and some across the basin but with poor correlation elsewhere (i.e., to Episode III deposits). We interpret this to support the local, alpine nature of glaciation in the Paganzo Basin, a result that is likely in nearby Episode II glacial deposits (Henry et al., 2014; Gulbranson et al., 2014; Limarino et al., 2014a).

5.3. Episode III heavy mineral provenance

In Fig. 4 we show the boulder pavement in the Meyers Hills, southern Ellsworth Mountains, reported in Matsch and Ojakangas (1992). This basal contact is also rich in garnets suggesting a proximal source (see insets, Fig. 13). Additional analysis identified most of the garnets as pyrope (Mg-rich) garnets of an ultramafic source. In separating zircons from the diamictite samples we also characterized the heavy mineral populations (Table 2) and found that samples 4–8, 13 and 14 (2 sites) all contain concentrations of pyrope garnets thereby providing an additional provenance tracer (Fig. 13). In outcrop appearance, the diamictite at all these locales look like classic “Dwyka” (see Appendix 3b), and all but sample 8 (KwaZulu Natal) are found in the deformed rocks of the Permian Gondwanide belt. To properly characterize the pre-Gondwanide depositional setting of the Karoo Basin, we made a palinspastic restoration (plane strain) and plotted the restored sites and pyrope garnet concentrations. We also plotted the grounding lines in the Ellsworth Mtns. and Falkland Islands to create an ice flow map. The pyrope-rich garnet source is likely east of the Ellsworth Mountains but from a different source than the Pagoda Formation diamictites found in the Transantarctic Mountains (see below) as there are no pyrope garnets in samples 16–19 and the Pagoda Formation is younger (Isbell et al., 2003).

5.4. Episode III new age constraints

Only a few of the youngest detrital zircon ages were close to the presumed late Paleozoic depositional age of their respective diamictites (Table 1; Appendix 1). The two samples from eastern Australia, in the Tamworth belt, the Rocky Creek and Currabubula formations (Sites 20–21), had several young zircons so we calculated maximum depositional ages for each (MDA; Fig. 11). These ages are consistent with other ages for igneous materials in the section that are part of the local island arc system (Roberts et al., 2004; Fielding et al., 2008) and the zircons are likely from reworked ash deposits. We also included the U-Pb ages of euhedral zircons found in the Permian Polarstar Formation in (reworked ash bed eudedral zircons; Craddock et al., 2017a, 2017b, 2017c), and near (ash beds; Elliot et al., 2014), the Ellsworth Mountains where the Polarstar Formation overlies the Whiteout Conglomerate (Fig. 3).

5.5. Episode III granite clasts, Falkland Islands

The presence of Ordovician (447 Ma; Fig. 9) plutonic clasts within the Fitzroy Diamictite provides some constraints on the bedrock geology of the glaciated headlands. Within the Cape Belt of South Africa, plutonic rocks of late Ediacaran to Cambrian age form part of the Cape Granite Suite (Da Silva et al., 2000), which outcrops exclusively in southwestern South Africa. A better match in age is found in displaced terranes of the West Antarctica peninsula as well as the Amundsen Province of Marie Byrd Land, where Pankhurst et al. (1998) identify ca. 450 Ma calc-alkaline granite plutons. We note that the North Patagonia massif also contains similarly-aged granite plutons dated by $^{40}Ar/^{39}Ar$ techniques (Rapalini et al., 2013). All of these granitic source areas are west of the Falklands at the time of deposition (Fig. 1), which is consistent with the glacial flow direction observed by Frakes and Crowell (1967; west to east), but is inconsistent with the detrital zircon and pyrope garnet provenance of the diamictite matrix (Site 13). Statistically, the detrital zircons in the Fitzroy Diamictite are not similar to the adjacent east Dwyka diamictites (Site 7) but preserve a robust pyrope garnet population that diminishes from east (Ellsworth Mtns.; sample 14) to west (Sauce Grande Formation; Site 4; see below).

5.6. Episode III isolated and unlikely detrital zircon correlations

Visual inspection of the relative probability plots (Figs. 7, 8, 10–12) hints at the detrital zircon provenance correlations of adjacent sample sites (Fig. 1). Using the K-S statistical analysis makes these correlations more analytical with two end-members: detrital zircon populations that are isolated outliers (no correlations) and distal sites that happen to have similar detrital zircon populations despite separations of +1000 km and differences in age.

Six of the 30 samples do not have a detrital zircon population that correlates with any other samples (K-S result: 0.00; Appendix 2). These include: Site 11 (Oman-1, the top of the core; see below), which does not correlate with the two samples lower in the same core or any other distal sample; Sites 7 and 8 (east Dwyka and KwaZulu Natal, South Africa) with no horizontal detrital zircon correlation, despite a rich pyrope garnet concentration like its neighbors (Fig. 13); Site 12 (Talchir Formation, India), no correlation with anything; Sites 20 and 21 (east Australia) correlate almost perfectly with each other (K-S result: 0.986; the two samples were thereby combined in 1 column in Appendix 2) but with nothing else in the study (K-S result: 0.00), and Site 22 (Carnarvon Basin, western Australia) where the two upper samples in the Warroora #1 core (see well log in Appendix 3f) do not correlate with the bottom of the core but correlate with the Canning Basin.

Sample 10 (Oman-1) makes the minimum K-S correlation threshold ($P = .050$) with the Sauce Grande Formation (Site 4, Argentina) and is discarded due to the 3000 km separation with no supporting ice flow connection. Site 11 (Madagascar) correlates with the Paraná Basin (Site 3; 0.159), the Pensacola (Site 16; 0.096) and Queen Elizabeth (Site 18; 0.186) ranges, Antarctica despite separations of 3000, 3500 and 4500 km, respectively. The Congo (Site 9) correlates (0.618) with Site 22 in western Australia despite being separated by 4000 km, and India has no correlatives. There are other oddball correlations: The Falkland Islands (Site 13) and Pensacola Mountains (Site 16) correlate with each other and the western Dwyka Grp. (Site 5) but not with the adjacent eastern Dwyka Grp. (Site 7), but all four of these samples have pyrope garnets.

5.7. Episode III vertical detrital zircon correlations

We have three sites with drill core through LPIA diamictites that allow for analysis of provenance through time in a single location. Oman (Site 11; Fig. 5 and Appendix 3) provides 3 samples from the Al Khlata Formation, specifically samples Oman-1 (glacial zone P1, top), Oman-2 (glacial zone P3) and Oman-3 (glacial zone P9, bottom). All three core samples are populated with abundant of non-pyrope garnet and pyrite (Table 2, Fig. 5). The detrital zircon populations all have age peaks of varying intensity (Fig. 8) at ~525 Ma (East Africa orogeny), ~620 Ma (amalgamation of the Arabian shield-Pan-African orogeny), and ~800 Ma (Arabian basement) that are zircons derived locally. Older zircon populations are likely from Africa: ~1000 Ma (Grenville-equivalent Namaqua-Natal Province) and 2500–3000 Ma (Kaapvaal craton) and not India, based on the ice flow data in Oman and the provenance outlier status of India (Appendix 2). The K-S analysis shows Oman-1 (top) has poor correlations anywhere, including samples Oman-2 and Oman-3 lower in the core. Oman-2 and Oman-3 have a K-S correlation coefficient of 0.346. Samples Oman 2 and 3 also correlate with the North Qiantang terrane (Fig. 1; K-S values of 0.051 and 0.923). This suggests that the older samples correlate with the nearby, offshore North Qiantang terrane, but not with the younger (P1) glacial advance. We thereby define an “Oman” ice cap which flowed to the northeast.

The Carnarvon Basin in western Australia (Site 22) provides the Warroora #1 core where 3 of 4 cores yielded detrital zircons. Heavy mineral populations are garnet-rich in the upper samples and rutile-rich in the lower sample (Table 2). The sample details are: AUS-4 (412.4–416.4 m depth; mostly Archean Yilgarn zircons), AUS-5 (478.2–483.7 m, no zircons recovered), AUS-10 (830.3–831.8 m; Proterozoic Badgeradda and Centralian Group and Archean Yilgarn zircons), and, AUS-17 (1374.6–1375.9 m; Proterozoic Pan-African and Pinjarra orogen zircons). Statistical analysis indicates no correlation within the three samples of the core; the only horizontal correlation is between the basal diamictite and the Lhasa terrane (0.618; Site 23). Ice flow indicators around the Carnarvon Basin are mixed (local) and generally northerly, suggesting northerly transport of Australian zircons to the Lhasa terrane, perhaps from Antarctica.

5.8. Episode III aross-basin detrital zircon correlations

Detrital zircon U-Pb age probability distribution plots indicate the Grant Group in the Canning Basin was sourced predominantly from proximal Proterozoic and Phanerozoic terranes with ages of 1800–1500, 1300–1000, and 600–500 Ma (Fig. 11). Statistical analysis of the three samples from the same unit in the Canning Basin, from 3 wells, separated by ~100 km each, have K-S correlation coefficients > 0.90, so across-basin provenance correlation is excellent. Accordingly, many of the detrital zircon ages are equivalent with orogenic events in terranes to the south and east of the Canning Basin, notably the Arunta Inlier, Musgrave Block, and Capricorn Orogen. A lack of Archaean detrital zircons, as observed by other Western Australian provenance investigations of Permian sediments (Cawood and Nemchin, 2000), highlights the importance of considering regional models in the interpretation of U-Pb age data (e.g. Kohn et al., 2002), and the three Canning Basin samples correlate nicely with the detrital zircon populations in the Lhasa terrane (Fig. 12; Appendix 2). The Canning Basin and Carnarvon-Perth Basins, where the Grant and Lyons Groups are age-equivalent (mid-Ghezelian – early Sakmarian), also correlate statistically and were connected to the open ocean to the northwest toward the Lhasa terrane. We thereby identify a “Mawson” ice cap that flowed to the northwest (Figs. 5 and 16; Appendix 3d) and deposited glacial sediment on the nearby exotic terrane (see ternary analysis below; Fig. 14).

5.9. Episode III detrital zircon correlations

The pyrope garnet populations from Sites 4–8, 13 and 14 provide one line of evidence of an ultramafic garnet source in continental Antarctica and, based on the glacial striations and grounding line in the Meyers Hills, southern Ellsworth Mountains, for ice motion into the southern Karoo Basin all the way to the Sauce Grande Formation, Ventana Mountains, Argentina (Fig. 12). The Sauce Grande Formation (Site 4) passes the K-S correlation coefficient minima (0.050) with 9 other sites, with a correlation coefficient total of 3.015. The two other highest correlations are for the Pensacola Mountains (Site 16; 8 correlations = 2.69) and the adjacent Ellsworth Mountains (Site 14; 6 correlations = 2.991). The highest detrital zircon correlation in the study is between the Ellsworth and Pensacola populations: 0.998. The Sauce Grande Formation detrital zircon population thereby correlates with both Itarare Formation till samples to the north in the Paraná Basin (0.077, 0.58; we don't have heavy mineral splits to look for pyrope garnets), as well as robustly with the western Dwyka diamictite in South Africa (0.34), the Falkland Islands (0.725) and the Pensacola Mountains, Antarctica (0.737). Sites 6,7,8 (Dwyka Diamictite) and 15 (Heimefront Range, Antarctica) do not correlate at all. One ice flow model could be a significant ice sheet in northwest Antarctica that flowed west across the southern Karoo Basin to the Sauce Grande Formation (~4000 km), an interpretation supported by cumulative probability plots (Fig. 15).

Africa	AFR
Argentina Sauce Grande	4
Brazil Itarare	3
Brazil Parana	2
Congo	9
Dwyka C	6
Dwyka E	7
Dwyka W	5
Ellsworth	14
Falklands	13
Fatamina	1e
Heimefront	15
Himalaya	HIM
Huaco A Tupo	1c
Huaco B Tupo	1d
India	12
KZN	8
Laurentia	LAU
Lesser	23b
Lhasa	23
Madagasgar	11
Malanzan	1b
N.Quiag	24b
North Qia	24a
Ohio Range	17
Oman 1	10a
Oman 3	10c
Oman2	10b
Pensacola	16
Queen Alex	18
Queen Liz	19
Rocky Creek	20
S. America	SAM
S. Qiang	24c
Sisne lower	SL
Sisne Middle	SM
Sisne upper	SU
Tethyan	Teth
Unquillal	1a
W Aus M-T	22b
W.Aus B	22a
Canning Australia	25

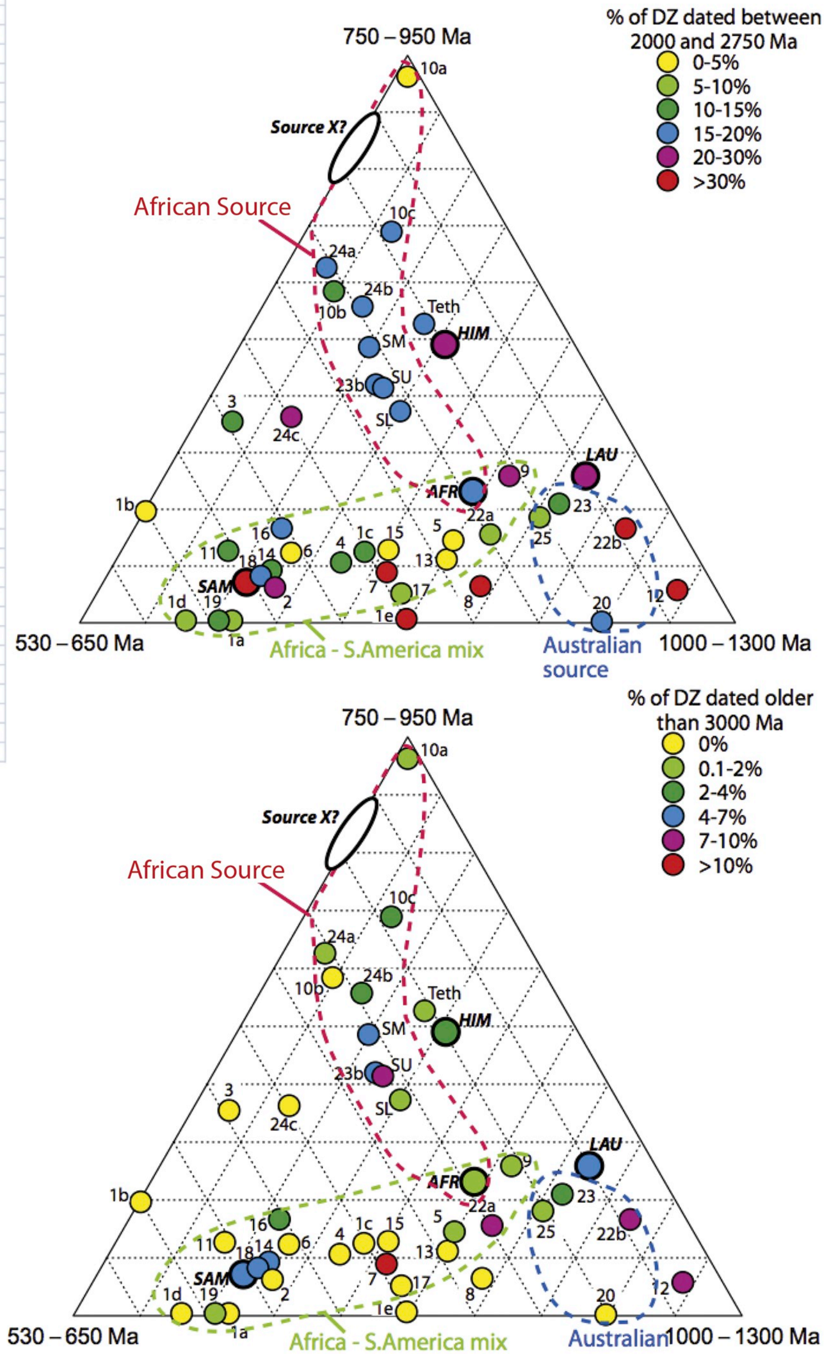

Fig. 14. Ternary plots of diamictite detrital zircon ages compared to detrital zircon ages from modern river sediment (Rino et al., 2008).

The more traditional view of ice flow trajectories for deposition of the Dwyka diamictites in the greater Karoo Basin argue for a highland to the northeast with flow to the southwest (Appendix 3a). This is complicated by the lack of ice flow data in the Cape fold belt, poor K-S correlation data between Dwyka Sites 5–8, and the preponderance of pyrope garnets in the Dwyka (see Fig. 13). All the southern Africa, Falkland, and Ellsworth diamictites (Sites 5–8, 11, 13, 14) include age spectra peaks at ~560 Ma (Pan-African orogen) and 1000 Ma (Namaqua-Natal belt = Grenville) with varying concentrations of 2700–3000 Ma zircons and rocks of these ages are north, south and beneath (buried) southern Africa (see text below concerning Archean zircons in the diamictites; Jacobs et al., 2003, Jacobs et al., 2008; Robb et al., 2006; Cornell et al., 2006). There was likely an ice divide separating the southerly Dwyka till deposition from diamictite deposition in the north (Cargonian Highland). Isbell et al. (2008a, 2008b) have demonstrated the complexity of local sedimentation and ice flow dynamics in the Dwyka diamictites in the north, supported by studies of Dwyka-aged eskers (deWit et al., 2016). Local, detailed detrital zircon studies will better define these issues.

5.10. Episode III continental-scale sedimentation and provenance patterns

In order to discriminate the possible sediment source of the zircon grains in the glacial deposits analyzed and compiled here, we have

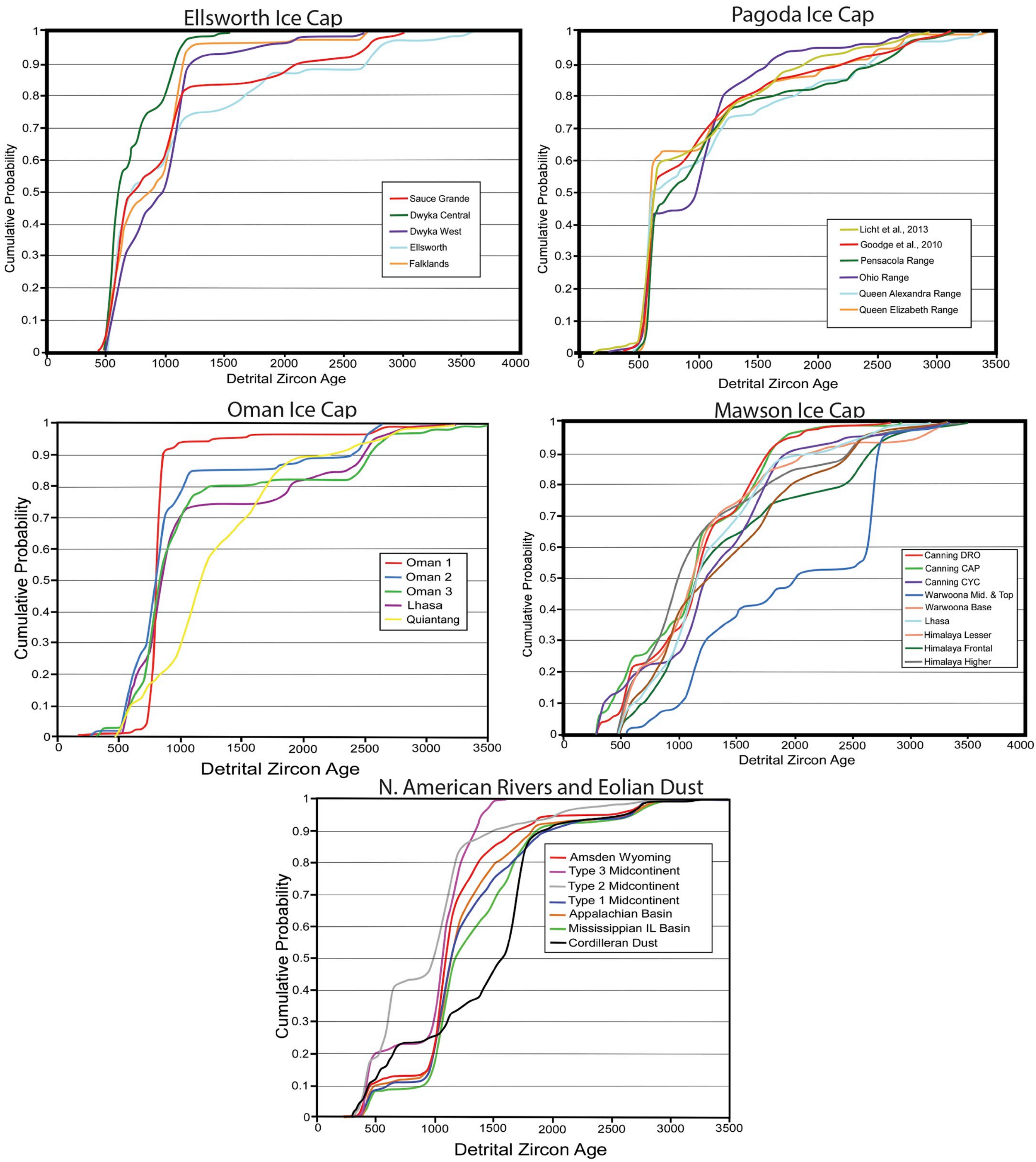

Fig. 15. Proposed Gondwana (Episode III) ice caps using detrital zircon cummulative probability plots: (A) Ellsworth, (B) Pagoda, (C) Oman, (D) Mawson and (E) Pennsylvanian eolian detrital zircons from the southwest USA (Soreghan et al. 2002) and fluvial detrital zircons from the North American midcontinent (Kissock et al., 2017). See Fig. 16.

separated the detrital zircons into five age groups that are observed in sediments from major rivers (Saylor et al., 2013) and can be correlated with major orogenic events on the globe: 1. Zircons that range in age from 530 to 650 Ma, which corresponds to African and South American orogenic events related to the formation of Gondwana, 2. Zircons that range in age from 750 to 950 Ma, which correlate with the breakup of Rodinia, 3. 1000–1300 Ma which, corresponds to the Grenville orogeny in North and South America as well as the age-equivalent events Africa and Antarctica, 4. Zircons that were dated between 2000 and 2750 Ma, which correspond to the formation of late Archean shields and the

Paleoproterozoic amalgamation of these terranes, and 5. Older than 3000 Ma, which represent the older cores of Archean shields.

These five populations were normalized and projected on two ternary plots (Fig. 14a,b). The apexes of both of these plots represent populations 1–3 from the list above, while the colour of the symbols represents the proportion of 2000–2750 Ma zircons on Fig. 14a, and the proportion of > 3000 Ma zircon on Fig. 14b. We plotted all of our samples on these two figures in addition to the proportions of these zircon populations from major rivers draining the present- day continents of Africa, North America, South America and the Himalaya. These detrital zircon data were used as a proxy for the detrital zircon signature of the African continent (AFR), Himalayan orogen (HIM), Laurentian continent (LAU), and South American continent (SAU).

The resulting plots indicate that most of our samples (80% or 30 out of 38) generally plot along two major trends: a trend that appears to be mixing the African (AFR) and South American (SAM) signature, and another trend between the African and an unidentified source that would have ~20% 2000–2750 Ma zircons, 55% 750–950 Ma zircons, ~25% 530–650 Ma zircons and minimal to none of both 1000–1300 Ma and > 3000 Ma zircons. Based on the regional context of our detrital zircon samples and the tectonic history of the Indian plate and the Arabian platform, both of which lack major late Mesoproterozoic (Grenville-age) and Paleozoic events, it seems likely that this unidentified sediment source is the Indio-Arabian plates.

Most of our South American, South African and Trans-Antarctic samples (e.g., Paraná, Karoo Basin, Ellsworth Mountains, Ohio Range, Queen Alex and Queen Elizabeth) fall along the SAM-AFR mixing trend. On the other hand, our Oman, North Quiangtang samples seem to represent mixing of the African source (AFR) and the proposed Indo-Arabian source. Several of our samples that don't fall along these two trends appear to come from the Australian continent (western Australian and easternAustralia samples) and have high proportions of Archean and early Proterozoic ages (> 2000 Ma). We infer these to be dominated by a local Australian signature that has a high proportion of Paleoproterozoic and older zircons. Finally, the Lhasa terrane and central India samples appear to have detrital zircon populations that do not fall along the trends described above, potentially because they are spatially isolated from any of the other samples.

This type of broad-scale analysis can be useful in identifying large-scale depositional fairways during glaciation events. A possible explanation for the patterns we observe is the existence of two or three major ice-shields that were at least periodically connecting smaller ice-shields. One of the shields would cover large regions of South America, South Africa and Antarctica, in which case we should expect that significant areas of Archean (> 2600 Ma) basement would be covered under the present-day Antarctic ice; the oldest Antarctic zircon is 3568 Ma. The other ice shield would cover large regions of the Arabian plate, India and portions of Australia, mixing sediment from these source areas.

5.11. Episode III out-of-Antarctica detrital zircon correlations

Goodge et al. (2010) presented the first data on the rock types, and ages

of glacial sediment delivered to coastal Antarctica north of North Victoria Land, a study duplicated for the Byrd Glacier and sites downstream in the Ross Sea area (Fig. 15) by Licht and Palmer (2013). Cumulative probability plots of all the zircon ages (see K-S data in Appendix 3) confirm the common provenance of zircons delivered to modern coastal Antarctica and detrital zircons delivered to the Permian Pagoda Formation in the Transantarctic Mountains (Sites 16–19; see Isbell et al., 2003, Isbell et al., 2008a, 2008b). We have named this the "Pagoda ice cap" (Fig. 16).

The Whiteout Conglomerate (Site 14, Ellsworth Mountains, Antarctica) has the most pyrope garnets (Table 2), the oldest detrital zircon in the study (3568 Ma; Appendix 1), and the remarkable boulder pavement loaded with pyrope garnets (Fig. 4), so we think this allows us to propose an "Ellsworth ice cap" that sourced ultramafic rocks east of the Ellsworth Mountains (Fig. 15). Diamictites in the Ellsworth depositional system also included carbonate clasts with Cambrian archeocyathids (Fig. 13) sourced in the Cambrian Heritage Group sediments in the Ellsworth Mountains and delivered to the west (Cooper and Oosthuizen, 1974; Isbell et al., 2008a, 2008b). The provenance of this ice cap includes the SAM-AFR affiliations of the ternary analysis (Fig. 14) but the Whiteout Conglomerate (Dwyka-equivalent) does not correlate well with the Pagoda Formation diamictites in the Transantarctic Mountains by age or K-S analysis (we analyzed data sets from Elliot et al., 2014 and Bader et al. 2017 and found no correlation) and is thereby older and unique (Isbell et al., 2008a, 2008b; Isbell et al., 2012). We therefore propose that the Ellsworth ice cap was centered along coastal Antarctica in the Late Carboniferous and flowed west depositing glacial sediment as far as the Sauce Grande Formation in Argentina (Fig. 13). A cumulative probability plot for Sites 4–7, 13 and 14, supports this hypothesis (Fig. 15). The glacial diamictites in the Heimefront range, Antarctica (Site 15; Appendix 3e) represent an outlier, not correlating with any other site but may be the older equivalent of the glacially-derived rocks described by Veevers and Saeed (2008) for the Prince Charles Mountains, Antarctica. Neither the Ellsworth or Pagoda ice centers, based on their detrital zircon provenance, are in any way connected to the "Mawson ice cap", which flowed north on the opposite side of Antarctica (see below).

5.12. Episode III equatorial glaciation and exotic terranes

Tectonic reconstructions for the late Paleozoic include a variety of ("Peri-Gondwana") terranes in low-latitude locations off the northern coast of Gondwana (Fig. 1; Blakey, 2008). Four of these terranes have since been accreted to Asia as part of the greater Himalayan-Tibet plateau and contain LPIA diamictites (Gehrels et al., 2011 and references therein; Sites 24 and 25; Appendix 3 h). The diamictites contain dropstones and thus are of glacial origin. As the Tethys, Lhasa and North and South Qiangtang terranes have since been intensely deformed during accretion to Asia, they were larger in the late Paleozoic and had greater surface areas, making their glacial proximity to Oman and Australia more likely. Sites 10 and 25 (Oman-3; K-S correlation = 0.923 with North Qiangtang; Oman-2; K-S correlation with North Qiangtang = 0.053) correlate well and, in general tectonic terms, must be nearly equatorial. Site 23 (Canning Basin; K-S correlations of 0.264, 0.154, 0.083, and 0.51 with the Tethys samples) and Site 22 (Carnarvon Basin; K-S correlations = 0.618 with Lhasa) support ice flow from northwest Australia to the Tethys-Lhasa terranes. The detrital zircon cumulative probability plots in Fig. 15 support the presence of a Permian ice cap centered over Oman and an ice cap flowing northwest from Antarctica, across Australia to the Tethys-Lhasa terranes (Fig. 16).

5.13. Episode III five ice centers and ice volumes

We can thus propose that there were at least five ice centers on Gondwana, from oldest to youngest (Fig. 16):

- 1. The "**Dwyka ice center**"centered around present-day Zimbabwe, from which ice flowed W and SW, around the Cargonian Highland, to deposit the Dwyka Group diamictites (depositional distance: ~2000 km);
- 2. The"**Ellsworth ice center**"centered east of the Ellsworth Mountains, from which ice flowed west with a source rich in pyrope garnets and Cambrian archeocyathids (Fig. 13; depositional distance: ~2000 km);
- 3. The "**Mawson ice center**" situated along the Australia-Antarctic coast, from which ice flowed NW through the Carnarvon and Canning basins to the Tethys and Lhasa terranes (depositional distance: ~1500 km);

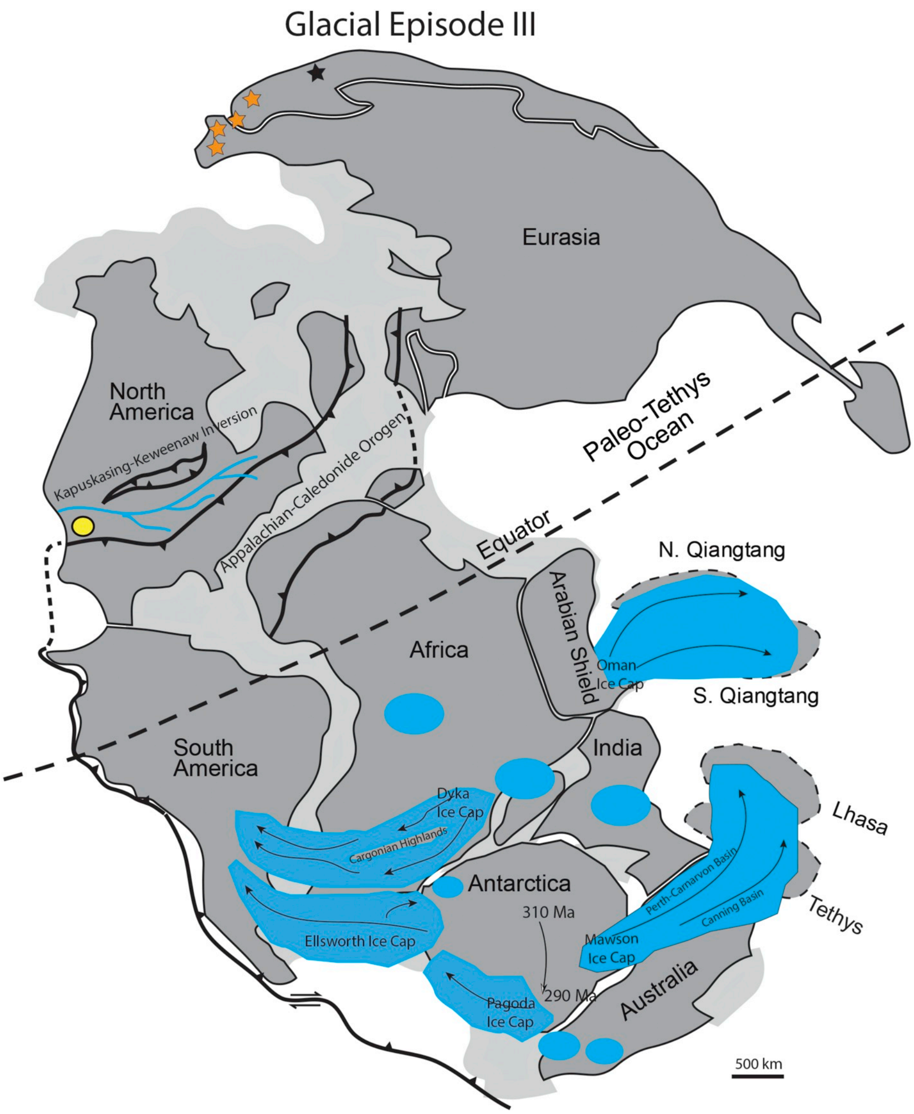

Fig. 16. Pangea during the Permo-Carboniferous with regional Gondwana ice centers based on detrital zircon provenance (Figs. 14 and 15) with the paleopole. Blue ellipses are local ice centers. In the Northern Hemisphere, possible glacial tillites (orange stars) and non-glacial diamictites (black star; see Isbell et al., 2016) are plotted, as are glacial loess deposits (yellow circle; Soreghan et al., 2002) and rivers draining the Appalachian Mountains (Kissock et al., 2017) west and around the inverted Kapuskasing-Keweenaw highland (Craddock et al., 2017a, 2017b, 2017c). See Fig. 15 for detrital zircon comparisons and cummulative probability plots.(For interpretation of the references to colour in this figure legend, the reader is referred to the web version of this article.)

- 4. The "**Pagoda ice center**", inland of Site 19 (Transantarctic Mountains; see Isbell et al., 2003, Isbell et al., 2008a, 2008b for images of grounding line deformation), where the ice flowed north, toward the current South Pole (depositional distance: ~1000 km);
- 5. A lower latitude "**Oman ice center**" covering Oman-Qiangtang, where ice flowed to the NE (depositional distance: ~1500 km).

Our proposal of five Episode III ice centers is supported by ice flow striation observations and detrital garnet, archeocyathid and zircon provenance data but also presents a different mechanism for ice flow and diamictite deposition far from an ice center. Pleistocene continental ice centers, and their remnants in Greenland and Antarctica, did (do) not leave evidence of diamictite deposition ~2000 km offshore although ice streams that drain the Antarctic ice cap into the Ross and Weddell Seas have flow distances of 1000–2000 km. Only the Pagoda and Ellsworth deposits preserve a grounding line, but it appears that most of the LPIA glacial deposits may be marine in origin. The Dwyka Group diamictites are remarkably uniform (no interbedded sands, etc.) in outcrop across southern Africa, southern Argentina, the Falkland Islands and Ellsworth Mountains (Fig. 4b, Appendix 3c) yet there appear to have been two unique ice centers to delineate the Dwyka and Ellsworth systems (Fig. 16). The Ellsworth ice center was located east of the Ellsworth Mountains and the grounding line, tillite deposition (east), and diamictite deposition (west) is located in the Meyers Hills of the southern Ellsworth Mountains (Matsch and Ojakangas, 1992), indicating westward flow. The Whiteout Conglomerate, Dwyka Group, Fitzroy and Sauce Grande formations have a common detrital zircon provenance (Fig. 15a) and pyrope garnet concentrations (Fig. 13) decrease from east to west. How big was the Antarctic ice center (ice volume) to get diamictite deposition ~2000 km west of the ice center? Antarctica was centered over the South Pole during much of Episode III, but how much of the polar continent was covered in ice centers that fed the Ellsworth, Mawson and Pagoda systems.

The Mawson ice center presents a different, complex fluvial-glacial depositional system (Fig. 6; Appendices 3 e,f) sourced in Antarctica (Wilkes Land), and spread over western Australia and the Tethys and Lhasa terranes (Fig. 16). Paleo-ice flow indicators (Fig. 6) and detrital zircon provenance data (Fig. 15 d, with the exception of the Waroora) support our model. Without the detrital zircon data it would be difficult to prove how the south Carnarvon and Canning basins were connected as both represent cratonic arms of an open sea connected to the Tethys and Lhasa terranes. Evidence of that open marine connection is vague as the Permian has not been reached by drilling along the North West Shelf, but is seen in structurally dissected sections in the Gondwanan part of Timor-Leste Basin (Davydov et al., 2013; Haig et al., 2014; Haig et al., 2017). The oceanic connection played out somewhat differently in both basins with a greater fluvial input in the Canning during the mid-Ghezelian – early Sakmarian (likely the age of both the Grant and

Lyons groups) so clearly there is a temporal connection. The older glacial section in Warroora #1 on the northern Gascoyne Platform and south Carnarvon Basin, is much the same age as the non-marine Reeves Formation in the Canning Basin (latest Visean to ~Bashkirian). Strata of latest Visean – Serpukhovian age further east (northern Merlinleigh sub-basin, south Carnarvon Basin) are restricted to a siliciclastic section in Quail #1 (Quail Formation) and a possible equivalent unit in outcrop (Harris Sandstone, next to the eastern edge of the basin). There are also outcrops of this age much farther south in the northern Perth Basin (formerly assigned to the Nangetty Fm but their glacial character has recently been questioned by Playford and Mory, 2017). Perhaps the five Episode III ice centers present a different type of glacial environment with far-field ice movement and diamictite deposition, similar to the paradigm of far-field fluvial distribution proposed by Rainbird et al. (1992) for Grenville orogen detrital zircons that is now uniformly accepted.

5.14. Episode III late Paleozoic snowball earth?

The LPIA in the southern supercontinent of Gondwana has a broad correlation with the 55 cyclothems in the midcontinent of North America reported by Heckel (1986) and Rygel et al. (2008) over a ~10 million year period (Westphalian and Stephanian) as ice volume fluctuated (Fig. 15). These Pennsylvanian cyclothems are found in the Appalachian-Ouachita foreland but southeast of the Kapuskasing-Keweenaw inversion uplift in North America (Craddock et al., 2017a, 2017b, 2017c). In Europe, the cyclothems are east of the Variscan highlands and west of the Ural uplift with precise ash bed age control in the Donets Basin (Khodjanyazova et al., 2014). Coal seams are ubiquitous, found in the northern hemisphere cyclothems and several Gondwana glacial basins (Heckel, 2008; Isbell et al., 2012). The northern hemisphere also includes Pennsylvanian loess in the Ancestral Rocky Mountains of the southwest US (Soreghan et al., 2008), which includes eolian detrital zircons that have a North American provenance but no K-S correlation with the fluvial detrital zircons moving from the Appalachian highlands west (Kissock et al., 2017). Neither the eolian nor fluvial detrital zircons correlate with any of our southern hemisphere Gondwana diamictite detrital zircon populations (K-S = 0.0). Glacial diamictites are reported in a variety of high-latitude Siberia locations (Mikhaylov et al., 1970; Hambrey and Harland, 1981; Chumakov, 1994; Chumakov and Zharkov, 2003), although Isbell et al. (2016) report that the Siberian Atkan Formation is a Permian non-glacial diamictite. Did the LPIA have a glacial presence in the northern hemisphere, and thereby all of Pangea?

5.15. Episode III tectonic implications

As Gondwana moved during the late Paleozoic, the majority of the Episode III glaciation occurred between 310 and 290 Ma when Antarctica was centered over the South Pole (paleopoles, Figs. 1 and 16) with three of our proposed ice caps (Ellsworth, Pagoda, Mawson) flowing away from Antarctica. The older Dwyka and youngest Oman ice caps formed far from the South Pole and at moderate to low latitudes, respectively, and flowed off unknown highlands. Yeh and Shellnutt (2016) have documented the presence of mid-Permian high-temperature mafic intrusions along the northern margin of Gondwana in terranes they group as "Cimmeria", and include some of our exotic terranes. They have argued that the ice mass caused crustal flexure, then decompression through melting, which initiated rifting of Cimmeria from Gondwana. We find this unlikely as Gondwana was not covered by a single, massive ice sheet (Isbell et al., 2012; this study) and most of the LPIA glacial deposits are diamictites (with dropstones) so there is little crustal depression associated with floating ice.

6. Conclusions

The LPIA spanned 338–256 Ma with three separate glacial episodes where ice volumes and ice flow run-out (1000–2000 km), as documented by glacial diamictite deposition, increasingly dominated the southern landscape as Gondwana rotated. We did not sample the Episode I glacial deposits in northern South America (Lopez-Gamundi and Buatois, 2010). Episode II glacial deposits in the Paganzo Basin are the oldest samples we studied in the LPIA and their heavy mineral and detrital zircon provenances are of a local origin. Episode III glaciation dominated the LPIA with large ice caps centered in Zimbabwe (oldest, SW flow), coastal Antarctica (Ellsworth ice cap, westward flow), the Pagoda ice cap (flow toward the current South Pole), and lesser ice caps in SW Australia-Antarctica (Mawson ice cap, north flow) and Oman (youngest, northeast flow; youngest) where ice flow, and deposition of diamictites, reached distances of 1000 to 2000 km. Evidence of LPIA glaciation in the northern hemisphere is probable.

Acknowledgements

Craddock and Ojakangas started this project in the Ellsworth Mountains (1979-80) and progressed with piecemeal funding. Tohver acknowledges Australian Research Council grant LP0991834, and Riccomini Brazilian Council for Scientific and Technological Development grant CNPQ 307871/2010-0. Nancy Vickery and Bob Brown are thanked for contributing samples from eastern Australia. Macalester students who participated in this effort were: Alex Nereson, Maria Princen, Nick Culter, Dale Dybvig, Jesse Geary and Jake Moen. Matthew Horstwood (NERC Lab, U.K.) is thanked for aiding the analysis of the Canning Basin detrital zircons. We thank Petroleum Development Oman and especially Irene Gomez Perez for the drill cores from the Al Khlata Formation. The sample material for our study was released by the Ministry of Oil and Gas of the Sultanate of Oman (MOG Ref. 7312/12531) which is gratefully acknowledged. Martin and Redfern acknowledge the joint financial support provided by Natural Environment Research Council (UK) Studentship NER/S/A/2004/13012. Gerhard Spaeth kindly contributed the Heimefront Range field photo and Jim Collinson contributed TAM field images. A. J. Mory publishes with the permission of the Director, Geoscience Resources Strategy. The Laserchron crew at the University of Arizona was awesome over many decades! Pucks containing the detrital zircons analyzed in this study, except the Canning Basin, Australia (contact Jonathan Redfern, University of Manchester) and Sites 23 and 24 (contact the Laserschron Center, University of Arizona), will be housed at the Byrd Polar Research Center, Ohio State University, for future use. Doug Cole and one anonymous reviewer greatly improved the clarity and presentation of the manuscript.

Gondwanide fold-and-thrust belt showing the palinspastic locations of diamictite samples and their populations of pyrope garnets (inset PL images; see Table 2) and Cambrian archeocyathid clasts (2 mm diameter; Webers et al., 1992, see text.

The ice grounding line and striation directions in the Meyers Hills of the Ellsworth Mountains, Antarctica are from Matsch and Ojakangas (1992).

Appendix A. Supplementary data

Supplementary data to this article can be found online at https://doi.org/10.1016/j.earscirev.2019.01.014.

References

Adie, R.J., 1952. The position of the Falkland Islands in a Reconstruction of Gondwanaland. Geol. Mag. 89, 401–410.

Agassiz, L., 1840. On glaciers, and the evidence of their having once existed in Scotland, Ireland, and England. Proc. Geol. Soc. Lond. 3, 327–332.

Ahmad, N., 1981. Late Paleozoic Talchir tillites of Peninsular India. In: Hambrey, M.J., Harland, W.B. (Eds.), Earth's Pre-Pleistocene Glacial Record. Cambridge University Press, pp. 326–330.
Aldiss, D.T., Edwards, E.J., 1999. The Geology of the Falkland Islands. British Geological Survey Technical Report, WC/99/10.
Al-Hussein, M., 2015. Arabian ORBITAL STRATIGRAPHY revisited-AROS. Geoarabia 20, 183–216.
Azcuy, C.L., 1975. Miospores del Namuriano y Westphaliano de la comarca Malanzán-Loma Larga, Provincia de la Rioja, Argentina I. Localización y descripciones sistematicás. Ameghiniana 12, 1–69.
Backhouse, J., 1991. Permian palynology of the Collie Basin, Western Australia. Rev. Palaeobot. Palynol. 67, 237–314.
Backhouse, J., 1993. Palynology and correlation of Permian sediments in the Perth, Collie and Officer Basins, Western Australia. Geol. Surv. W. Aust. Rep. 34, 111–128.
Bangert, B., Stollhofen, H., Lorenz, V., Armstrong, R., 1999. The geochronology and significance of ash-fall tuffs in the glaciogenic Carboniferous-Permian Dwyka Group of Namibia and South Africa. J. Afr. Earth Sci. 29, 33–49.
Barrett, P.J., 1965. Geology of the area between the Axel Heiberg and Shackleton Glaciers, Queen Maud Range, Antarctica: part 2—Beacon group. N. Z. J. Geol. Geophys. 8, 344–363.
Betts, P.G., Giles, D., Lister, G.S., Frick, L.R., 2002. Evolution of the Australian lithosphere. Aust. J. Earth Sci. 49, 661–695.
Bigarella, J.J., Salamuni, R., Fuck, R.A., 1967. Striated surfaces and related features developed by the Gondwana ice sheets (State of Paraná, Brazil). Palaeogeogr. Palaeodimatol. Palaeoecol. 3, 265–276.
Birgenheier, L.P., Fielding, C.R., Rygel, M.C., Frank, T.D., Roberts, J., 2009. Evidence for dynamic climate change on sub-106-year scales from the late Paleozoic glacial record, Tamworth Belt, New South Wales, Australia. J. Sediment. Res. 79, 56–82.
Blakey, R.C., 2008. Gondwana paleogeography from assembly to breakup — a 500 m.y. odyssey. In: Fielding, C.R., Frank, T.D., Isbell, J.L. (Eds.), Resolving the Late Paleozoic Ice Age in Time and Space. Vol. 441. Geological Society of America Special Paper, pp. 1–28.
Blanford, W.T., Blanford, H.F., Theobald, W., 1856. On the geological structure and relations of the Talcheer Coal Field, in the District of Cuttack. Geol. Surv. India Mem. 1, 1–98.
Bodorkos, S., Crowley, J., Holmes, E., Laurie, J., Mantle, D., McKellar, J., Mory, A.J., Nicoll, R., Phillips, L., Smith, T., Stephenson, M., Wood, G., 2016. New ages for Permian palynostratigraphic biozones in the Sydney, Gunnedah, Bowen, Galilee and Canning basins, Australia. Permophiles 63, 19–21.
Botha, R.C.N., Botha, G.A., 2002. Geological Description of Sheet 2930CB Pietermaritzburg; Explanation Sheet 2930 CB, Scale 1:50,000. Council for Geoscience, South Africa (39 pp).
Bourman, R.P., Alley, N.F., 1999. Permian glaciated bedrock surfaces and associated sediments on Kangaroo Island, South Australia: implications for local Gondwanan ice-mass dynamics. Aust. J. Earth Sci. 46, 523–531.
Brakel, A.T., Totterdell, J.M., 1990. The Permian Palaeogeography of Australia. Bureau of Mineral Resources Geology and Geophysics Record 1990/60. http://www.ga.gov.au/metadata-gateway/metadata/record/14350/.
Buggisch, W., 1987. Stratigraphy and very low grade metamorphism of the Sierras Australes of the Province of Buenos Aires, Argentina and implications in Gondwana correlations. Zentralblatt Mineralogie Geologie Paläontologie 1, 819–837.
Buggisch, W., Wang, X., Alekseev, A.S., Joachimski, M.M., 2011. Carboniferous–Permian carbon isotope stratigraphy of successions from China (Yangtze platform), USA (Kansas) and Russia (Moscow Basin and Urals). Palaeogeogr. Palaeoclimatol. Palaeoecol. 301, 18–38.
Cagliari, J., Lavina, E.L.C., Philipp, R.P., Tognoli, F.M.W., Basei, M.A.S., Faccini, U.F., 2014. New Sakmarian ages for the Rio Bonito formation (Paraná Basin, southern Brazil) based on LA-ICP-MS U–Pb radiometric dating of zircons crystals. J. S. Am. Earth Sci. 56, 265–277.
Catuneanu, O., Hancox, P.J., Rubidge, B.S., 1998. Reciprocal flexural behaviour and contrasting stratigraphies: a new basin development model for the Karoo retroarc foreland system. South Afr. Basin Res. 10, 417–439.
Catuneanu, O., Wopfner, H., Cairncross, B., Rubidge, B.S., Smith, R.M.H., Hancox, P.J., 2005. The Karoo basins of south-central Africa. In: Catuneanu, O., Guiraud, R., Eriksson, P., Thomas, R.J., Shone, R., Key, R. (Eds.), Phanerozoic Evolution of Africa. J. Afr. Earth Sci. 43. pp. 211–253.
Cawood, P.A., Nemchin, A.A., 2000. Provenance record of a rift basin: U/Pb ages of detrital zircons from the Perth Basin, Western Australia. Sediment. Geol. 134, 209–234.
Chumakov, N.M., 1994. Evidence of Late Permian glaciation in the Kolyma River Basin: a repercussion of the Gondwana glaciations in northeast Asia? Stratigr. Geol. Correl. 2, 426–444.
Chumakov, N.M., Zharkov, M.A., 2003. Climate during the Permian–Triassic biosphere reorganizations. Article 2. Climate of the Late Permian and Early Triassic: general inferences. Stratigr. Geol. Correl. 11, 361–375.
Coates, D.A., 1969. Stratigraphy and sedimentation of the Sauce Grande Formation, Sierra de la Ventana, southern Buenos Aires Province, Argentina. Gondwana Stratigr. IUGS Symp. Buenos Aires, UNESCO Earth Sci. 2, 799–819.
Collo, G., Astini, R.A., Cawood, P.A., Buchan, C., Pimentel, M., 2009. U–Pb detrital zircon ages and Sm–Nd isotopic features in low-grade metasedimentary rocks of the Famatina belt: implications for late Neoproterozoic–early Paleozoic evolution of the proto-Andean argin of Gondwana. J. Geol. Soc. 166, 303–319.
Compston, W., Pidgeon, R.T., 1986. Jack Hills, evidence of more very old detrital zircons in Western Australia. Lett. Nat. 321, 766–769.
Cooper, M.R., Oosthuizen, R., 1974. Archaeocyatha-bearing erratics from the Dwyka Subgroup (Permo-Carboniferous) and their importance to continental drift. Nature 247, 396–398.
Cornell, D.H., Thomas, R.J., Moen, H.F.G., Reid, D.L., Moore, J.M., Gibson, R.L., 2006. The Namaqua-Natal Province. In: Johnson, M.R., Anhaeusser, C.R., Thomas, R.J. (Eds.), The Geology of South Africa: The Geological Society of South Africa and Council for Geoscience, pp. 325–379.
Craddock, J.P., 2011. Provenance of Late Paleozoic Gondwana Tillites: Gondwana-14. Buzios, Brazil, pp. 131.
Craddock, J.P., Thomas, R., 2011. Detrital Zircon Provenance of the Dwyka Diamictite, Cape Fold Belt, S. Africa and the Falkland Islands, GeoSynthesis Conference, Cape Town, South Africa, pp. 56–57.
Craddock, J.P., McGillion, M.S., Webers, G.F., Yoshida, M., 1998. Strain analysis across the Ventana-Ellsworth fold-and-thrust belt: South African. J. Earth Sci. 27, 49–50.
Craddock, J.P., Konstantinou, A., Nereson, A., Webers, G.F., Ojakangas, R.W., Fitzgerald, P., Gehrels, G., 2008. Detrital Zircon and heavy mineral provenance of the Ellsworth Mountains, Antarctica and Gondwana-wide Carboniferous Diamictite: Gondwana. 13. China. pp. 35.
Craddock, J.P., Schmitz, M.D., Crowley, J.L., Larocque, J., Pankhurst, R.J., Juda, N., Konstantinou, A., Storey, B., 2017a. Precise U-Pb zircon ages and geochemistry of Jurassic granites, Ellsworth-Whitmore terrane, central Antarctica. Geol. Soc. Am. Bull. 129, 118–136.
Craddock, J.P., Fitzgerald, P., Konstantinou, A., Nereson, A., Thomas, R.J., 2017b. Detrital Zircon provenance of upper Cambrian-Permian Strata and Tectonic evolution of the Ellsworth Mountains, West Antarctica. Gondwana Res. 45, 191–207.
Craddock, J.P., Malone, D.H., Porter, R., Luczaj, J., Konstantinou, A., Day, J.E., Johnston, S.T., 2017c. Paleozoic reactivation structures in the Appalachian-Ouachita-Marathon foreland: Far-field deformation across Pangea. Earth-Sci. Rev. 169, 1–34.
Crostella, A., Iasky, R.P., 1997. Structural interpretation and hydrocarbon potential of the Giralia area, Carnarvon Basin. W. Aust. Geol. Surv. Rep. 52, 1–38.
Crowell, J.C., 1978. Gondwanan glaciation, cyclothems, continental positioning, and climate change. Am. J. Sci. 278, 1345–1372.
Crowell, J.C., 1999. Pre-Mesozoic Ice Ages: their bearing on understanding the climate system. Geol. Soc. Am. Mem 192, 1–106.
Crowell, J.C., Frakes, L.A., 1970. Phanerozoic glaciation and the causes of ice ages. Am. J. Sci. 268, 193–224.
Crowley, T.J., Baum, S.K., 1991. Estimating Carboniferous sea-level fluctuations from Gondwana ice extent. Geology 19, 975–977.
Crowley, T.J., Baum, S.K., 1992. Modeling late Paleozoic glaciation. Geology 20, 507–510.
Da Silva, L.C., Gresse, P.G., Scheepers, R., McNaughton, N.J., Hartmann, L.A., Fletcher, I., 2000. U-Pb SHRIMP and Sm-Nd age constraints on the timing and sources of the Pan-African Cape Granite Suite, South Africa. J. Afr. Earth Sci. 30, 795–815.
Dalziel, I.W.D., Elliot, D.H., 1982. West Antarctica: Problem child of Gondwanaland. Tectonics 1, 3–19.
Darwin, C., 1846. Geological Observations on South America. Being the Third Part of the Geology of the Voyage of the Beagle. Under the Command of Capt. FitzRoy, R.N. During the years 1832 to 1836. Smith, Elder and Co, London.
Davydov, V.I., Haig, D.W., McCartain, E., 2013. A latest Carboniferous warming spike recorded by a fusulinid-rich bioherm in Timor Leste: implications for East Gondwana deglaciation. Palaeogeogr. Palaeoclimatol. Palaeoecol. 376, 22–38.
DeCelles, P.G., Gehrels, G.E., Quade, J., Lareau, B., Spurlin, M., 2000. Tectonic implications of U-Pb zircon ages of the Himalayan orogenic belt in Nepal. Science 288, 497–499.
DeCelles, P.G., Gehrels, G.E., Najman, G.E.Y., Martin, A.J., Carter, A., Garzanti, E., 2004. Detrital geochronology and geochemistry of Cretaceous–Early Miocene strata of Nepal: implications for timing and diachroneity of initial Himalayan orogenesis. Earth Planet. Sci. Lett. 227, 313–330.
deWit, M.C.J., 2016. Dwyka eskers along the northern margin of the main Karoo basin: in Origin and Evolution of the Cape Mountains and Karoo basin. Regional Geology Reviews 87–98. https://doi.org/10.1007/978-3-319-40859-0_9.
Deynoux, M., Miller, J.M.G., Domack, E.W., Eyles, N., Fairchild, I.J., Young, G.M. (Eds.), 1994. Earth's Glacial Record. Cambridge University Press, Cambridge, United Kingdom, pp. 266.
Dillinger, A., George, A.D., Parra-Avila, L.A., 2018. Early Permian sediment provenance and paleogeographic reconstructions in southeastern Gondwana using detrital zircon geochronology (Northern Perth Basin, Western Australia). Gondwana Res. 59, 57–75. https://doi.org/10.1016/j.gr.2018.02.020.
Drobe, M., de Luchi, M.L., Steenken, A., Wemmer, K., Naumann, R., Frei, R., Siegesmund, S., 2011. Geodynamic evolution of the Eastern Sierras Pampeanas (Central Argentina) based on geochemical, Sm–Nd, Pb–Pb and SHRIMP data. Int. J. Earth Sci. 100, 631–657.
Du Toit, A.L., 1921. The Carboniferous glaciation of South Africa. South Afr. J. Geol. 24, 188–227.
Du Toit, A.L., 1929. The continental displacement hypothesis as viewed by du Toit. Am. J. Sci. 17, 179–183.
Du Toit, A.L., 1937. Our Wandering Continents: An Hypothesis of Continental Drifting. Oliver and Boyd.
Elliot, D.H., Fanning, M., Laudon, T.S., 2014. The Gondwana Plate margin in the Weddell Sea sector: zircon geochronology of the upper Paleozoic (mainly Permian) strata of the Ellsworth Mountains and eastern Ellsworth Land. Antarctic Gondwana Res. 29, 234–247.
Evans, D.A.D., 2000. Stratigraphic, geochronological, and paleomagnetic constraints upon the Neoproterozoic climatic paradox. Am. J. Sci. 300, 347–433.
Eyles, N., 2008. Glacioepochs and the supercontinent cycle after ~3.0 Ga: tectonic boundary conditions for global cooling. Palaeogeogr. Palaeoecol. Palaeoclimatol. 258, 89–129.
Eyles, N., Young, G.M., 1991. Geodynamic controls on glaciation in Earth history. In:

Deynoux, M., Miller, J.M.G., Domack, E.W., Eyles, N., Fairchild, I.J., Young, G.M. (Eds.), Earth's Glacial Record. Cambridge University Press, pp. 1–28.
Falcon-Lang, H.J., 2004. Pennsylvanian tropical rain forests responded to glacial–interglacial rhythms. Geology 32, 689–692.
Fielding, C.R., Frank, T.D., Isbell, J.L., 2008. The late Paleozoic ice age—a review of current understanding and synthesis of global climate patterns. In: Fielding, C.R., Frank, T.D., Isbell, J.L. (Eds.), Resolving the Late Paleozoic Ice Age in Time and Space: Geological Society of America Special Paper. Vol. 441. pp. 343–354.
Forbes, G.A., Jansen, H.S.M., Schreurs, J., 2010. Al Khlata Formation. In: Lexicon of Oman Subsurface Stratigraphy. GeoArabia special Publication 5, Bahrain, pp. 156–165.
Fossa-Mancini, E., 1943. Supuestos Vestigios de Glacialciones del Paleozoico en la Argentina. Impr, Coni.
Frakes, L.A., Crowell, J.C., 1967. Facies and paleogeography of Late Paleozoic diamictite, Falkland Islands. Geol. Soc. Am. Bull. 78, 37–58.
Frakes, L.A., Crowell, J.C., 1969. Late Paleozoic glaciation; I, South America. Geol. Soc. Am. Bull. 80, 1007–1041.
Frakes, L.A., de Figueiredo Filho, P.M., 1967. Glacial rocks of the Paraná Basin exposed along the Sorocaba- Itapetininga road. In: Bigarella, J.J., Pinto, I.D., Decker, R. (Eds.), Problems in Brazilian Gondwana Geology, Curitiba, I International Symposium on the Gondwana Stratigraphy and Palaeontology, pp. 103–106.
Frakes, L.A., Kemp, E.M., Crowell, J.C., 1975. Late Paleozoic glaciation: Part VI, Asia. Geol. Soc. Am. Bull. 86, 454–464.
Frakes, L.A., Francis, J.E., Syktus, J.I., 1992. Climate Modes of the Phanerozoic. Cambridge University Press, Cambridge (274 pp).
Frank, T.D., Birgenheier, L.P., Montañez, I.P., Fieldging, C.R., Rygel, M.C., 2008. Late Paleozoic climate dynamics revealed by comparison of ice-proximal stratigraphic and ice-distal isotopic records. In: Fielding, C.R., Frank, T.D., Isbell, J.L. (Eds.), Resolving the Late Paleozoic Ice Age in Time and Space: Geological Society of America Special Paper. Vol. 41. pp. 331–342.
Gehrels, G.E., DeCelles, P.G., Ojha, T.P., Upreti, B.N., 2006a. Geologic and U-Th-Pb geochronologic evidence for early Paleozoic tectonism in the Kathmandu thrust sheet, central Nepal Himalaya. Geol. Soc. Am. Bull. 118, 185–198.
Gehrels, G.E., DeCelles, P.G., Ojha, T.P., Upreti, B.N., 2006b. Geologic and U-Pb geochronologic evidence for early Paleozoic tectonism in the Dadeldhura thrust sheet, far-west Nepal Himalaya. J. Asian Earth Sci. 28, 385–408.
Gehrels, G., Valencia, V., Pullen, A., 2006c. Detrital zircon geochronology by laser ablation multicollector ICPMS at the Arizona LaserChron Center, Olszewski, T., Geochronology: emerging opportunities. Paleontol. Soc. Pap. 12, 67–76.
Gehrels, G.E., Valencia, V., Ruiz, J., 2008. Enhanced precision, accuracy, efficiency, and spatial resolution of U-Pb ages by laser ablation-multicollector-inductively coupled plasma-mass spectrometry. Geochem. Geophys. Geosyst. 9, Q03017. https://doi.org/10.1029/2007GC001805.
Gehrels, G., Kapp, P., DeCelles, P., Pullen, A., Blakey, R., Weislogel, A., Ding, L., Guynn, J., Martin, A., McQuarrie, N., Yin, A., 2011. Detrital zircon geochronology of pre-Tertiary strata in the Tibetan-Himalayan orogeny. Tectonics 30, TC5016. https://doi.org/10.1029/2011TC002868.
Glen, R.A., 2005. The Tasmanides of eastern Australia. Geol. Soc. Lond. Spec. Publ. 246, 23–96.
Goodge, J.W., Fanning, C.M., Brecke, D.M., Licht, K.J., Palmer, E.F., 2010. Continuation of the Laurentian Grenville province across the Ross Sea margin of East Antarctica. J. Geol. 118, 601–619.
Gorter, J.D., Jones, P.J., Nicoll, R.S., Golding, C.J., 2005. A reappraisal of the Carboniferous stratigraphy and the petroleum potential of the southeastern Bonaparte Basin (Petrel sub-basin), northwestern Australia. APPEA J. 45, 275–296.
Gorter, J.D., Poynter, S.E., Bayford, S.W., Caudullo, A., 2008. Glacially influenced petroleum plays in the Kulshill Group (Late Carboniferous Early Permian) of the southeastern Bonaparte Basin, Western Australia. APPEA J. 48, 69–113.
Grossman, E.L., Yancey, T.E., Jones, T.E., Bruckschen, P., Chuvashov, B., Mazzullo, S.J., Mii, H.S., 2008. Glaciation, aridification, and carbon sequestration in the PermoCarboniferous; the isotopic record from low latitudes. Palaeogeogr. Palaeoclimatol. Palaeoecol. 268, 222–233.
Grunow, A.M., Dalziel, I.W.D., Kent, D.V., 1987. Ellsworth-Whitmore Mountains crustal block, western Antarctica; New paleomagnetic results and their tectonic significance. In: McKenzie, G.D. (Ed.), Gondwana Six; Structure, tectonics, and Geophysics. Geophysical Monograph 40. American Geophysical Union, Washington, D.C., pp. 161–171.
Gulbranson, E.L., Montanez, I.P., Schmitz, M.D., Limarino, C.O., Isbell, J.L., Marenssi, S.A., Crowley, J.L., 2010. High-precision U-pb calibration of carboniferous glaciation and climate history, Paganzo group, NW Argentina. Geol. Soc. Am. Bull. 122, 1480–1498.
Gulbranson, E.L., Isbell, J.L., Montanez, I.P., Limarino, C.O., Marenssi, S.A., Meyer, K., Hull, C., 2014. Reassessment of mid-Carboniferous glacial extent in southwestern Gondwana, Rio Blanco Basin. Gondwana Res. 25, 1369–1379.
Haig, D.W., McCartain, E., Mory, A.J., Gilsel, B., Davydov, V.I., Dixon, M., Ernst, A.J., Groflin, S., Håkansson, E., Keep, M., Dos Santos, Z., Shi, G.R., Soares, J., 2014. Postglacial Early Permian (late Sakmarian-early Artinskian) shallow-marine carbonate deposition along a 2000 km transect from Timor to west Australia. Palaeogeogr. Palaeoclimatol. Palaeoecol. 409, 180–204.
Haig, D.W., Mory, A.J., McCartain, E., Backhouse, J., Håkansson, E., Ernst, A., Nicoll, R.S., Shi, G.R., Bevan, J.C., Davydov, V.I., Hunter, A., Keep, M., Martin, S.K., Peyrot, D., Kossavaya, O., Dos Santos, Z., 2017. Late Artinskian-Early Kungurian (Early Permian) warming and maximum marine flooding in the East Gondwana interior rift, Timor and Western Australia, and comparisons across East Gondwana. Palaeogeogr. Palaeoclimatol. Palaeoecol. 468, 88–121.
Haines, P.W., Allen, H.J., 2017. Geological Reconnaissance of the Southern Murraba Basin, Western Australia: Revised Stratigraphic Position Within the Centralian Superbasin and Hydrocarbon Potential. Geological Survey of Western Australia, Record 2017/4, pp. 38.
Haines, P.W., Hand, M., Sandiford, M., 2001. Palaeozoic synorogenic sedimentation in central and northern Australia: a review of distribution and timing with implications for the evolution of intracontinental orogens. Aust. J. Earth Sci. 48, 911–928.
Haines, P.W., Allen, H.J., Wingate, M.T.D., Kirkland, C.L., Hocking, R.M., 2011. Ice movement direction and detrital provenance age for early Permian glacial deposits, Amadeus Basin, eastern Western Australia. In: Håkansson, E., Trotter, J.A. (Eds.), Programme & abstracts: The XVII International Congress on the Carboniferous and Permian, Perth 3–8 July 2011. Geological Survey of Western Australia Record 2011/20, pp. 63.
Haldorsen, S., Von Brunn, V., Maud, R., Truter, E.D., 2001. A Weichselian deglaciation model applied to the Early Permian glaciation in the northeast Karoo Basin, South Africa. J. Quat. Sci. 16, 583–593.
Halvorson, G.P., Hoffman, P.F., Schrag, D.P., Maloof, A.C., Rice, A.H.N., 2005. Toward a Neoproterozoic composite carbon. Geol. Soc. Am. Bull. 117, 1181–1207.
Hambrey, M.J., Harland, W.B., 1981. Earth's Pre-Pleistocene Glacial Record. Cambridge University Press, pp. 1004.
Hand, S.J., 1993. Palaeogeography of Tasmania's Permo-Carboniferous glacigenic sediments. In: Findlay, R.H., Unrug, R., Banks, M.R., Veevers, J.J. (Eds.), Gondwana Eight: Assembly, Evolution and Dispersal. A.A Balkema, Rotterdam, pp. 459–469.
Hand, M., Mawby, J., Kinny, P., Foden, J., 1999. U-Pb ages from the Harts Range, central Australia: evidence for early Ordovician extension and constraints on Carboniferous metamorphism. J. Geol. Soc. Lond. 156, 715–730.
Hankel, O., 1994. Early Permian to Middle Jurassic rifting and sedimentation in East Africa and Madagascar. Geol. Rundsch. 83, 703–710.
Harley, S.L., Kelly, N.M., 2007. Ancient Antarctica: the Archaean of the East Antarctic shield. Dev. Precambrian Geol. 15, 149–186.
Harrington, H.J., 1947. Explicacio´n de las Hojas Geolo´gicas Sierras de Curamalal y de la Ventana, Provincia Buenos Aires, Servicio Nacional de Minerı´a y Geologı´a. Bol. 61.
Haskell, T.R., Kennett, J.P., Prebble, W.M., Smith, G., Willis, I.A.G., 1965. The geology of the middle and lower Taylor Valley of south Victoria Land, Antarctica. Trans. R. Soc. N. Z. 2, 170–189.
Heckel, P.H., 1986. Sea-level curve for Pennsylvanian eustatic marine transgressive-regressive depositional cycles along midcontinent outcrop belt, North America. Geology 14, 330–334 10.1130/0091-7613(1986)14 < 330:SCFPEM > 2.0.CO;2.
Heckel, P.H., 1994. Evaluation of evidence for glacio-eustatic control over marine Pennsylvanian cyclothems in North America and consideration of possible tectonic effects. In: Dennison, J.M., Ettensohn, F.R. (Eds.), Tectonic and eustatic controls on sedimentary cycles. Tulsa, Oklahoma, SEPM (Society for Sedimentary Geology). Concepts Sedimentol. Paleontol. 4. pp. 65–87.
Heckel, P.H., 2008. Pennsylvanian cyclothems in midcontinent North America as far-field effects of waxing and waning of Gondwana ice sheets. Special Paper 441, Boulkder. In: Fielding, C.R., Frank, T., Isbell, J.L. (Eds.), Resolving the Late Paleozoic Ice Age in Time and Space: Geological Society of America Special Paper, pp. 275–289.
Heckel, P.H., Clayton, G., 2006. The Carboniferous System. Use of the new official names for the subsystems, series, and stages. Geol. Acta 4, 403–407.
Henry, L.C., Isbell, J.L., Limarino, C.O., 2014. The late Paleozoic El Imperial Formation, western Argentina: glacial to post-glacial transition and stratigraphic correlation with arc-related basins. Gondwana Res. 25, 1380–1395.
Hoffman, P.F., Schrag, D.P., 2002. The snowball Earth hypothesis: testing the limits of global change. Terra Nova 14, 29–155.
Hyde, W.T., Crowley, T.J., Tarasov, L., Paltier, W.R., 1999. The Pangean ice age: studies with a coupled climate-ice sheet model. Clim. Dyn. 15, 619–629.
Isbell, J.L., 2010. Environmental and paleogeographic implications of glaciotectonic deformation of glaciomarine deposits within Permian strata of the Metschel Diamictite, southern Victoria Land, Antarctica. In: López-Gamundí, O.R., Buatois, L.A. (Eds.), Late Paleozoic glacial events and postglacial transgressions in Gondwana. Geological Society of America Special Paper. Vol. 468. pp. 81–100.
Isbell, J.L., Miller, M.F., Wolfe, K.L., Lenaker, P.A., 2003. Timing of late Paleozoic glaciation in Gondwana: was glaciation responsible for the development of northern hemisphere cyclothems? In: Chan, M.A., Archer, A.W. (Eds.), Extreme Depositional Environments: Mega End Members in Geologic Time. Vol. 370. Geological Society of America Special Paper, pp. 5–24.
Isbell, J.L., Cole, D.I., Catuneanu, O., 2008a. Carboniferous-Permian glaciation in the main Karoo Basin, South Africa: stratigraphy, depositional controls, and glacial dynamics. Geol. Soc. Am. Spec. Pap. 441, 71–82.
Isbell, J.L., Cole, D.I., Catuneanu, O., 2008b. Carboniferous-Permian glaciation in the main Karoo Basin, South Africa: stratigraphy, depositional controls and glacial dynamics. In: Fielding, C.R., Frank, T.D., Isbell, J.L. (Eds.), Resolving the Late Paleozoic Ice Age in Time and Space. Vol. 441. Geological Society of America Special Paper, pp. 71–82.
Isbell, J.L., Henry, L.C., Gulbranson, E.L., Limarino, C.O., Fraser, M.L., Koch, Z.L., Ciccioli, P.L., Dineen, A.A., 2012. Glacial paradoxes during the late Paleozoic ice age: evaluating the equilibrium line altitude as a control on glaciation. Earth Sci. Rev. 22, 1–19.
Isbell, J.L., Biakov, A.S., Vedernikov, I.L., Davydov, V.I., Gulbranson, E.L., Fedorchuk, N.D., 2016. Permian diamictites in northeastern Asia: their significance concerning the bipolarity of the late Paleozoic ice age. Earth Sci. Rev. 154, 279–300.
Jacobs, J., Fanning, C.M., Bauer, W., 2003. Timing of Grenville-age vs Pan-African medium- to high-grade metamorphism in western Dronning Maud Land (East Antarctica) and significance for correlations in Rodinia and Gondwana. Precambrian Res. 125, 1–20.
Jacobs, J., Pisarevsky, S., Thomas, R.J., Becker, T., 2008. The Kalahari Craton during the assembly and dispersal of Rodinia. Precambrian Res. 160, 142–158.

Joachimski, M.M., Bitter, P.H.V., Buggisch, W., 2006. Constraints on Pennsylvanian glacioeustatic sea-level changes using oxygen isotopes of conodont apatite. Geology 34, 277–280.

Johnstone, M.H., Pudovskis, V., 1955. Warroora No 1 Test Geological Completion Report. Western Australia Geological Survey (S-series, S51 V30 unpublished).

Keidel, J., 1922. Sobre la distribución de los depósitos glaciares del pérmico conocidos en la Argentina y su significación para la estratigrafía de la serie de Gondwana y la paleografía de hemisferio austral. Casa Ed. Coni. 1, 23–35.

Keidel, J.U.A.N., 1940. Paleozoic glaciation in South America. Proc. 8th Am. Sci. Congr., Washington 4, 89–108.

Kemp, E.M., Balme, B.E., Helby, R.A., Kyle, R.A., Playford, G., Price, P.L., 1977. Carboniferous and Permian palynostratigraphy in Australia and Antarctica: a review: Bureau of Mineral Resources, Australia. J. Aust. Geol. Geophys. 2, 177–208.

Key, R.M., Tidi, J., McGeorge, I., Aitken, G., Cadman, A., Anscombe, J., 1998. The Lower Karoo Supergroup geology of the south-eastern part of the Gemsbok sub-basin of the Kalahari Basin, Botswana. South Afr. J. Geol. 101, 225–236.

Khodjanyazova, R.R., Davydov, V.I., Montanez, I.P., Schmitz, M.D., 2014. Climate- and eustasy-driven cyclicity in Pennsylvanian fusulinid assemblages, Donets Basin (Ukraine). Palaeogeogr. Palaeoclimatol. Palaeoecol. 396, 41–61.

Kissock, J.K., Finzel, E.S., Malone, D.H., Craddock, J.P., 2017. Lower–Middle Pennsylvanian strata in the North American midcontinent record the interplay between erosional unroofing of the Appalachians and eustatic sea-level rise. Geosphere 11, 1–21.

Koch, Z.J., Isbell, J.L., 2013. Processes and products of grounding-line fans from the Permian Pagoda Formation, Antarctica: insight into glacigenic conditions in polar Gondwana. Gondwana Res. 24, 161–172.

Kohn, B.P., Gleadow, A.J.W., Brown, R.W., Gallagher, K., O'Sullivan, P.B., Foster, D.A., 2002. Shaping the Australian crust over the last 300 million years: insights from fission track thermotectonic imaging and denudation studies of key terranes. Aust. J. Earth Sci. 49, 697–717.

Larsson, K., Lindström, S., Guy-Ohlson, D., 1990. An Early Permian palynoflora from Milorgfjella, Dronning Maud Land, Antarctica. Antarct. Sci. 2, 331–344.

Laurie, J.R., Bodorkos, S., Nicoll, R.S., Crowley, J.L., Mantle, D.J., Mory, A.J., Wood, G.R., Backhouse, J., Holmes, E.K., Smith, T.E., Champion, D.C., 2016. Calibrating the middle and late Permian palynostratigraphy of Australia to the geologic time-scale via U–Pb zircon CA-IDTIMS dating. Aust. J. Earth Sci. 3, 701–730.

Levell, B.K., Braakman, J.H., Rutten, K.W., 1988. Oil-bearing sediments of Gondwanan glaciation in Oman. Am. Assoc. Pet. Geol. Bull. 72, 775–796.

Licht, K.J., Palmer, E.F., 2013. Erosion and transport by Byrd Glacier, Antarctica during the last glacial maximum. Quat. Sci. Rev. 62, 32–48.

Limarino, C., Gutierrez, P., 1990. Diamictites in the Agua Colorada Formation (northwestern Argentina): new evidence of Carboniferous glaciation in South America. J. S. Am. Earth Sci. 3, 9–20.

Limarino, C.O., Césari, S.N., Net, L.I., Marenssi, S.A., Gutiérrez, P.R., Tripaldi, A., 2002. The Upper Carboniferous postglacial transgression in the Paganzo and Río Blanco Basins (northwestern Argentina): facies and stratigraphic significance. J. S. Am. Earth Sci. 15, 445–460.

Limarino, C.O., Cesari, S.N., Spalletti, L.A., Taboada, A.C., Isbell, J.L., Geuna, S., Gulbranson, E.L., 2014a. A paleoclimatic review of southern South America during the late Paleozoic: a record from icehouse to extreme greenhouse conditions. Gondwana Res. 25, 1396–1421.

Limarino, C.O., Alonso-Muruaga, P.J., Ciccioli, P.L., Loinaze, V.S.P., Césari, S.N., 2014b. Stratigraphy and palynology of a late Paleozoic glacial paleovalley in the Andean Precordillera, Argentina. Palaeogeogr. Palaeoclimatol. Palaeoecol. 412, 223–240.

Lindström, S., 1995. Early Permian palynostratigraphy of the northern Heimefrontfjella mountain-range, Dronning Maud Land, Antarctica. Rev. Paleobot. Palynol. 89, 359–415.

Linol, B., de Wit, M.J., Milani, E.J., Guillocheau, F., Scherer, C., 2015. New regional correlations between the Congo, Paraná and Cape-Karoo basins of southwest Gondwana. In: Geology and Resource Potential of the Congo Basin. Springer, Berlin Heidelberg, pp. 245–268.

Liu, C., Jarochowska, E., Du, Y., Vachard, D., Munnecke, A., 2017. Stratigraphical and δ 13 C records of Permo-Carboniferous platform carbonates, South China: responses to late Paleozoic icehouse climate and icehouse–greenhouse transition. Palaeogeogr. Palaeoclimatol. Palaeoecol. 474, 113–129.

Long, W.E., 1962. Sedimentary rocks of the Buckeye Range, Horlick Mountains, Antarctica. Science 136, 319–321.

López-Gamundí, O.R., 1997. Glacial–postglacial transition in the late Paleozoic basins of Southern South America. In: Martini, I.P. (Ed.), Late Glacial and Postglacial Environmental Changes: Quaternary Carboniferous–Permian, and Proterozoic. Oxford University Press, Oxford U.K., pp. 147–168.

Lopez-Gamundi, O.R., Buatois, L.A., 2010. Introduction: Late Paleozoic glacial events and postglacial transgressions in Gondwana. In: Lopez-Gamundi, O.R., Buatois, L.A. (Eds.), Late Paleozoic Glacial Events and Postglacial Transgressions, Gondwana: Geological Society of America Special Paper 468, (v–viii).

Ludwig, K., 2008. Isoplot 3.6. 4. Berkeley Geochronology Center Special Publication, pp. 77.

Maack, R., 1961. A modificação da paisagem natural pela colonização e suas consequências no norte do Paraná. Bol. Paranaen. Geogr. 2-3, 29–46.

Maidment, D.W., Williams, I.S., Hand, M., 2007. Testing long-term patterns of basin sedimentation by detrital zircon geochronology, Centralian Superbasin, Australia. Basin Res. 19, 335–360.

Mantovani, M.S.M., Brito Neves, B.B., 2005. The Paranápanema Lithospheric Block: its importance for Proterozoic (Rodinia, Gondwana) Supercontinent Theories Gondwana Research. Vol. 8. pp. 303–315.

Marshall, J.E.A., 1994. The Falkland Islands: a key element in Gondwana paleogeography. Tectonics 13, 499–514.

Martin, J.R., 2008. Sedimentology, Provenance and Ice-Sheet Dynamics of the Late Palaeozoic Glaciation in Oman and the Canning Basin (West Australia): An integrated Outcrop and Subsurface study of the Permo-Carboniferous Glaciogenic Suites of Arabia and Western Australia. Ph. D. thesis. Manchester University (unpublished).

Martin, J.R., Redfern, J., Mory, A.J., Williams, B.P.J., 2007. Facies Architecture and Reservoir Prediction in Ancient Glaciogenic Sediments: A Case Study Using Integrated Outcrop and Subsurface Studies of the Grant Group (Canning Basin, West Australia). AAPG Annual Conference, Long Beach, California.

Martin, J.R., Redfern, J., Aitken, J.F., 2008. A regional overview of the late Paleozoic glaciation in Oman. In: Fielding, C.R., Frank, T.D., Isbell, J.L. (Eds.), Resolving the Late Paleozoic Ice Age in Time and Space. Geological Society of America Special Publication, pp. 175–186.

Martin, J.R., Redfern, J., Williams, B.J.P., 2012. Evidence for multiple ice centres during the late Palaeozoic ice age in Oman: outcrop sedimentology and provenance of the Late Carboniferous–Early Permian Al Khlata Formation. In: Huuse, M., Redfern, J., Le Heron, D.P., Dixon, R.J., Moscariello, A., Craig, G. (Eds.), Glaciogenic Reservoirs and Hydrocarbon Systems. 368. Geological Society, London, pp. 229–256 Special Publications.

Matsch, C.L., Ojakangas, R.W., 1992. Stratigraphy and sedimentology of the Whiteout Conglomerate; an upper Paleozoic glacigenic unit, Ellsworth Mountains, West Antarctica. Geol. Soc. Am. Mem. 170, 37–62.

McQuarrie, N., Robinson, D., Long, S., Tobgay, T., Grujic, D., Gehrels, G., Ducea, M., 2008. Preliminary stratigraphic and structural architecture of Bhutan: implications for the along strike architecture of the Himalayan system. Earth Planet. Sci. Lett. (72), 105–117.

Mikhaylov, Y.A., Ustritskiy, I., Chernyak, G.Y., Yavshits, G.P., 1970. Upper Permian glaciomarine sediments of the northeastern USSR. Doklady. Earth Sci. Sect. 190 (1–6), 100–102 in Russian.

Millar, I.L., Pankhurst, R.J., 1987. Rb-Sr geochronology of the region between the Antarctic Peninsula and the Transantarctic Mountains; Haag Nunataks and Mesozoic granitoids; Gondwana six; structure, tectonics, and geophysics. Geophys. Monogr. 40, 151–160.

Mitchell, C., Taylor, G.K., Cox, K.G., Shaw, J., 1986. Are the Falkland Islands a rotated microplate? Nature 319, 131–134.

Montañez, I.P., Poulsen, C.J., 2013. The Late Paleozoic ice age: an evolving paradigm. Annu. Rev. Earth Planet. Sci. 41, 629–656.

Montañez, I.P., McElwain, J.C., Poulsen, C.J., White, J.D., DiMichele, W.A., Wilson, J.P., Griggs, G., Hren, M.T., 2016. Climate, pCO2 and terrestrial carbon cycle linkages during late Palaeozoic glacial-interglacial cycles. Nat. Geosci. 9, 824.

Mory, A.J., 2010. A review of mid-Carboniferous to Triassic stratigraphy, Canning Basin, Western Australia. Geol. Surv. W. Aust. 107, 1–130.

Mory, A.J., Redfern, J., Martin, J.R., 2008. A review of Permian–Carboniferous glacial deposits in Western Australia. In: Fielding, C.R., Frank, T.D., Isbell, J.L. (Eds.), Resolving the Late Paleozoic Ice Age in Time and Space. 441. Geological Society of America Special Paper, pp. 29–40.

Moxness, L.D., Isbell, J.L., Pauls, K.P., Limarino, C.O., Schencman, J., 2018. Sedimentology of the mid-Carboniferous fill of the Olta paleovalley, eastern Paganzo Basin, Argentina: implications for glaciation and controls on diachronous deglaciation in western Gondwana during the late Paleozoic Ice Age. J. S. Am. Earth Sci. 84, 127–148.

Myrow, P.M., Hughes, N.C., Goodge, J.W., Fanning, C.M., Williams, I.S., Peng, S., Bhargava, O.N., Parcha, S.K., Pogue, K.R., 2010. Extraordinary transport and mixing of sediment across Himalayan central Gondwana during the Cambrian–Ordovician. Geol. Soc. Am. Bull. 122, 1660–1670.

Net, L.I., 2002. Control de la composición de la fracción clástica sobre el tipo de cemento en areniscas carboníferas de la Cuenca Paganzo, Argentina. AAS Revista 9, 1–30 (AAS = Asociación Argentina de Sedimentología).

Net, L.I., Limarino, C.O., 1999. Paleogeografía y correlación estratigráfica del Paleozoico Tardío de la Sierra de Los Llanos, provincia de La Rioja, Argentina. Rev. Asoc. Geol. Argent. 54, 229–239.

Net, L.I., Limarino, C.O., 2006. Applying sandstone petrofacies to unravel the Upper Carboniferous evolution of the Paganzo Basin, northwest Argentina. J. S. Am. Earth Sci. 22, 239–254.

Net, L.I., Alonso, M.S., Limarino, C.O., 2002. Source rock and environmental control on clay mineral associations, Lower Section of Paganzo Group (Carboniferous), Northwest Argentina. Sediment. Geol. 152, 183–199.

O'Brien, P.E., Christie-Blick, N., 1992. Glacially-grooved surfaces in the Grant Group, Grant Range, Canning Basin and the extent of the late Paleozoic Pilbara ice sheets: Bureau of Mineral Resources. J. Aust. Geol. Geophys. 13, 87–92.

Osborne, G.D., Browne, W.R., 1921. Note on a glacially-striated pavement in the Kuttung Series of the Maitland District. Proc. Linnean Soc. NSW 46, 59–262.

Pankhurst, R.J., Weaver, S.D., Bradshaw, J.D., Storey, B.C., Ireland, T.R., 1998. Geochronology and geochemistry of pre-Jurassic superterranes in Marie Byrd Land: Antarctica. J. Geophys. Res. 103, 2529–2547.

Pérez Loinaze, V.S., Césari, S.N., 2012. Palynology of late Serpukhovian glacial and postglacial deposits from Paganzo Basin, northwestern Argentina. Micropaleontology 335–350.

Playford, G., Mory, A.J., 2017. Composition and occurrence of the Grandispora maculosa zonal assemblage (Mississippian) in the subsurface of the Carnarvon Basin and the Coolcalalaya Sub-basin of Western Australia, and its Gondwanan distribution. Revista Italiana di Paleontologiia e Stratigrafia 123, 275–318.

Playford, P.E., Cockbain, A.E., Low, G.H., 1976. Geology of the Perth Basin, Western Australia. Geol. Surv. W. Aust. Bull. 124, 1–311.

Playford, P.E., Hocking, R.M., Cockbain, A.E., 2009. Devonian reef complexes of the Canning Basin, Western Australia. Geol. Surv. W. Aust. 145, 1–44.

Poscher, G., 1994. Permokarbone glaziale und periglaziale Sedimentation in den Kottas-Bergen der Heimefrontfjella, Dronning Maud Land, Antarktis. Zbl. Geol. Paläont. Teil 1 (1992), 1373–1386.
Preiss, W., Preiss, A., 2015. Glacial striations at Orroroo – Permian Cretaceous or Pleistocene? South Aust. MESA J. 70, 33–37.
Rainbird, R.H., Heaman, L.M., Young, G., 1992. Sampling Laurentia: detrital zircon geochronology offers evidence for an extensive Neoproterozoic river system originating from the Grenville orogen. Geology 20, 351–354.
Ramos, A., Chemale, F., Naipauer, M., Pazos, P.J., 2014. A provenance study of the Paleozoic Ventania System (Argentina): transient complex sources from Western and Eastern Gondwana. Gondwana Res. 26, 719–740.
Ramos, V.A., Cingolani, C., Junior, F.C., Naipauer, M., Rapalini, A., 2017. The Malvinas (Falkland) Islands revisited: the tectonic evolution of southern Gondwana based on U-Pb and Lu-Hf detrital zircon isotopes in the Paleozoic cover. J. S. Am. Earth Sci. 76, 320–345.
Rapalini, A., Lopez de Luchi, M., Tohver, E., Cawood, P.A., 2013. The South American ancestry of the North Patagonian Massif. geochronological evidence for an autochthonous origin? Terra Nova 25, 337–342.
Rino, S., Kon, Y., Sato, W., Maruyama, S., Santosh, M., Zhao, D., 2008. The Grenvillian and Pan-African orogens: World's largest orogenies through geologic time, and their implications on the origin of superplume. Gondwana Res. 14, 51–72.
Robb, L.J., Brandl, G., Anhaeusser, C.R., Thomas, R.J., 2006. Archaean granitoid intrusions. In: Johnson, M.R., Anhaeusser, C.R., Thomas, R.J. (Eds.), The Geology of South Africa. The Geological Society of South Africa and Council for Geoscience, pp. 57–94.
Roberts, J., James, L., 2010. Stratigraphic relationships of Carboniferous volcanogenic successions in the Clifton-Carroll block and the Werrie Syncline, northern Tamworth belt, southern New England. Aust. J. Earth Sci. 57, 193–205.
Roberts, J., Claoue-Long, J., Jones, P.J., Foster, C.B., 1995. SHRIMP zircon age control of Gondwanan sequences in Late Carboniferous and Early Permian Australia. Geol. Soc. Lond. Spec. Publ. 89, 145–174.
Roberts, J., Jones, P.J., Jenkins, T.B.H., 1996. Revised correlations for Carboniferous marine invertebrate zones of eastern Australia. Alcheringa 17, 353–376.
Roberts, J., Wang, X., Fanning, M., 2003. Stratigraphy and correlation of Carboniferous ignimbrites, Rocky Creek region, Tamworth Belt, Southern New England Orogen, New South Wales. Aust. J. Earth Sci. 50, 931–954.
Roberts, J., Offler, R., Fanning, M., 2004. Upper Carboniferous to Lower Permian volcanic successions of the Carroll–Nandewar region, northern Tamworth Belt, southern New England Orogen, Australia. Aust. J. Earth Sci. 51, 205–232.
Roberts, J., Offler, R., Fanning, M., 2006. Carboniferous to Lower Permian stratigraphy of the southern Tamworth Belt, southern New England Orogen, Australia: boundary sequences of the Werrie and Rouchel Blocks. Aust. J. Earth Sci. 53, 249–284.
Rocha-Campos, A.C., 1967. The Tubarão Group in the Brazilian portion of the Paraná Basin. In: Bigarella, J., Decker, R.D., Pinto, I.D. (Eds.), Problems in Brazilian Gondwana Geology, Curitiba, pp. 27–102.
Rocha-Campos, A.C., Santos, P.R. Dos, Canuto, J.R., 2008. Late Paleozoic glacial deposits of Brazil: Paraná Basin. In: Fielding, C.R., Frank, T.D., Isbell, J.L. (Eds.), Resolving the Late Paleozoic Ice Age in Time and Space. Vol. 441. Geological Society of America, pp. 97–114 Special Paper.
Rygel, M.C., Fielding, C.R., Frank, T., Birgeinheier, L.R., 1996. The magnitude of late Paleozoic glacioeustatic fluctuations: A synthesis. Journal of Sedimentary Research 78, 500–511. https://doi.org/10.2110/jsr.2008.058.
Santos, P.R., Rocha-Campos, A.C., Canuto, J.R., 1996. Patterns of Late Palaeozoic deglaciation in the Paraná Basin, Brazil. Palaeogeogr. Palaeoclimatol. Palaeoecol. 125, 165–184.
Saylor, J.E., Knowles, J.N., Horton, B.K., Nie, J., Mora, A., 2013. Mixing of source populations recorded in detrital zircon U-Pb age spectra of modern river sands. J. Geol. 121, 17–33.
Schandelmeier, H., Bremer, F., Holl, H.G., 2004. Kinematic evolution of the Morondava rift basin of SW Madagascar—from wrench tectonics to normal extension. J. Afr. Earth Sci. 38, 321–330.
Schmidt, D.L., Williams, P.L., 1969. Continental glaciation of late Paleozoic age, Pensacola Mountains, Antarctica. In: Gondwana stratigraphy (IUGS symposium, Buenos Aires, 1967). Earth Science Series 2. pp. 617–649.
Shen, S.Z., Zhang, H., Shi, G.R., Li, W.Z., Xie, J.F., Mu, L., Fan, J.X., 2013. Early Permian (Cisuralian) global brachiopod palaeobiogeography. Gondwana Res. 24, 104–124.
Soreghan, M.J., Soreghan, G.S., Hamilton, M.A., 2008. Paleowinds inferred from detrital ziron geochronology of upper Paleozoic loessite, west equatorial Pangea. Geology 30, 695–698.
Southgate, P., Sircombe, K., Lewis, C., 2011. New insights into Reservoir Sand Provenance in the Exmouth Plateau and Browse Basin: Australian Petroleum Production and Exploration Association Conference, 10–13 April 2011, Perth. (Extended Abstract).
Sporli, K.B., Craddock, C., 1992. Structure of the Heritage Range, Ellsworth Mountains, West Antarctica: Webers, G. F., Craddock, C., Splettstoesser, J. F. Geol. Soc. Am. Mem. 170, 375–392.
Stollhofen, H., Werner, M., Stanistreet, I.G., Armstrong, R.A., 2008. Single-zircon U-Pb dating of Carboniferous-Permian tuffs, Namibia, and the intercontinental deglaciation cycle framework. Geol. Soc. Am. Spec. Pap. 441, 83–96.
Storey, B.C., Hole, M.J., Pankhurst, R.J., Millar, I.L., Vennum, W., 1988. Middle Jurassic within-plate granites in West Antarctica and their bearing on the break-up of Gondwanaland. J. Geol. Soc. Lond. 145, 999–1007.
Streel, M., Theron, J.N., 1999. The Devonian-Carboniferous boundary in South Africa and age of the earliest episode of the Dwyka glaciation: New palynological result. Episodes 22, 41–44.
Tessensohn, F., Kleinschmidt, G., Talarico, F., Buggisch, W., Brommer, A., Henjes-Kunst, F., Kroner, U., Millar, I.L., Zeh, A., 1999. Ross-age amalgamation of East and West Gondwana: evidence from the Shackleton Range. Antarctica: Terra Antartica 6, 317–325.
Thomas, R.J., von Brunn, V., Marshall, C.G.A., 1990. A tectono-sedimentary model for the Dwyka Group in southern Natal, South Africa. South Afr. J. Geol. 93, 809–817.
Trewin, N.H., Macdonald, D.I.M., Thomas, C.G.C., 2002. Stratigraphy and sedimentology of the Permian of the Falkland Islands; lithostratigraphic and palaeoenvironmental links with South Africa. J. Geol. Soc. Lond. 159, 5–19.
Veevers, J.J., 2004. Gondwanaland from 650–500 Ma assembly through 320 Ma merger in Pangea to 185–100 Ma breakup: supercontinental tectonics via stratigraphy and radiometric dating. Earth Sci. Rev. 68, 1–132.
Veevers, J.J., Powell, M., 1987. Late Paleozoic glacial episodes in Gondwanaland reflected in transgressive–regressive depositional sequences in Euramerica. Geol. Soc. Am. Bull. 98, 475–487.
Veevers, J.J., Saeed, A., 2008. Gamburtsev Subglacial Mountains provenance of Permian–Triassic sandstones in the Prince Charles Mountains and offshore Prydz Bay: integrated U–Pb and TDM ages and host-rock affinity from detrital zircons. Gondwana Res. 14, 316–343.
Veevers, J.J., Tewari, R., 1995. Permian–Carboniferous and Permian–Triassic magmatism in the rift zone bordering the Tethyan margin of southern Pangea. Geology 23, 467–470.
Veevers, J.J., Conaghan, P.J., Powell, C.McA., Cowan, E.J., McDonnell, K.L., Shaw, S.E., 1994. Eastern Australia. In: Veevers, J.J., Powell, C.M. (Eds.), Permian–Triassic Pangean Basins and Fold Belts along the Panthalassan Margin of Gondwanaland. 184. Geological Society of America Memoir, pp. 11–171.
Veevers, J.J., Saeed, A., Belousova, E.A., Griffin, W.L., 2005. U–Pb ages and source composition by Hf-isotope and trace-element analysis of detrital zircons in Permian sandstone and modern sand from southwestern Australia and a review of the paleogeographical and denudational history of the Yilgarn Craton. Earth Sci. Rev. 68, 245–279.
Veevers, J.J., Belousova, E.A., Saeed, A., Sircombe, K., Cooper, A.F., Read, S.E., 2006. Pan-Gondwanaland detrital zircons from Australia analysed for Hf-isotopes and trace elements reflect an ice-covered Antarctic provenance of 700–500 Ma age, TDM of 2.0–1.0 Ga, and alkaline affinity. Earth Sci. Rev. 76, 135–174.
Vermeesch, P., 2004. How many grains are needed for a provenance study? Earth Planet. Sci. Lett. 224, 441–451.
Visser, J.N.J., 1987. The palaeogeography of part of southwestern Gondwana during the Permo-Carboniferous glaciation. Palaeogeogr. Palaeoclimatol. Palaeoecol. 61, 205–219.
Visser, J.N.J., 1990. The age of the late Palaeozoic glaciogene deposits in southern Africa. S. Afr. J. Geol. 93, 366–375.
Visser, J.N.J., 1997. Deglaciation sequences in the Permo-Carboniferous Karoo and Kalahari basins of southern Africa: a tool in the analysis of cyclic glaciomarine basin fills. Sedimentology 44, 507–521.
Visser, J.N.J., Van Niekerk, B.N., Van der Merwe, S.W., 1997. Sediment transport of the late Palaeozoic glacial Dwyka Group in the southwestern Karoo Basin. S. Afr. J. Geol. 100, 223–236.
Von Brunn, V., 1996. The Dwyka Group in the northern part of KwaZulu-Natal, South Africa: sedimentation during late Palaeozoic deglaciation. Palaeogeogr. Palaeoclimatol. Palaeoecol. 125, 141–163.
Von Charpentier, J., de Charpentier, J., 1841. Essai Sur Les Glaciers et Sur le Terrain Erratique du Bassin du Rhône. (M. Ducloux).
Von Gosen, W., Buggisch, W., Dimieri, L.V., 1990. Structural and metamorphic evolution of the Sierras Australes, Buenos Aires province, Argentina. Geol. Rundsch. 79, 797–821.
Von Gosen, W., Buggisch, W., Krumm, S., 1991. Metamorphism and deformation mechanisms in the Sierras Australes fold and thrust belt (Buenos Aires province, Argentina). Tectonophysics 185, 335–356.
Watts, D.R., Bramall, A.M., 1981. Palaeomagnetic evidence for a displaced terrain in Western Antarctica. Nature 93, 638–641.
Webers, G.F., Craddock, C., Splettstoesser, J.F., 1992. Geologic history of the Ellsworth Mountains, West Antarctica: St. Paul, MN, Webers, G. F., Craddock, C., Splettstoesser, J. F. Geol. Soc. Am. Mem. 170, 1–8.
Wegener, A., 1915. Die Entstehung der Kontinente und Ozeane. On the Origin of Continents and Oceans, English translation of 3rd edition by J. G. A. Skerl (1924). Methuen, London (212 pp).
Wegener, A., 1966. The Origin of Continents and Oceans. Courier Corporation.
Wescott, W.A., Diggens, J.N., 1998. Depositional history and stratigraphical evolution of the Sakamena Group (Middle Karoo Supergroup) in the southern Morondava Basin, Madagascar. J. Afr. Earth Sci. 27, 461–479.
Wolmarans, L.G., Kent, L.E., 1982. Geological investigations in Western Dronning Maud Land, Antarctica – a synthesis. South Afr. J. Ant. Res Supplement 2, 93 pp.
Yeh, M.W., Shellnutt, J.G., 2016. The initial break-up of Pangaea by Late Paleozoic Glaciation. Nat. Sci. Rep. 6, 31442.
Ziegler, A.M., Hulver, M.L., Rowley, D.B., 1997. Permian World topography and climate. In: Martini, I.P. (Ed.), Late Glacial and Postglacial Environmental Changes. Quaternary Carboniferous–Permian, and Proterozoic. Oxford University Press, Oxford, U.K., pp. 111–146.